

**KERNFORSCHUNGSZENTRUM
KARLSRUHE**

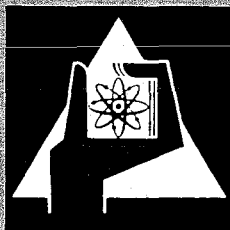
Juni 1971

KFK 1399

Institut für Angewandte Reaktorphysik
Projekt Schneller Brüter

Physics Investigations of Sodium-Cooled Fast Reactors
SNEAK-Assembly 2

F. Helm, G. Jourdan, S. Pilate, H. Reichel



GESELLSCHAFT FÜR KERNFORSCHUNG M. B. H.

KARLSRUHE

Als Manuskript vervielfältigt

Für diesen Bericht behalten wir uns alle Rechte vor

**GESELLSCHAFT FÜR KERNFORSCHUNG M. B. H.
KARLSRUHE**

KERNFORSCHUNGSZENTRUM KARLSRUHE

Juni 1971

KFK 1399

Institut für Angewandte Reaktorphysik
Projekt Schneller Brüter

Physics Investigations of Sodium-Cooled Fast Reactors

SNEAK-Assembly 2

Compiled by

F. Helm, G. Jourdan, S. Pilate¹⁾, H. Reichel²⁾

With contributions from

W. Bickel, L. Bindler¹⁾, R. Böhme, R. Buyl³⁾, B. Dorr, P. Engelmann,
E. Fischer, F.W.A. Habermann³⁾, P. Mc Grath, W.J. Oosterkamp, F. Plum,
J. Quenon¹⁾, A.M. Raberain³⁾, P. Voß²⁾, H. Walze, H. Wehmann²⁾, G. Wittek

1) Belgonucleaire

2) Interatom

3) Euratom

A b s t r a c t

SNEAK Assembly 2 was aimed at measuring physics parameters of a fast sodium cooled breeder core having a number of features typical for the prototype SNR. Particular attention was given to a close simulation of the radial geometry. The three modifications 2A, 2B, and 2C denote respectively a purely uranium fuelled core, a core with a 90 degree sector fuelled with SNEAK plutonium and a core where the 90 degree plutonium sector was extended to about 150 degrees using MASURCA fuel. In the latter configuration an extensive series of experiments with simulated control rods was performed.

The experimental results were compared to detailed calculations. In particular, the application of three dimensional synthesis calculations to the control rod experiments should be noted.

The work covered by this report was performed in close cooperation between the Gesellschaft für Kernforschung, the industrial consortium for the SNR, and the French MASURCA group at Cadarache.

7. Juni 1971

Zusammenfassung

Die Anordnung SNEAK-2 diente zur physikalischen Untersuchung eines schnellen natriumgekühlten Brüter-Cores, das wesentliche Züge des Prototyps SNR trug. Insbesondere wurde die radiale Geometrie des SNR so gut wie möglich angenähert. Die drei Modifikationen 2A, 2B und 2C bezeichnen ein Core mit reinem Uran-Brennstoff, ein Core mit einem 90 Grad-Plutonium-Sektor und ein Core, in dem der 90 Grad Sektor durch Verwendung von MASURCA Brennstoff auf etwa 150 Grad erweitert worden war. In der letzten Konfiguration wurde eine Reihe von Experimenten mit simulierten Kontrollstäben durchgeführt.

Die experimentellen Ergebnisse wurden mit detaillierten Berechnungen verglichen. Besonders sollte die Anwendung dreidimensionaler Synthese-Rechnungen bei der Auswertung der Kontrollstabexperimente erwähnt werden.

Die in diesem Bericht beschriebenen Untersuchungen wurden in enger Zusammenarbeit zwischen der Gesellschaft für Kernforschung, dem Industriekonsortium für den SNR und der französischen MASURCA-Gruppe in Cadarache durchgeführt.

Contents

	Page
1. Introduction	1
2. General Description of the Experimental Techniques	2
2.1 Reactivity Determinations	2
2.2 Determination of Material Worth	3
2.3 Fission Chamber Measurements	4
2.4 Foil Measurements	6
2.5 Activation of SNEAK-PuO ₂ UO ₂ Platelets	7
2.6 Sodium Void Measurements	8
3. General Description of the Calculation Methods	8
3.1 Methods of Current Use	8
3.2 Treatment of the Heterogeneity	9
3.3 Transport Methods	10
3.4 Synthesis Method	10
3.5 Other Methods	11
3.5.1 REMO-Correction	11
3.5.2 MONTE-CARLO Method	11
3.5.3 First Order Perturbation and REAC-Code	11
4. SNEAK-2A	12
4.1 Critical Experiment	12
4.2 Reaction Rate Traverses in the Core and Blanket	13
4.3 B ² -Determination	16
4.4 Material Worth Measurements	17
4.5 Sodium Void Traverse	17

	Page
5. SNEAK-2B	18
6. SNEAK-2C	20
6.1 Calculation of k_{eff} for SNEAK-2	21
6.2 Fission Rates in the Core	22
6.2.1 Measurements	22
6.2.2 Method of Calculation	23
6.2.3 Results and Discussion	23
6.3 Fission Rate Traverses with Storage Position	24
6.3.1 Measurements	24
6.3.2 Method of Calculation	25
6.3.3 Results and Discussion of Fission Rates	25
6.3.4 Results and Discussion of the Power Density Traverse	26
6.3.5 Possible Origins of the Discrepancies	26
6.4 Sodium Void	27
6.4.1 Experimental Technique	27
6.4.2 Methods of Calculation	27
6.4.3 Discussion of the Results	28
7. SNEAK-2C (Control Rod Experiments)	29
7.1 General Scope of the Control Rod Experiments in SNEAK-2C	29
7.1.1 Basic Considerations	29
7.1.2 Simulation of Control Rods in SNEAK	30
7.1.3 Description of the Rod Experiments	31
7.2 Reactivity Changes with a Single Control Rod	33
7.2.1 Experiments performed	33
7.2.2 Method of Calculations	33

	Page	
7.2.3	Meaning of Comparisons	34
7.2.4	Conversion of the Experimental Results to Δk	35
7.2.5	Diffusion Theory Results	35
7.2.6	Discussion of the Diffusion Theory Results	36
7.2.7	Effect of using MOXTOT instead of NAP	37
7.2.8	Effect of Computational Approximations	37
7.2.9	Transport Corrections	38
7.2.10	Reactivity of a Central Void	38
7.3	Reactivity Changes with three Control Rods	39
7.3.1	Experiment performed	39
7.3.2	Diffusion Results	40
7.3.3	Discussion of the Diffusion Theory Results	40
7.3.4	Characteristics Curve of a B_4C Rod	41
7.4	Traverses with a Single Rod	41
7.4.1	Measurements performed	41
7.4.2	Method of Calculation	42
7.4.3	Fission Rates, Diffusion Theory Results	42
7.4.4	Power Density, Diffusion Theory Results	43
7.4.5	Discussion of the Diffusion Theory Results	44
7.4.6	Effect of using MOXTOT instead of NAP	45
7.4.7	Transport Correction	45
7.4.8	Traverse measured in a Central Void in the Core	46
7.5	Traverses with three Control Rods	46
7.5.1	Measurements performed	46
7.5.2	Results from Fission Rates and Power Density	47
7.5.3	Discussion of the Diffusion Theory Results	47
7.6	Sodium Void with Control Rods	48

	Page
7.6.1 Method of Calculation	48
7.6.2 Discussion of the Results	48
8. Direct Application to the SNR Design	49
8.1 k_{eff}	49
8.2 Power Distribution	50
8.3 Control Rod Worths	51
8.4 Sodium Void	52
8.5 Conclusions	53

1. Introduction

In the series of assemblies SNEAK-2-SNR the properties of a sodium-cooled fast core with two enrichment zones were investigated. Uranium and plutonium fuel was used. Geometry and composition showed the main characteristics of the SNR - an exact simulation of the SNR was not attempted as the task of the assemblies consisted in testing calculational methods rather than directly predicting the neutronic data of the prototype.

Design and evaluation of the experiments were performed in close cooperation between the Institute of Angewandte Reaktorphysik of the Kernforschungszentrum Karlsruhe and the industrial consortium for the construction of the SNR.

The experimental program concentrated on the measurements of most interest at the present design status of the SNR - such as power distributions and the reactivity worth of control rods.

The measurements were performed in part as a common experiment with French scientists of the fast critical facility MASURCA. For several months about 90 kg of plutonium from MASURCA was used in SNEAK. Since MASURCA materials are in the form of rodlets while SNEAK is using platelets some effort had to be part into adapting the compositions. Finally the cells built of SNEAK platelets could be arranged in such a way that the integral composition of the unit cells formed with MASURCA rodlets were well matched.

The program was subdivided into three assemblies which are shortly described in the following:

SNEAK-2A was a cylindrical core fuelled with uranium only. The enrichment ratio of the outer and inner zone was about 4:3.

After some basic measurements (critical data, reaction rates, material worths, spectra) a 90 degree plutonium fuelled sector was introduced

as an substitution experiment (SNEAK-2B). The evaluation of this experiment made possible an extrapolation to the critical size of a pure plutonium core.

Finally in order to reduce the spectral transients in the plutonium sector it was surrounded by an about 15 cm thick buffer zone using MASURCA plutonium as a fuel. In this configuration (SNEAK-2C) power traverses and sodium void traverses were measured along the sector axis and finally an extended experimental program about control rods, (their reactivity, their material shadowing and their influence on the surroundings) was conducted.

The experimental work on SNEAK-2-SNR started in May 1969 and was completed in November of the same year.

2. General Description of the Experimental Techniques

2.1 Reactivity Determinations

In the course of SNEAK-2 experiments reactivities and changes of reactivity were measured. During the investigations of simulated SNR control rods, the changes of configurations were performed in steps small enough to allow a measurement of the associated reactivity change by calibrated SNEAK shim rods. In between steps the accumulated negative reactivity was compensated by adding core elements at the edge. Recalibrations of shim rods were performed often during the experiments. The calibrations of the SNEAK shim rods were performed by driving them into or out of the core. Rod position and chamber current from three BF_3 ionization chambers in the radial blanket were measured. From this record the reactivity characteristic of the rod was calculated by solving the inverse kinetic equations on the DDP 124 computer.

The variation in the flux was measured in one of the existing linear channels. Because of the neutron flux caused by spontaneous fission of

plutonium and (α, n) effects in the oxygen, reactivities were compared at a fixed power level in a state slightly subcritical by about 1.8 cents.

The reactivity measurements are estimated to be accurate within 5%. The experimental uncertainty is associated with the following points:

An effect of the simulated SNR control rod to be measured on the calibrated SNEAK shim rod used in the measurement. In order to minimize this error, the SNEAK shim rods are recalibrated several times during the measurements and after each large core reloading. Also the shim rod used is always located far from the rod to be measured.

An effect of the position of the ionization chamber located at the outside of the core on the flux signal obtained during the rod calibration.

A source of possible systematic error lies in the β_{eff} value used for converting ρ into Δk . To a minor extent the result of the shim rod calibration (solution of the inverse kinetic equations) is also influenced by the assumed value of β_{eff} . This value is extracted from a calculation and it is known that such calculations may give values in error of a few % for an uranium core and 5 to 10% for a plutonium core.

2 Determination of Material Worths

In SNEAK-2A, determinations of the reactivity worths were made for a number fuel isotope samples (U^{235} , U^{238} , Pu^{239} , Pu^{240}), sodium, and some other materials (Fe, Al, B^{10} , Ta).

The measurements were made using a pile oscillator element which was connected to the piston of a driving mechanism driven by compressed air. The element consisted of a square tube $47 \times 47 \text{ mm}^2$ with 1 mm wall thickness⁺⁾.

^{+) moving in a guide tube of the same wall thickness.}

The oscillator stroke of 80 cm served to move the sample from the center of the core to a position outside the blanket. The amount of time for this movement was 3 seconds. The time the sample stayed in the core was generally 20 seconds. One oscillates a cell containing a sample against a normal cell. The pile oscillator element was filled with core material in such a way that the regular lattice was nearly undisturbed in both end positions of the oscillator. Thus the sample was actually inserted into the regular lattice.

The reactivity worths were determined from the flux signals by solving the inverse kinetic equations on the DDP 124 computer. The results were corrected for linear reactivity drift. The influences of the sample container and of the guide tube were determined experimentally and eliminated.

The experimental technique and the calculation method are described in detail in /1/. The experimental uncertainties are mainly caused by statistics and non linear drift effects (around 5% for the fissionable isotopes, 1% for the absorbers).

2.3 Fission Chamber Measurements

Radial and axial reaction rate distributions were measured with fission chambers. The radial measurements were made through the core and the blanket up to the fuel element storage position, the axial measurements were made only within the core.

The fission chambers used were of the type FC4 (20th Century Electronics) such of a type developed in Cadarache. The type FC4 (U^{235} , U^{238} , Pu^{239} , Np^{237}) had a diameter of 6.35 mm. The chambers developed in Cadarache had a diameter of 8 mm and were designated as 552 C (U^{235}), 871 C (U^{238}), 961 C (Pu^{239}), 772 C (Np^{237}). In addition to the main isotope the chamber deposits contained the impurities given in Table 6.

The radial fission rate measurements were made with FC4 chambers at the core midplane in the horizontal channel $Y = 19$. The fission chambers were

moved from north to south. The dimensions of the horizontal channel were 9.45 mm (height) by 11.0 mm (width). It consisted of core and reflector elements with installed windows (see Fig. 2 and 13).

In order to guarantee an undisturbed movement of the chambers, a steel tube with an outer diameter of 8.0 mm and a thickness of 0.5 mm was used to guide the chambers. The chambers were connected to a coaxial-cable.

The experimental apparatus consisted of fission chamber, preamplifier, amplifier with discriminator, interface electronics and the DDP 124 computer. The experiment was run completely automatically. The power level was regulated in such a way, that in the core center about 5000 counts/s were measured. This was achieved within the range of 100 W to 500 W.

The statistical error of the measurements was 0.7% in the core. From the outer edge of the core up to the fuel element storage position the statistical error was less than 2.5% for the U^{235} and the Pu^{239} chambers and less than 5.5% for the U^{238} chamber.

Measurements for the axial reaction rate distributions were made at different core positions with a special element loaded with platelets which are bored through resulting in a vertical channel within the element. To permit an undisturbed movement of the chambers a steel tube with a diameter of 10 mm and a wall thickness of 0.5 mm was introduced. Because the diameter of the axial channel was larger than that of the radial channel, the 8 mm chambers developed in Cadarache were used. These chambers had a thicker deposit of fissionable material and gave a higher counting rate.

The measurements were corrected for the effect of the dead time (around 3.5 μ sec.) The measurements were not corrected for chamber impurities. It was estimated by using calculated reaction rates, that this correction is always negligible for U^{235} and Pu^{239} chambers (<0.1%). For U^{238} chambers the effect is small (<0.3%) in the core but it increase in the blanket with distance from the core boundary. It is 0.7% at the core boundary and 4% at a distance of 16 cm.

2.4 Foil Measurements

Fission rates were measured from irradiated pairs of pure uranium metal foils of depleted (0.44 w/o U^{235}) and enriched (20.04 w/o U^{235}) uranium. The two foils of different enrichment were enveloped in 10 μ m thick aluminium foils. The integral γ activity of the fission products above 660 keV was counted as a measure for the amount of fissions during irradiation.

The U^{238} capture rate was determined by the γ -X-ray coincidence method in the 106 keV range and calibrated with an Am^{243} sample /2/.

All foils were calibrated with foils irradiated inside absolutely calibrated parallel plate fission chambers. The accuracy of this method is about 2% /3/.

In the core of SNEAK-2A, axial traverses in the element 18/19 and radial traverses in direction west-east were made from foil measurements which were taken up to the blanket. Uranium foils with a diameter of 25.4 mm and a thickness of 0.1 mm were used. The foils were activated for 2 hours at a reactor power of 250 W.

In the core of SNEAK-2C azimuthal traverses were measured with inserted simulated SNR absorbers in the Z2 zone (see chapter 7). For these measurements foils with a diameter of 9.5 mm and a thickness of 0.1 mm were used.

The measurements of the azimuthal traverses were made with absorbers inserted in the following positions:

Na follower in position 1

B_4C in position 1, Na B_4C (half inserted) in the positions 1, 2, 3

B_4C (full inserted) in the positions 1, 2, 3.

In order to cross-check the results with fission chamber measurements one foil was located in the element 18/19 at the core center. The radial traverses also went through the core center.

The axial traverses were measured at the position 26/18 from 5 mm under the core midplane to either 16 cm or 22.5 cm above the core midplane.

2.5 Activation of SNEAK-PuO₂UO₂ Platelets

Since no channel existed for measurement of azimuthal fission rate traverses, foils and PuO₂UO₂ platelets were used instead of chambers.

By γ -counting the fission products in the activated PuO₂UO₂ platelets above 1.17 MeV the total fission rate distribution which corresponds to the power distribution was determined. In order to absorb the low energy γ -radiation a lead shield of 9 mm thickness and a collimator were used. To minimize the background interference the NaI detector with the collimator were placed in a leadwalled container with a wall thickness of 10 cm.

Because several points per platelet were measured the distribution of the γ -background over one platelet had to be determined. The decline in the count rates near the edge was also taken into consideration. This decline is caused by the design of the counting device and the different neutron flux in the centre and at the edge of one element.

The platelets were used both for the measurement along the azimuthal traverses in increasing distance from a simulated SNR absorber and for measurement along axial traverses.

In addition the activation of platelets was determined in the core center and at a position in the Z1 zone near the zone boundary in order to provide a cross-check with the fission chamber traverses.

The accuracy of the technique is estimated to be 1.5%. This includes a 0.7% statistical error associated with the γ -count rate, a 0.4% error associated with the calibration of the discriminator, and a 0.4% uncertainty in the fuel content of the platelets.

2.6 Sodium Void Measurements

For the measurement of Na void traverses Na platelets were substituted by empty steel cans in different core zones. The reactivity changes for different configurations were measured with calibrated shim rods.

Axial and radial traverse measurements were performed. For the axial traverses sodium was removed in 4 central elements in regions of increasing height starting from the core center plane. The radial traverse was measured along the central axis of the Pu-sector. In the first step 3 cells of the 4 central elements were voided. After that, the voided zone was displaced in steps of one element width radially outward. This procedure was performed up to the boundary of the breeder blanket. In the breeder blanket itself only one measurement was made.

As the unit cells in the various zones contained different numbers of Na-platelets the number of cells voided per element was 3 (= 15 Na-platelets) in Z1, 5 (= 15 Na-platelets) in Z2 and 7 (= 14 Na-platelets) in the breeder blanket. Thus the number of Na-platelets in the void zone remained more or less constant throughout the radial traverse.

A radial traverse of the Na-void coefficient was also measured while three simulated SNR absorbers were inserted. The absorbers were placed at the boundary of the two zones of enrichment at different distances from each other. The traverses contained three measuring points between the absorber positions and core center and two points outward from the absorber positions.

3. General Description of the Calculation Methods

3.1 Methods of Current Use

The evaluations were primarily performed with multigroup diffusion theory.

All the calculations were made with the 26-group KFK-NAP-PMB cross-section set /4/. Some of the calculations were repeated using the MOXTOT set /5/, which mainly differs from the NAP-PMB set by lower U^{238} capture cross-sections.

The one-dimensional diffusion programs utilized were the 6731 code of the NUSYS system at Karlsruhe, HEIDI at Interatom and PANOPLIE at Belgonucleaire. The two-dimensional programs were, respectively, DIXY (Karlsruhe), MUGDI (Interatom) and SQUID (Belgonucleaire).

Some of the two-dimension diffusion calculations were performed in 26 groups. These were for k_{eff} corresponding to the critical reactors (RZ model) and for the calculation of a correction for cylindrisation. However most of them, and particularly the control rod calculations (Chapter 7), were made using 4-group condensed cross-sections. The latter were obtained by means of one-dimensional weighting spectra calculated for each zone. The deviations due to the approximation of the condensation were minimized by an adequate choice of the few-group scheme and by finely subdividing the zones of the reactor /6/.

The transverse buckling values used in the one-dimensional or two-dimensional (XY) calculations were constant, space- and energy- independent values, except for the case of material reactivity worth calculations. The space- and energy- dependent bucklings were extracted from previous one-dimensional calculations in the transverse direction, or two-dimensional calculations in RZ geometry. Such procedures on the B^2 were found to be satisfactory from checks with more elaborate geometrical models (two-dimensions, RZ or three-dimensions, see also § 3.4).

3.2 Treatment of the Heterogeneity

The fine structure of the neutron flux and reaction rates within the SNEAK cell, consisting of a stack of thin platelets, was calculated by the cell program ZERA of Karlsruhe /7/. This program is based on the collision probability method.

ZERA also generates heterogeneity corrected cell averaged cross-sections which are introduced into one-dimensional diffusion models, for the calculations of the heterogeneity corrections on k_{eff} and reaction rate traverses.

3.3 Transport Methods

The one-dimensional S_N transport programs DTK of GfK, MUSN of Interatom and DTF-IV of Belgonucleaire have been used to determine the transport corrections on k_{eff} and on reaction rate traverses.

The correction on k_{eff} was obtained by adding the axial and radial corrections. The axial correction resulted from an appropriate weighting of the axial corrections associated with each of the radial zones.

The order of the transport approximation was generally chosen to be S_4 ; in some criticality calculations the orders 6 and 8 were also used. No appreciable gain was found when passing from order 6 to order 8. Order 4 calculations give 90% of the transport correction obtained with order 6.

Some two-dimensional (RZ) transport calculations were performed by Belgonucleaire using the DOT code /8/; they were applied to the calculation of reactivity changes due to central control rods and reaction rate distributions around them (see Chapter 7).

It must be noted that the one-dimensional transport programs use transport cross-sections weighted by the current while the DOT program uses flux weighted values.

These two-dimensional calculations used 4-group cross-sections, condensed with weighting spectra obtained by one-dimensional DTF-IV.

3.4 Synthesis Method

The computer program KASY of GfK /9/ builds three-dimensional fluxes by a linear combination of the form:

$$\phi (XYZ) = \sum_k Z_k (Z) \cdot H_k (XY),$$

where the two-dimensional trial functions H_k are used as input data, and the one-dimensional mixing functions Z_k are calculated by the code on the basis of a variational principle. In addition, the code also calculates k_{eff} .

This program was used in the evaluation of the control rod experiments (see Chapter 7). The trial functions were the fluxes calculated by DIXY in the (XY) geometry for the different axial slices of the reactor. The synthesis was performed along the axial direction Z.

The validity of the synthesis approximation had been tested successfully, with respect to direct three-dimensional results obtained with a Belgo-nucleaire version of the program TRITON /10/. A separate report /11/ is devoted to the use of the synthesis method and to the tests performed. Its general conclusion is that, for the problems considered, the accuracy requirements are fulfilled by the synthesis technique.

3.5 Other Methods

3.5.1 The REMO correction /4/, developed at Karlsruhe, was applied to the criticality calculations. This correction consists of improving the 26-group elastic removal cross-sections by weighting the data of the nuclear data file KEDAK with the collision density spectra calculated in each particular zone of the reactor.

3.5.2 The Monte-Carlo program MOCA /12/ of Interatom was applied to criticality calculations. In order not to exceed large computer times the k_{eff} was calculated only within 0.5%. The result was regarded only as a goodness check.

3.5.3 The reactivity worths were calculated by 1st order perturbation theory applied to one-dimensional diffusion calculations (FOP)

and by the code REAC /1/ which is based on collision probability theory. With the latter code it is possible to take into account the heterogeneity of the sample and the lattice.

4. SNEAK-2A

The figures 1a and 1b show a vertical and a horizontal section through the critical core configuration of SNEAK-2A-SNR together with the critical dimensions which were used in the calculations. The core zone R2 has been subdivided in two concentric parts, named R2' and R2'', because the elements of the zone R2'' are made of slightly modified cells. Fig.2a-d show the structure of the unit cells used in each zone and the rest cells used at the upper and lower core boundary.

Fig.3a-c show the structure of the cells of the shim- and safety-rods. Table 1a gives the compositions of each reactor zone. Two types of compositions are shown: The first one is the composition for the k_{eff} -calculations; it includes contributions of the SNEAK shim rods and of the rest cells. The second type was used in the calculation of the reaction rates, it corresponds to the composition of the pure unit cells.

In considering the analysis, it must be taken into account that an increased hydrogen content was found in the Na_2CO_3 platelets used in SNEAK-2A only after the experiments were completed. By a later analysis the average H-content of these platelets was determined and the k_{eff} -calculations could be properly corrected. However it was not possible to calculate accurate corrections for local parameters such as spectrum, material worth and reaction rates since one could not determine the H-content of the individual Na_2CO_3 platelets in the vicinity.

4.1 Critical Experiment

a) Result of the experiment

The measured k_{eff} with inserted shim rods and control rods was:

$$k_{\text{eff}} \text{ (experimental)} = 1.0000$$

b) Methods and results of the k_{eff} calculations

The calculations for the critical experiment were done with the methods which are described in more detail in Chapter 2. The basic calculation was a two-dimensional homogeneous diffusion calculation with four groups in RZ geometry. The condensation scheme used is given in Table 7. The calculations for the condensation spectra, the heterogeneity, REMO and transport correction were done in one-dimensional geometry with 26-groups. A correction for cylindrisation was found by comparing 1D cylindrical with 2D XY diffusion calculations. The average mesh size was 1 cm for the 1D calculations and 2 cm for the 2D calculations. The cross-section set NAPPMB was used for all these calculations. Some calculations were repeated with the MOXTOT set.

Table 8 gives the results of the homogeneous diffusion calculations. Table 9 gives the results of the heterogeneity, REMO and transport correction for both cross-section sets. In all these results the changed content of hydrogen in the Na_2CO_3 platelets was not considered. Table 10 gives the results of the calculations with the new compositions (Table 1b) which considered the higher averaged content of hydrogen.

One observes that the NAP set produces a slight underestimate in k_{eff} while with the MOXTOT set one obtains a significant overestimate.

4.2 Reaction Rate Traverses in the Core and Blanket

In the uranium core SNEAK-2A-SNR fission traverses were measured with U^{235} and U^{238} chambers (Typ FC4) and with foils, capture traverses

R1 zone: Generally the effect is very small (<0.5%) in all traverses.

R2 zone: The effect depends on the reaction rates considered.
It is
for U²³⁵ fission < + 1%
for U²³⁸ fission < + 4.5%

In the axial direction it is

in the core for U²³⁵ < 2.5%
for U²³⁸ < 6%

in the blanket (increasing with distance from the core boundary)
for U²³⁵ up to 10.5%
for U²³⁸ up to 12.5%

In addition to these corrections the influence of the cross-section set on the traverses was checked. In the core a very small difference was found between NAP- and MOXTOT-set. (<0.6%) At the core blanket boundary the difference is ~ 3% for all traverses.

Fig. 4 to 6 give the results of the measurements and the calculations for the different axial reaction rate traverses. The comparison of the measured and calculated curves, and of the chamber and foil measurements, show a good agreement in all cases in the core. Fig. 7 gives the curves of the measured and calculated axial power distribution. The radial traverses are shown in Fig. 8 to 11. Here too, the agreement between calculated and measured data, and between chamber and foil measurements is good. The influence of the higher content of hydrogen in the compositions has been calculated and was found very small (<0.5% in the core and <1% at the boundary).

Foil measurements in the radial blanket zone were performed in two locations only. Therefore an evaluation of this experiment was not considered to be meaningful.

4.3 B_m^2 Determination

The material buckling B_m^2 of the central zone R1 in SNEAK-2A has been determined on the basis of the measured fission rate traverses.

The principle of the method, developed in Cadarache, and detailed in /13/, is briefly the following.

Fission rate traverses are measured for a number of different fission chambers (generally U^{235} , U^{238} , Pu^{239} , and Np^{237}). Due to the different spectral sensitivities of the chambers the measured traverses will not be the same.

An idealized detector which would filter out the transients and therefore yield the correct traverse for a buckling measurement must have a spectral sensitivity proportional to the product of the diffusion coefficient with the adjoint flux $D\phi^+$.

In the order to arrive at a semi experimental result for such an idealized detector one calculates the traverses for an idealized $D\phi^+$ detectors and for the actual chamber isotopes by multigroup calculations. It is then possible to find an "experimental" $D\phi^+$ traverse which correlates to the calculated $D\phi^+$ traverse in the same way as measured and calculated traverses correlate for the isotopes in the chamber. From this $D\phi^+$ traverse the value of B_m^2 is derived.

The application of this principle to SNEAK-2A gives the following results /14/.

$$B_m^2 = 1.620 \pm .003 \cdot 10^{-3} \text{ cm}^{-2}$$

This "experimental" value is to be compared with the following results of calculations.

cross-section set:	homogeneous	heterogeneous	REMO correction	het.+REMO
NAP-PMB	1.533	1.548	+ .005	1.553
MOXTOT	1.727	1.735	+ .003	1.732
SETR 25/21 Cadarache	-	-	-	1.592

The prediction of the B_m^2 by calculation is to be compared with the prediction of the k_{eff} for the SNEAK-2A core (see part 4.1). This comparison is coherent. One finds again a slight underestimate (of B_m^2 , therefore k_{∞} , and

of k_{eff}) with NAP, and a rather significant overestimate with MOXTOT. The french set SETR 25 gives a very good prediction as well for the B^2 of R1, as for the k_{eff} of SNEAK-2A (0.995, including heterogeneity and transport corrections) /15/.

4.4 Material Worth Measurements

The material worth measurements were performed with the pile oscillator. The calculated results were obtained with the following methods:

- 1) one-dimensional perturbation theory and homogeneous cross sections in 26 groups
- 2) the code REAC which takes into account the heterogeneity of the probe and the surrounding medium
- 3) two-dimensional perturbation theory and homogeneous cross sections in 15 groups.

Table 11 gives the results from the different methods and for both cross-section sets used. The MOXTOT set was used only in the 2D calculations.

The influence of the changed hydrogen content, shown in Table 12, was checked with both sets. The increased hydrogen content used in these calculations corresponded to the average H-content of all Na_2CO_3 platelets.

Since it is possible that the hydrogen content of the platelets in the vicinity of the samples was deviating considerably from the average an interpretation of the measurements is quite difficult. Even if some trends may be deduced from the measured values definite conclusions can certainly not be reached.

4.5 Sodium Void Traverse

In the axial direction the local sodium void effect was measured with the pile oscillator. One sodium platelet was exchanged with an empty can.

The effect was calculated with two-dimensional perturbation theory in 15 energy-groups. Both cross-section sets were used. Fig. 12 shows the measured and calculated effect.

Here too the uncertain hydrogen content of the surrounding Na_2CO_3 platelets prohibits any definite conclusion. It may e.g. be responsible for the strong deviation of the point in core center from the rest of the traverse which appears to agree quite satisfactorily with the calculations.

5. SNEAK-2B

The transition from SNEAK-2A to SNEAK-2B consisted in substituting elements with SNEAK plutonium fuel for uranium fuelled elements in a small central zone and a 90° sector of the core. The site of the substituted zone was limited by the supply of SNEAK plutonium platelets. Fig. 13a-b show the unit cells used in the plutonium zones.

The substitution experiment had the purpose of

- a) studying the effect of boundary surfaces between uranium and plutonium fuelled zones and
- b) estimating the size of a pure plutonium core.

It consisted of eight steps: (Fig. 14 - 16)

- | | |
|---------------|--|
| Step 1: | Insertion of the central block of 16 Pu-elements. |
| Step 2 - 6: | Insertion of 5 diagonal rows of Pu-elements. |
| Step 7 and 8: | Insertion of two $\frac{1}{8}$ sectors yielding the 90° degree sector of the final configuration. |

The reactivities measured during the experiment are given in Table 13.

Steps number 2-6 (the diagonal rows) had the purpose to approximately determine the reactivity effect of the zone boundary and to show the decrease of its contribution to the individual steps as the thickness of the plutonium zone increases. This is illustrated in Fig. 17. For the

first substitution steps the reactivity effect per diagonal row is considerably larger than for the last ones where it finally becomes independent of the total size of the substituted zone. This is due to the fact that with the insertion of the first few rows of Pu-elements the reactivity effect of the U-Pu zone boundary is being built up. Its size may be found from the ordinate intersection of the asymptotic straight line in the diagram (Fig. 17).

Since asymptotic behaviour was not established completely only an estimate of the boundary effect could be made with yields a value of $4 \cdot 10^{-4}$ in $\frac{\Delta k}{k}$.

Steps No. 7 and 8, each consisting of introducing a $\frac{1}{8}$ Pu sector, again give a value for the boundary effect but also allow an extrapolation to the reactivity of a purely plutonium fuelled core.

The boundary effect is found from the difference of the reactivities added by the two steps (step 7 is to be taken with respect to the configuration after step 1). It is included in step 7 which builds up zone boundaries but not in step 8. Its value is found to be $3.5 \cdot 10^{-4}$ in reasonable agreement with the result from the diagonal row substitutions.

The critical size of an extrapolated plutonium fuelled core was found under the assumption that the effect of step 1 plus the eightfold effect of step 8 represents approximately the reactivity difference between the pure uranium and the pure plutonium core. This difference was found to be +0.8%. With a calculated $\frac{\Delta r}{\Delta k} = 1.6 \frac{\text{cm}}{\% \Delta k}$ the extrapolated plutonium core has a radius 1.3 cm smaller than that of SNEAK-2A. Its geometry is therefore given by the following data:

radius of the Z_1 zone 45.11 cm
radius of the Z_2 zone 65.17 cm
thickness of the radial blanket 30.0 cm
thickness of the axial blanket 30.5 cm

For this extrapolated core k_{eff} calculations were performed using the compositions given in Table 2. The calculational methods were the same as

described above. The results are given in Table 14. The 2D diffusion calculations were performed with the MOXTOT set. In addition 1D diffusion calculations were performed with both the MOXTOT- and NAPPMB-sets for a comparison of the results. One observes that in this case of a plutonium fuelled core both sets give very similar results. For either set the reactor is calculated slightly subcritical.

6. SNEAK-2C

By enlarging the Pu sector of SNEAK-2B with a buffer zone the next assembly, SNEAK-2C, was built. The material of this buffer zone was MASURCA material in the form of rodlets. The arrangement of the SNEAK platelets cells had been chosen in such a way that the compositions of both zones were very similar. Table 3a gives the compositions originally used for the two MASURCA-Pu-zones. The composition of the Z1 zone had to be modified later, because there was an error in the data of the depleted uranium rodlets. Table 3b gives the modified composition. Most of the calculations were done with the uncorrected compositions. The influence of the correction was estimated later by a few calculations to be small.

Fig. 18 shows the cells of the Z1 and Z2 MASURCA zone. Fig. 19 shows the cross-section of SNEAK-2C

In this assembly the following measurements were performed

- 1) Criticality (Chapter 6.1)
- 2) Reaction rate traverses through core blanket, and a simulated fuel element storage position in the radial direction (see Chapter 6.3)
- 3) Sodium void traverses with and without control rods (see Chapter 6.4 and 7.6)
- 4) Control rod experiments: reactivity changes and reaction rate traverses (see Chapter 7).

6.1 Calculation of k_{eff} for SNEAK-2C

Because of the complicated sector geometry of SNEAK-2C it becomes very difficult to perform exact criticality calculations with one or two dimensional programs. The following types of reference calculations were used

1) 4 group 2D-RZ diffusion calculations

These calculations can be applied only when SNEAK-2C is split in two halves each of which can be approximated by cylindrical geometry. The mean value of the multiplication constant for the two systems then is used as the reference value of k_{eff} .

For this type of calculations the right and left side of SNEAK-2C (Fig. 19) are each considered as one half of a system with cylindrical symmetry. The following subdivision into zones is used

Right side		Left side	
Zone	Radius (cm)	Zone	Radius (cm)
Z1 (SNEAK Pu)	45.6	Z1 (SNEAK Pu)	12.3
Z2 (SNEAK Pu)	66.0	Z2 (MASURCA Pu)	28.8
blanket	96.5	R1 (uranium)	45.1
		R2 (uranium)	66.5
		blanket	96.5

2) 4 group 2D-XY diffusion calculations

Here the main uncertainty is caused by the transverse bucklings which have to be introduced. They were derived as region and group-dependent buckling from RZ-calculations.

All calculations were performed with the NAP - PMB set. A comparison NAP - PMB - MOXTOT was made by one-dimensional diffusion calculations.

The effect of group condensation was also estimated by comparing 1D calculation with 26 and 4 groups.

Transport corrections were found by S_4 -calculations with the one-dimensional transport code MUSN.

A correction for cylindrisation was applied to the 2D RZ calculations by adding the difference between an XY and a 1D cylindrical calculation. The results of the calculations show Table 15.

Corrections for heterogeneity and averaging errors in the group cross-sections (REMO) were not applied. Their order of magnitude can be estimated from calculations for SNEAK-2A and 2B to be about +0.5%.

The one-dimensional results with the MOXTOT set gave a k_{eff} which was 1.7% higher than the NAPPMB result. Therefore the MOXTOT result corresponding to the values derived above for NAPPMB would be $k_{eff} = 1.007$.

Calculations with the Monte Carlo Code MOCA (NAPPMB set) in which 60 neutrons were followed through 170 generations gave an average multiplication factor of 0.985 ± 0.003 .

2D XY diffusion calculations (4 group, NAPPMB set) also were used as a basis for three-dimensional XY/Z calculation with the synthesis code KASY. No significant deviations were found from the results given in Table 15.

A comparison of the criticality calculations for SNEAK-2A, SNEAK-2B (extrapolated) and SNEAK-2C shows their results are quite compatible.

6.2 Fission Rates in the Core

6.2.1 Measurements

Radial fission rate traverses of the isotopes U^{235} , U^{238} , Pu^{239} were measured in the two zones of the core which was surrounded by a blanket of depleted uranium as shown in Fig. 19. The measured values had

a statistical accuracy of 0.7%. They were corrected for dead time losses.

6.2.2 Method of Calculation

The fission rate traverses were calculated using diffusion theory in XY geometry with NAP-PMB group constants condensed to 4 groups. The effect of condensation was estimated by one-dimensional calculations the transport effect by one- and two-dimensional calculations (S_4). A correction of the cross-sections with regard to the heterogeneity of the cells was not performed.

The axial leakage was taken into account by means of space and energy dependent bucklings which were taken from a RZ calculation.

The power density was derived from the measurements by using the following calculated spectral indices:

$$\sigma_{f9}/\sigma_{f5} = 0.961, \sigma_{f8}/\sigma_{f5} = 0.0295$$

The contributions of the isotopes to the power density were the following

	in Z1	in Z2
U ²³⁵	3.0 %	2.0 %
U ²³⁸	11.9 %	8.5 %
Pu ²³⁹	82.5 %	86.7 %
Pu ^{240, 241, 242}	2.6 %	2.8 %

6.2.3 Results and Discussion

Fig. 20 shows the fission rates obtained by diffusion calculations corrected for condensation and transport effects. The first correction is smaller

than 1% within the whole core for all isotopes, whereas the latter reaches 2% in the case of U^{238} in the outer zone and stays below 1% for U^{235} and Pu^{239} .

The comparison of the calculated and measured rates, which are both normalized to unity in the center shows a maximum overestimation of 2.9% and 1.6% for U^{235} and Pu^{239} respectively. The traverse of U^{238} is estimated too low by less than 1%. In particular the transition between the two zones is well reproduced.

The deviations in the power distribution which here also was normalized to unity in the core center are mainly due to the Pu^{239} contribution. They are somewhat reduced by the underestimation of the U^{238} contribution. The relative deviation of the experimental and calculated power density traverses is given for some points in Table 22. The larger values found are about 1.5%.

6.3 Fission Rate Traverses with Storage Position

6.3.1 Measurements

The experimental arrangement is shown in Fig. 21. The fission rates were measured in order to get a quantitative information about the power level of the fuel elements in the storage position. The elements are surrounded and separated from the core by a zone of aluminium or steel (exact compositions see Table 4), the first of which is supposed to simulate the sodium-reflector of the SNR while the configuration with steel simulates the conditions in PHENIX. The storage position was filled either with 4 fuel elements of type R2 or with the surrounding material.

Since the storage position has practically no influence on the two core-zones and the inner part of the blanket, the results of the four fission rate measurements (taken with steel and Al with fuel elements or not) were averaged for these zones.

6.3.2 Method of Calculation

The methods of calculation are described in chapter 6.2.2. As in this section, the corrections for transport- and condensation effects were obtained with one-dimensional calculations. Therefore they are not correct in the neighbourhood of the filled storage position which cannot be described in one-dimensional geometry.

Because it is difficult to determine the radial dependence of the axial bucklings, the calculation of the flux was performed with different bucklings for the outer regions of the arrangement:

- 1) B_z^2 values for all regions taken from a RZ calculation,
- 2) $B_z^2 = 0$ for the storage position, all others unchanged,
- 3) $B_z^2 = 0$ for blanket and storage position, the rest unchanged.

Only the results corresponding to the first assumption will be compared in detail with measurements. The effect of taking the second or third assumption instead of the first one will be described briefly.

6.3.3 Results and Discussion of Fission Rates

Fig. 22 shows as an example the calculated and measured fission rates of the isotopes U^{235} , U^{238} and Pu^{239} for the case of the filled storage position surrounded by Al. The theoretical values represent diffusion calculations with 4 groups, corrected for transport and condensation effects. B_z^2 values of all regions were taken from a RZ calculation.

As in 6.2.3 the agreement within the core was quite good. In the breeder blanket an underestimate of about 50% for all three rates is to be noticed. This underestimate is increasing with the distance from the core, so that the measured rates are three times larger than the calculated ones in the storage position.

Table 16 gives relative deviations of calculated and measured fission rates at different points for the four cases (with or without RZ elements, surrounded by aluminium or steel).

The discrepancies are similar in all four cases. They are somewhat smaller in case of steel, which means that the coupling of core and storage position is better reproduced for steel than for aluminum.

6.3.4 Results and Discussion of the Power Density Traverse

Fig. 23 shows the calculated power density traverse for the case of R2 elements in the Al storage position. The fission rates discussed in chapter 6.3.3 were combined using the spectral indices for the core center which were given in 6.2.2. The same indices were used for the combination of the experimental fission traverses in order to get an experimental power density traverse. This is also given in Fig. 23. Both traverses are normalized to unity in the center. The relative deviations for the outer regions are numerically given in Table 22.

The inner part of the core (up to $R = 60$ cm) shows agreement of both power density traverses within 1%. The deviations increase in the breeder blanket in the outer part of which they reach nearly 50% (35%) for aluminum (steel). The calculated power densities in the storage position surrounded by aluminum or steel are smaller by about 65% and 34%, respectively, than the experimental ones.

6.3.5 Possible Origins of the Discrepancies

Two points arising from experimental uncertainties have to be considered. The first is the streaming-effect in the radial channel, which increases the flux at larger distances from the core. Another uncertainty of the experimental results is due to the empty aluminum matrix which surrounds the whole arrangement.

The most important methodical uncertainty arises from the choice of axial bucklings. The fission rate traverses taken for comparison were calculated with the bucklings of a RZ calculation. They are somewhat questionable because of the special geometry of the storage position. When taking an axial leakage of zero for the storage position and the surrounding material, the fission rates are increased by 8% in the outer part of the blanket and by 15% in the storage position. In the extreme case of $B_z^2 = 0$ in all zones, except the two core zones, the fission rate traverses are increased by factors of up to 1.8 and 3 in the blanket and storage position, respectively.

6.4 Sodium Void

In safety considerations for the SNR the sodium void effect represents an important factor. Therefore axial and radial sodium void traverse measurements were performed in SNEAK-2C. Comparison of experimental and theoretical results should give information on the reliability of predictions for this effect.

6.4.1 Experimental Technique

A general description of the experimental technique was given in 2.6. In addition to that it should be noted, that these experiments have shown the necessity of measuring small reactivity changes of about 1% directly versus the unperturbed reference case. Otherwise disturbing influences of possible reactor-drifts cannot be excluded. Figures 24 and 25 show the geometry of the experiments.

6.4.2 Methods of Calculation

The volumes of the voided zones and the reactivity changes observed in SNEAK-2C were small. Therefore the calculations were generally performed by means of first order perturbation theory. Only for some cases $\Delta k/k$ was determined directly by diffusion calculations, showing good agreement with perturbation results.

In general the plutonium sector was extended for the calculations to a full cylinder. That calculations have shown that the influence of the outer uranium zones are small and can be neglected.

One- and two-dimensional programs were used. The 26 energy groups (NAPPMB or MOXTOT set) used in 1D-codes were reduced to 17 or 15 groups for 2D-programs. The last groups which give small contributions to the total effect were collapsed.

Universal bucklings were used in 1D-investigations.

The calculations using the MOXTOT set were performed with homogeneous cross-sections and also with cross-sections corrected for the heterogeneity of the cell composition (ZERA-code).

For the conversion of the reactivity $\Delta k/k$ into cents the calculated value $\beta_{\text{eff}} = 5.1 \times 10^{-3}$ was used.

6.4.3 Discussion of the Results

In Tables 17 and 18 and Figures 26, 27 the comparison of experimental with calculated results of sodium void traverses is shown. In axial direction the most positive effect is obtained for a void extension over half the core height. In radial direction the local void effect is positive in the inner Z1 zone. Beyond the sign changes to negative due to rapidly increasing neutron leakage.

Obviously sodium void calculations are extremely sensitive to the cross-section set used and to heterogeneity corrections. In case of the axial traverse (third step) for instance the ratio C/E (calculated value / experimental value) varies between 0.8 (MOXTOT, heterogeneous) and 1.43 (NAPPMB, homogeneous).

The experimental results are better reproduced if MOXTOT group constants are used.

In the central zone a remarkable improvement is achieved by consideration of heterogeneity while in the outer regions this correction makes the disagreement even worse.

One must keep in mind that the uncertainty in β_{eff} is of the order of 10%, and that the measurements in ϵ also have errors of about 10% for such small reactivities.

7. SNEAK-2C (Control Rod Experiments)

7.1 General Scope of the Control Rod Experiments in SNEAK-2C

7.1.1 Basic Considerations

It was decided between GfK (IAR) and the Industrial Consortium SNR to perform two series of control rod experiments in SNEAK-2C:

- 1.) SNR type rod experiments;
- 2.) Central rod experiments.

The first series of experiments is directly related to the design of the compensation rods of SNR.

As illustrated in Fig. 28 superimposed on the SNEAK lattice, the SNR reactor will comprise two rings of control rods. These are:

- a) 12 metallic tantalum compensating rods located at the boundary between the two core zones;
- b) 6 B^{10} enriched B_4C safety rods located at an inner ring in the central core zone.

The compensating rods will be, during normal operation, approximately one-half inserted at full power reactor start-up. The safety rods will be, during normal operation, out of the core. Three of them, constituting the normal scram system, will consist of enriched B_4C rod bundles with followers while the remaining three will form the secondary shut-

down system by having the capability of being very rapidly inserted into the core in empty wrapper tubes.

All the SNR control rods will be spaced with 30 cm from center to center.

The second series of experiments, central rod experiments, was designed in such that geometrical effects interfere as little as possible with presumably the most important causes of discrepancies, that is, cross-section sets and methods of calculations. A central rod is obviously the best case for a meaningful comparison between theory and experiment.

Since then, another series of control rod experiments had been decided upon and performed in SNEAK-6 (Part A). A central position again was considered, but in a core as cylindrical as possible, and with a height closer to that of the SNR.

7.1.2 Simulation of Control Rods in SNEAK

Four SNEAK square elements are equivalent in surface to 1.09 times one hexagonal SNR assembly. One SNR control rod was therefore simulated in SNEAK by 4 SNEAK elements.

A mock-up of the SNR tantalum rods was designed as shown in Fig. 29. Each of the 4 SNEAK elements comprising the mock-up contain 2 thick rods (22 mm diameter) and 2 thin rods (13 mm diameter) inserted into an aluminum matrix and surrounded on two sides by steel platelets. The rods were either metallic tantalum or aluminum so that either the absorber portion or the follower portion of the SNR control rod could be simulated. The sodium present in SNR was replaced by aluminum which was assessed to be an acceptable substitute.

The B_4C rods were constructed with B_4C boxes (natural B_4C powder, 1.6 g/cm³ density, contained in steel boxes). The corresponding follower portion was made of Na platelets, which gives approximately the same ratio Na/steel as in SNR.

In the experiments therefore, one had two different control rods with follower, designated below as Al-Ta and Na-B₄C. Table 5 shows the atomic compositions of the control rods simulated in SNEAK, compared with those of SNR.

7.1.3 Description of the Rod Experiments

In the first series of experiments, the SNR conditions were simulated as closely as possible with the rods placed on the boundary of the core zones Z1/Z2 at approximately 30 cm distance from each other. As it was impossible, due to material limitations, to build a full-size plutonium core in SNEAK, a sector core was built.

The sector had an angle of 90°. The MASURCA plutonium, on loan from the French C.E.A., served as a buffer zone to decouple the 90° SNEAK plutonium sector from the uranium zone and to improve the experimental conditions.

The start-up core (SNEAK-2C) is shown in Fig. 30.

Shadowing effects were investigated with the rod positions (Fig. 32). The measurements were performed with one rod (Na/B₄C or Al/Ta) at the Z1/Z2 boundary, and with three rods (Na/B₄C only) at the Z1/Z2 boundary. In the latter instance particular attention was given to the case of a partially inserted rod bank.

The shadowing effect was investigated by measuring the reactivity worth of the inner of the three rods for different azimuthal positions of the two outer rods. These outer rods remained always on the Z1/Z2 boundary with their absorber fully or half inserted. The distance between the outer and inner rods (center-to-center) was respectively 11 cm, 30 cm (reference case), 37 cm and 52 cm.

In the central position, both types of control rods were investigated; Al/Ta and Na/B₄C. In addition, the reactivity worth of a void was measured by removing the four central elements from the core. Such a case,

particularly difficult to compute accurately, is close to the case of the planned secondary shut-down system of SNR which hollow elements are provided in the central zone of the core during normal operation.

Also, the complete characteristic curve, $\delta k(h)$, of a Na-B₄C rod, consisting of only one SNEAK element, was measured in an off-center position in the central core zone. The characteristic curve was measured twice, with the three outer rod positions mentioned above filled with, respectively, Na and B₄C.

The material composition in the rod positions is the following. Below the lower core plane the rod positions contained normal blanket material. From a level 20 cm above the upper core boundary, the rods consisted of B₄C for safety reasons.

However, the axial distribution of the composition corresponds relatively well to that of the SNR rods.

The measurements performed consisted of:

- 1.) the reactivity changes between successive configurations in which the rods (4 elements) were made of:
 - a. core medium (reference state);
 - b. follower (Al or Na);
 - c. absorber half inserted (Al-Ta or Na-B₄C);
 - d. absorber fully inserted (Ta or B₄C);
- 2.) the distributions of U²³⁵, U²³⁸ and Pu²³⁹ fission rates:
 - axially, in a position close to the control rods, for the half insertion of a rod or rod bank;
 - radially and azimuthally, for the full insertion of a rod or rod bank.

Table 19 lists the measurements (35 reactivity changes, 19 fission rate traverses) which were performed. The experimental methods used have been described in Chapter 2.

The entire program of control rod measurements included the loading of 5 core configurations, the largest core containing 85 core elements more than the first one, to compensate for the high absorber reactivities introduced (up to 2.5% δk).

Fig. 30 and 31 represent, respectively, the first two and the last three core configurations of the series together with the exact positions of the control rods.

7.2 Reactivity Changes with a single Control Rod

7.2.1 Experiments performed

The experiments performed with a single control rod are listed in Table 19.

A control rod of the SNR type was placed at different radial positions, designated as:

5, center of the core;

1, mean the boundary of the two core zones at a mean radius of 49.0 cm;

1a and 1b, slightly displaced from position 1 inwards to a mean radii of 43.5 and 38.1 cm.

The absorber material was, either B_4C (with a Na follower) used at the four positions, or Ta (with a Al follower) used at positions 5 and 1.

7.2.2 Method of Calculations

All the measured reactivity changes were calculated with diffusion theory, using the following models:

- a) two dimensions (XY) with a constant B_z^2 value;
- b) three dimensions XY/Z (synthesis⁽⁺⁾).

A few cases were recalculated with transport theory (see § 7.2.9).

All cases were calculated using the NAP-PMB cross-sections, condensed from 26 to 4 groups.

Some of the calculations were repeated with the MOXTOT cross-sections.

The mesh spacing chosen was one half a SNEAK element (2.72 cm) in the horizontal plane (XY), and 3 cm in the axial direction Z.

The accuracy of k_{eff} was, respectively, $5 \cdot 10^{-5}$ in two dimensions, and $1 \cdot 10^{-5}$ in three dimensions (synthesis).

The reactivities deduced were simple differences of k_{eff} rather than differences divided by k_{eff} .

7.2.3 Meaning of the Comparisons

The calculational model was chosen to represent as closely as possible the actual conditions of the measurements. The exact core sizes were considered for each step of reactivity measured. Then the different steps were added to build, for example, the reactivity of a fully inserted control rod.

This type of calculation takes in account as well as possible, that the measured quantity was actually for each case the excess reactivity as determined by the critical position of SNEAK shim rods and not the total reactivity loss caused by the simulated SNR rods.

(+) The details of application of the synthesis technique are described in a separate report /11/.

7.2.4 Conversion of the Experimental Results to Δk

A perturbation calculation using two-dimensional (XY) diffusion fluxes with KEEPIN's data /16/ gave the following effective delayed neutron fraction for the core 1 of the series, reference state (without control rods):

$$\beta_{\text{eff}} = 510 \cdot 10^{-5} \Delta k.$$

The conversion of the experimental results from ρ to Δk was made considering the variation of β_{eff} , during the control rod experiments. The variation is a result of the addition of core elements at the edge of the core and of the large flux depression caused by the simulated control rods. On the basis of calculations, it has been estimated that β_{eff} was not very sensitive to the first cause but extremely sensitive to the second. The effect results in an increase of β_{eff} of the order of:

1 to 2% if one rod is placed at the core center;

1 to 4% if one rod is placed at the boundary of the core zones;

3 to 10% if three rods are placed at the boundary of the core zones.

The experimental values are given in the Table 20 below as directly obtained in ρ and as converted to Δk after correction for β_{eff} variations.

7.2.5 Diffusion Theory Results

The reactivity changes calculated by two- and three-dimensional diffusion theory are given in Table 20a and 20b. These are reactivity changes corresponding to, respectively:

a) the replacement of fuel by Na, Na-B₄C, B₄C, Al, Al-Ta or Ta;

and

b) the half or full insertion of an absorber (B₄C, Ta) in a follower (Na, Al).

7.2.6 Discussion of the Diffusion Theory Results

Part A of Table 20

There is a general trend to overestimate the reactivity changes by calculation. The deviation of the calculated results from the experimental ones range from:

- 1% to 11% in two-dimensional calculations (excepting Na);
- 2% to 8% in three-dimensional calculations (excepting Na).

The two- and three-dimensional results agree within 4% for the full insertion of absorbers with the three-dimensional results being generally the best.

When the position of the absorber is displaced from the center to the periphery, the deviation from experiment ranges

B_4C (full) : from - 1% to + 5% (2-D)
 from - 1% to + 1% (3-D)

Ta (full) : from + 4% to + 9% (2-D)
 from + 5% to + 5% (3-D)

The largest discrepancies are observed for Na, and to a lesser extent, for Al. The main reason is probably an inadequate treatment of the axial leakage of neutrons in these light materials. When the third dimension is taken into account, the calculation is improved. However there still remains a high overestimate at the center of + 24% for Na and + 8% for Al.

The replacement of fuel by a half inserted absorber is calculated (in three dimensions) as well as the full insertion of the same absorber.

Part B of Table 20

The reactivity changes corresponding to the half or full insertion of an absorber into a follower are differences of the reactivity changes

in Part A and therefore, the discrepancies observed in Part B are also differences of discrepancies found in Part A. For example, Part A shows a rather large overestimate for Na and a small one for B_4C ; the transition from Na to B_4C is therefore underestimated.

The transitions from half to full insertion are slightly overestimated:

+ 2 to + 1% for Na- B_4C to B_4C

+ 9 to + 8% for Al-Ta to Ta.

7.2.7 Effect of using MOXTOT instead of NAP

Some one-dimensional diffusion calculations, including a central control rod (position 5) have been made using both cross-section sets NAP-PMB and MOXTOT. The effect of using MOXTOT instead of NAP is found to be:

+ 3% (ref to B_4C), + 2% (ref to Ta), + 1% (ref to Na), 0 (ref to Al)

+ 4% (Na to B_4C), + 3% (Al to Ta).

7.2.8 Effect of Computational Approximations

The calculated values of Table 20 correspond to some simplifications in space and in energy (see § 3.1 and 7.2.2). The deviations introduced have been estimated on the basis of one-dimensional diffusion calculations.

In the case of a central control rod, the broad mesh spacing and the 4-group condensation introduce deviations of:

- 1% (ref to B_4C), - 3% (ref to Ta), - 5% (ref to Na), - 3% (ref to Al)

- 1% (na to B_4C), - 1% (Al to Ta).

In the case of a peripheral rod, the deviations are of the order of 1%.

The influence of the slightly too low (2%) B_Z^2 value used in the two-dimensional results is of the order of 1% of the measured values. The three-dimensional results are not influenced /11/.

7.2.9 Transport Corrections

The central rod worths have also been calculated with transport theory, by means of S_n codes for $n = 4$ (see § 3). These calculations were performed in one (R) and two dimensions (RZ). In the one-dimensional calculations the current weighted transport cross-sections ("STR") and the flux weighted transport cross-sections ("STRTR") were used while in the two-dimensional calculations, the flux weighted transport cross-sections ("STRTR") were used.

The results obtained, expressed in terms of a correction factor to be applied to the reactivities found by diffusion calculations, are as follow:

Position 5 (center)	1-D (R) STR	1-D (R) STRTR	2-D (RZ) STRTR
Fuel replaced by Na	.92	.74	.76
Fuel replaced by B_4C	.93	.93	.93
Fuel replaced by Al	.93	-	-
Fuel replaced by Ta	.94	.90	.91

One obtains transport corrections which have about the same magnitude as the deviations between diffusion theory and experiment such as given in Table 20.

7.2.10 Reactivity of a Central Void

An additional reactivity measurement was concerned with the removal of

the 4 central elements from the core and their replacement by empty structural tubes.

Two approximate methods of calculation, which allow the use of diffusion theory, were applied.

The first one consists of replacing the void by a fictitious medium, having all cross-sections equal to zero, and a finite diffusion coefficient calculated with reference to the surrounding core medium, according to a formula given by MÄRKL /17/.

The second one consists of applying, at the boundary of the core zone with the void, an inner boundary condition giving the current-over-flux ratio as a function of the ratio of void radius to core height and of the axial reflector saving /18/.

The compared values are as follows:

Experiment	698 10^{-5} Δk
first method, two dimensions (XY):	1170 10^{-5} Δk
three dimensions (XY/Z):	921 10^{-5} Δk
second method, two dimensions (RZ)	
14 cm reflector saving:	1181 10^{-5} Δk
1 cm reflector saving:	650 10^{-5} Δk

The second method gives the best results, when taking the assumption of a nearly zero reflector saving, as was already observed in /4/.

7.3 Reactivity Changes with three Control Rods

7.3.1 Experiment performed

The experiments performed with three control rods are listed in Table 19. They were concerned with the movement of a control rod (full out, half-in,

full-in) in the peripheral position 1 with two rods in neighboring positions at the same radius. The effect examined was, therefore, the shadowing of two neighboring rods upon a single rod in position 1. The two neighboring rods were displaced azimuthally, to distances from position 1 (center to center) of respectively 11 (2C,3C), 29.5 (2,3), 37 (2A,3A) and 52 cm (2B,3B). The 11 cm distance corresponds to directly adjoining positions. The configurations are shown in Fig. 31.

The absorber material was B_4C with a Na follower.

The measured reactivity changes are given in Table 21 below, as directly obtained in ρ , and as converted to Δk , after correction for β_{eff} variations (see § 7.2.4).

7.3.2 Diffusion Results

Table 22 also gives the reactivity changes calculated in (XY) and (XY/Z) geometry. The reactivity steps considered for the rod in position 1 are:

full out to half in (Na — Na- B_4C)
half in to full in (Na- B_4C — B_4C)
and full out to full in (Na — B_4C).

No transport corrections were calculated for these cases.

7.3.3 Discussion of the Diffusion Theory Results

The general observation from Table 21 is that the reactivity change as a result of the movement of a rod in position 1 from full out to half insertion is underestimated by 5% to 21% while from half to full insertion, the deviation ranges from + 1% to - 6%.

The trend of the calculations is that the agreement with experiments becomes worse with decreasing distance between the rods. This obviously

means that a portion of the shadowing effect of the rods is not described properly by the calculations. Diffusion theory is not able to describe properly the current across the boundary between a large bulk of highly absorbing medium and the core. Therefore, as the absorber becomes more concentrated in one region of the core, diffusion theory becomes worse.

7.3.4 Characteristic Curve of a B_4C Rod

In an off-center position in the central core zone Z1 the characteristic curve of a single SNEAK element (5.44 x 5.44 cm), loaded with a B_4C absorber section and a Na follower was measured in two conditions, namely in the presence of Na followers or B_4C absorbers in the three outer rod positions 1, 2, 3.

The characteristic curves are represented in Fig. 32. The calculated curves are the results of three-dimensional (XY/Z) calculations. For the comparison of measured and calculated values the conditions of half insertion was taken as a reference point. The calculation produces steeper curves than were measured. The curves for $(Na)_{1,2,3}$ are in disagreement by about 10% while the curves for $(B_4C)_{1,2,3}$ are in disagreement by a maximum of about 30%.

7.4 Traverses with a Single Control Rod

7.4.1 Measurements performed

All the measurements performed are listed in Table 19. They consist of spatial fission rate distributions for U^{235} , U^{238} and Pu^{239} in the radial, axial and azimuthal directions. The radial traverses were performed in the core midplane, the azimuthal traverses in horizontal planes at different heights and the axial ones in the central core axis and near the control rod position 1.

The measurements were performed with fission chambers (radially and axially) and by the activation of foils and PuO_2UO_2 SNEAK platelets (axially and azimuthally).

The statistical accuracy of the measured points in the core region was, respectively:

- radially: 0.7%;
- axially: 0.2 to 0.7% by chambers and by foils (U^{235});
1 to 2% by foils (U^{238}), 1.5% by platelets;
- azimuthally: 1.5% by platelets and 1 to 2% by foils.

The chamber measurements were corrected for the dead time, and also for the impurities of the chamber.

7.4.2 Method of Calculation

The calculations were the same as those performed for the reactivity changes: two-dimensional (XY) and three-dimensional (XY/Z) calculations in diffusion theory with NAP-PMB cross sections.

A few cases were also calculated in transport theory.

The effect of the calculational approximations, the broad mesh spacing, the 4 group condensation and the low B_Z^2 value (in two dimensions XY), was estimated by a one-dimensional calculation to be smaller than 0.5% in all the cases.

7.4.3 Fission Rates, Diffusion Theory Results

The fission rates obtained by diffusion theory are illustrated in Fig. 33 and 34. These rates are related to the cases with Ta in position 5 and B_4C in position 1.

One observes that the depression of the traverses within an absorber is well predicted for Pu^{239} , but greatly underpredicted for U^{238} (10%). The gradient at the boundary between the core and the absorber is calculated too steep.

The calculated axial traverses compare, in general, well with the experiment when there was a fully inserted control rod or none at all near the location of the measurements. In an axially unsymmetrical case however, such as $(\text{Na-B}_4\text{C})_1$ (Fig. 35), the degree of a symmetry is not correctly calculated. This could result from an inadequate treatment of the axial neutron leakage in the sodium follower (see § 7.2.6).

7.4.4 Power Density, Diffusion Theory Results

The goal of the traverse measurements was to obtain information on the spatial distribution of the power density in a core containing control rods. For this purpose, the fission rates measured for the different isotopes were combined using calculated values of spectral indices (see Chapter 6.2.2).

For the sake of comparison measured and calculated traverses were normalized so that the integral over the core part (weighted by r in the radial case) yielded unit average power density. All values therefore represent local-to-average ratios.

Four typical power distributions are illustrated in Fig. 36, 37, 38 and 39, referring to the cases, respectively of

- Fig. 36, radial, (B_4C) ;
- Fig. 37, radial, $(\text{B}_4\text{C})_1$;
- Fig. 38, axial, reference (Z2);
- Fig. 39, azimuthal, $(\text{B}_4\text{C})_1$.

In order to make the comparison complete, the reference radial traverse (without any control rod), presented in Chapter 6, § 6.2, is also included and compared to the cases with control rods.

The Table 22 gives the relative deviation between calculated and measured values for a series of typical points in the core.

7.4.5 Discussion of the Diffusion Theory Results

Radial Traverses

The reference traverse is predicted within 1.2% in the core.

The traverses with control rods fully inserted are in general calculated within:

- 2.4% for a central absorber rod (Ta_5 , $(B_4C)_5$);
- 2.0% for a central follower rod (Na_5);
- 1.5% ($(B_4C)_1$) or 2.4% (Ta_1) for an outer absorber rod.

In the zone of power depression around a central rod the power densities are slightly underestimated ((Ta_5, Na_5)) or slightly overestimated ($(B_4C)_5$).

The maximum in the inner zone is, respectively displaced inwards and 1% underestimated for (Na_5) , well predicted (0.5%) for $(Ta)_5$, 2% overestimated for $(B_4C)_5$.

The maximum in the outer zone is 1 to 2% overestimated in the three cases.

The power depression around an absorber rod in outer position 1 is well predicted also (within 1 to 2%).

Axial Traverses

The comparison is clearer and leads to the following conclusions:

- a) the calculated traverses have a steeper gradient than the measured ones. The maximum-to-average ratio is 1% overestimated;
- b) axial power distribution is calculated as well in the vicinity of a control rod fully inserted as in a reference fuel zone (far from any control rod);

- c) in the case of a partial insertion of a control rod, the axial assymetry is not well accounted for by the calculation. For example, in the case of $(\text{Na-B}_4\text{C})$, the maximum-to-average ratio is 3% overestimated. This may come from the deficient treatment of the sodium already discussed in connection with the reactivities.

Azimuthal Traverses

The power gradient in the vicinity of a control rod is overestimated by the calculation. The maximum of the traverse is calculated about 1% too high.

The main results obtained may be summarized as follows in terms of maximum-to-average power ratios with absorber rods inserted (B_4C , Ta):

- radially, 2% overestimate in both core zones;
- axially, 1% overestimate;
- azimuthally, 1% overestimate.

The calculation overestimates the power gradients when absorber rods are inserted in the core.

7.4.6 Effect of using MOXTOT instead of NAP

When using the MOXTOT cross-section set instead of the NAP set, the power density traverses, normalized as described above, are, in general, changed by less than 0.5%.

7.4.7 Transport Correction

Two-dimensional (RZ) and one-dimensional transport calculations, compared with corresponding diffusion calculations, yielded, as in the case with-

out control rods (Chapter 6), very small discrepancies in regions with core material. The transport effects are much larger inside control rods. The following effects were found in the central point of a central rod:

B_4C : - 6% for Pu^{239} and - 7% for U^{238} ;

Ta : - 5% for Pu^{239} and -19% for U^{238} ;

Na : - 1% for Pu^{239} and - 8% for U^{238} .

Transport theory predicts better the fission rate depression caused by an absorber, for U^{238} ; this is illustrated on Fig. 33, where the transport correction has been drawn.

The power density distribution is only slightly (1 to 2%) changed close to the absorber rod.

See Chapter 6.2, for the transport corrections in the core region in the absence of control rods, and in the blanket region.

7.4.8 Traverse measured in a Central Void in the Core

Axial fission traverses have also been measured in 4 empty central SNEAK tubes (see § 7.2.10). The approximate methods used for calculating the fluxes, in the case of the void with streaming-corrected diffusion coefficients, reproduce satisfactorily the traverses within the voided region of the core but underestimate the rates within the void in the blanket region. A recently developed method /19/ which couples a diffusion theory solution in the core medium with a transport theory procedure in the void zone better agreement in the traverses.

7.5 Traverses with three Control Rods

7.5.1 Measurements performed

The measurements performed are listed in Table 19. Radial, axial and

azimuthal fission rate traverses were measured for half and full insertion of three control rods ($\text{Na-B}_4\text{C}$) near the boundary of the two core zones. These traverses have been calculated only in diffusion theory.

7.5.2 Results from Fission Rates and Power Density

Fig. 40 and 41 illustrate the comparison of predicted and measured radial traverses in the case with three rods fully inserted. Fig. 40 represents the fission rates for the isotopes Pu^{239} and U^{238} , while Fig. 41 represents the total fission rate or power density, obtained and normalized as explained above in 7.4.4.

The relative deviations of the calculated to measured power density ratios for a series of typical points of the considered traverses have also been included in the recapitulating Table 22 already presented.

7.5.3 Discussion of the Diffusion Theory Results

One observes the following when passing from one to three control rods:

1.) Radially:

- a) full insertion $(\text{B}_4\text{C})_{1,2,3}$: there is a shift of the deviations (the sign is changed), but all the deviations remain smaller than 2%;
- b) half insertion $(\text{Na-B}_4\text{C})_{1,2,3}$: the maximum deviation is 3.4%; it must be remembered that the traverse is located in the plane separating the absorber (B_4C) and the follower (Na) parts of the rods.

2.) Axially:

The agreement becomes even better than in the case of one rod, the overestimate of the calculated power peak is reduced.

3.) Azimuthally:

The overestimate by 2.3% for $(B_4C)_1$ changes only slightly for $(B_4C)_{1,2,3}$ (2.0%). The sign of the discrepancy changes for $(Na-B_4C)_{1,2,3}$ from the upper core (B_4C) to the lower core (Na) .

As a conclusion, the influence of three rods on the power density distribution in the core is as well calculated as the influence of a single rod. The presence of several rods instead of one does not introduce any additional discrepancy between calculation and measurement.

7.6 Sodium Void with Control Rods

Five points of the radial sodium void traverse in the plutonium sector of SNEAK-2C were remeasured with B_4C rods in the positions 1, 2, 3 (typical SNR distances between rods) to get information about the influence of absorber material on the sodium void effect. In two points next to the absorber the void effect was also investigated with B_4C in the positions 1, 2c, 3c (three control rods collapsed). For the last configuration calculations were not accomplished. See Fig. 31 for the core configurations.

7.6.1 Method of Calculation

The sodium void traverse with B_4C rods in positions 1, 2, 3 was treated by perturbation theory using normal and adjoint fluxes from 4 group XY diffusion calculations. Group- and region-dependent bucklings were taken from RZ calculations for the reference core. Homogeneous NAPPMB cross-sections were used.

7.6.2 Discussion of the Results

In Table 23 measured and calculated reactivity values are presented. For comparison the experimental results without B_4C are added. The experimental values are also illustrated on Fig. 42.

In the core centre the sodium void reactivity is smaller than the corresponding value without B_4C rods, mainly due to the larger core volume (edge elements). In the other points a direct influence of the B_4C rods is observed. In particular the large flux gradient in the Z1 zone near the rod causes the Na void effect there to become more negative than in the unperturbed system.

In the Z2 zone the flux gradient is reduced by the presence of B_4C . The neutron leakage becomes smaller and the void effect is less negative than in the reference core.

The agreement between the measured and calculated traverses is quite good. At 27.2 cm the discrepancy is caused by the greater steepness of the experimental curve in this region.

8. Direct Application to the SNR Design

The main conclusions from the SNEAK-2 evaluation for a direct application to the SNR design are summarized in this chapter. They concern the prediction of the following parameters:

- k_{eff} ;
- power distribution;
- control rod worths;
- sodium void effect;

by means of the methods in current use or envisaged at this time for the SNR design calculations. The basic cross-section set used is NAP-PMB.

8.1 k_{eff}

The criticality calculations of most direct interest for the SNR design are relevant to the extrapolated full plutonium core SNEAK-2B (sector substitution experiment, Chapter 5). They give the following predictions for the critical core (with an uncertainty estimated to .003):

	NAPPMB set	MOXTOT set
Homogeneous diffusion	.980	.988
REMO correction	+ .009	+ .004
Heterogeneity correction	+ .001	+ .001
Transport correction	+ .006	+ .006
	<hr/>	<hr/>
	.996	.999

For a full uranium system (SNEAK-2A, Chapter 4), the predictions are approximately as good with NAPPMB (.991), but not so good with MOXTOT (1.023).

8.2 Power Distribution

In the core of a plutonium reactor without control rods (Chapter 6), the radial power density distribution normalized to a unit core average, is predicted by conventional diffusion methods within 1%; the maximum-to-average power ratio is 1% overestimated.

When this core contains control rods (Chapter 7), the maximum-to-average power ratios are, respectively: 2% overestimated radially and azimuthally, and 1% overestimated axially. This has been verified, as well in the case of a single rod inserted (absorber or follower) as in the case of three rods inserted. The power gradient in the vicinity of an absorber is slightly overestimated by diffusion.

On the power distribution in the core region, the effects of using either transport theory instead of diffusion, or the MOXTOT set instead of the NAP set, or heterogeneity corrected cross-sections instead of homogeneous ones, are always smaller than 1%.

In the radial blanket region, the power distribution is underpredicted with diffusion by about - 5% near the core boundary to about - 50% after 40 cm blanket thickness. Using transport theory instead of diffusion is general improves the prediction by about 5%.

Using the MOXTOT set instead of the NAP set improves also the prediction

by about + 1% near the core boundary to about + 15% after 40 cm blanket thickness.

In a mock-up type experiment one radial power distribution was also extended through a fuel element placed in a storage position outside the core blanket system. The results are given in Chapter 6.

8.3 Control Rod Worths

The evaluation of the SNEAK-2C control rod experiment (Chapter 7) leads to the following conclusions, as far as control rod worths are concerned (experimental accuracy: $\pm 5\%$):

- 1.) Simulation of the SNR shim rods, placed at the interface Z1/Z2; Ratios calculation (diffusion) over experiment, C/E, 3-D (XY/Z) values; 2-D (XY) values in brackets.

Reactivity changes	One single rod		One rod with 2 neighboring rods at 30 cm distance, Na to B ₄ C only
	Al to Ta	Na to B ₄ C	
Rod out - rod half in	1.10		.80
Rod half in - rod full in	1.08		.98
Rod out - rod full in	1.09 (1.10)	.98 (.96)	.87 (.91)

- 2.) Simulation of the SNR safety rods, in the central zone.

Reactivity change	One single rod, Na to B ₄ C
Rod out - rod full in	1.00 (.99)

- 3.) Systematical deviations found:

- a) For a single rod placed in central or peripheral position the reactivity difference (reference to Ta) is 4 to 5% overestimated with respect to (reference to B₄C).
- b) The reactivity of Na against reference is overestimated greatly with a conventional 2-D (XY) model and still somewhat in a 3-D (XY/Z) model.

- c) The shadowing effect of control rods is overestimated particularly in case of a partial insertion of the absorber.

4.) Complementary information:

- a) Using the MOXTOT set instead of NAP changes the reactivities by 3% or less;
- b) The simplifications in space and energy used in the current calculational methods introduce deviations of the order of 1%;
- c) Transport corrections have been obtained, see Chapter 7. They were found to be in general of the order of - 6 to - 10% (except for Na). Such corrections have the same magnitude as the deviations between diffusion theory and experiment. They should therefore receive more attention in the near future.

8.4 Sodium Void

In plutonium zones (Chapter 6), calculations by direct differences of k_{eff} or by perturbation (both methods agree fairly), reproduce the major part of the axial and radial sodium void traverses with a positive bias, the deviation is generally within 30%. Taking the heterogeneity of the SNEAK cell into account improves generally the agreement.

The MOXTOT set in general reproduces the experimental results better than the NAP set, by about 10%.

Two-dimensional (RZ) calculations give the best agreement, but one and a half dimensional models using constant B^2 values give deviations which are only 10% (of the total effect) larger.

The influence of the insertion of absorber rods on the sodium void effect is satisfactorily well predicted (Chapter 7).

A general result is that the calculations are on the safe side as they produce too positive effects.

8.5 Conclusions

The results of SNEAK-2 give a good survey of the accuracies reached by calculations of a system with features of the SNR. Complementary information will be provided by the data of SNEAK-6 /20/ to be published shortly. To some extent the results may already be used to apply corrections to the SNR design calculations. For other problems (in particular than associated with the two rings of control rods) further investigations in a more realistic system will have to be performed.

References

- /1/ W.J. Oosterkamp:
"The Measurement and Calculation of the Reactivity Worth of Samples in a Fast Heterogeneous Zero Power Reactor"
KFK 1036 (1969)
- /2/ H. Seufert, D. Stegemann:
"A Method for Absolute Determination of U²³⁸ Capture Rates in Fast Zero Power Reactors"
Nucl. Sci. and Eng. 28 (1967) 277
- /3/ R. Böhme, H. Seufert:
"Uranium Reaction Rate Measurements in the Steam-Cooled Fast Reactor SNEAK, Assembly 3A-2"
KFK 811 (1968)
- /4/ H. Huschke:
"Gruppenkonstanten für dampf- und natriumgekühlte schnelle Reaktoren in einer 26-Gruppendarstellung"
KFK 770 (1968)
- /5/ E. Kiefhaber et al.:
"Evaluation of Fast Critical Experiments by Use of Recent Methods and Data"
Proceedings of the BNES. Conf. on "The Physics of Fast Reactor Operation and Design", London 1969
- /6/ L. Bindler, A. Charlier, J. Quenon:
"Neutronic Methods of Fast Breeder Physics Analysis", and also "Control Rod Worth Calculations"
Meeting on Fast Reactor Analysis, Abelekeess (U,R,S,S) (1970)
- /7/ D. Wintzer:
"Zur Berechnung von Heterogenitätseffekten in periodischen Zellstrukturen thermischer und schneller Kernreaktoren"
KFK 743 (1969)

- /8/ F.R. Mynatt:
"Development of Two-dimensional Discrete Ordinates Transport Theory for Radiation Shielding"
Dissertation, Uni. of Tennessee (Febr. 1969)
- /9/ G. Buckel:
"Approximation der stationären drei-dimensionalen Mehrgruppen-Neutronen-Diffusionsgleichung durch ein Syntheseverfahren mit dem Karlsruher Synthese-Programm KASY"
KFK 1349, not published
- /10/ A. Daneri, G. Maggioni, E. Salina:
"TRITON, a Multigroup Diffusion-depletion Program in Three Dimensions for IBM-360
FIAT, FN-E-97 (May 1968)
- /11/ S. Pilate et al.:
"Three Dimensional Synthesis Method Tested and Applied in Fast Breeders"
KFK 1345 (1970)
- /12/ J. Lieberoth:
(MOCA), Nukleonik 11 (1963) 213
- /13/ N. Barberger et al.:
"Analysis of Experiments Performed in MASURCA"
Proceedings of the BNES. Conf. on "The Physics of Fast Reactor Operation and Design", London (1969)
- /14/ J.L. Campan:
Private Communications
- /15/ P. Hammer:
Private Communications
- /16/ G.R. Keepin et al.:
"Delayed Neutrons from Fissionable Isotopes of Uranium, Plutonium and Thorium"
Phys. Rev. 107 (1957) 1044

- /17/ H. Märkl:
"Berechnung des "Streaming Effektes" eines durch den Reaktor ver-
laufenden Hohlraumes, mittels Einführung eines fiktiven Mediums"
Nukleonik, Vol. 6, No. 6 (1964)
- /18/ E.L. Zimmermann:
"Boundary Values for the Inner Radius of a Cylindrical Annular
Reactor"
ORNL-2484 (Febr. 1958)
- or A. Stojadinovic:
Private Communications
- /19/ P. Mc Grath:
Private Communications
- /20/ G. Jourdan, H. Reichel:
Private Communications
- /21/ J.Y. Barré, G. Ravier:
Private Communications

1. The first part of the document discusses the importance of maintaining accurate records of all transactions and activities. It emphasizes that this is crucial for ensuring transparency and accountability in the organization's operations.

2. The second part outlines the various methods and tools used to collect and analyze data. This includes both traditional manual methods and modern digital technologies, highlighting the benefits of each approach.

3. The third section focuses on the challenges and risks associated with data management, such as data loss, security breaches, and compliance issues. It provides strategies to mitigate these risks and ensure the integrity of the data.

4. The final part of the document discusses the future of data management, including emerging trends like artificial intelligence and cloud computing, and how they will impact the way organizations handle their data.

Table 1a

Atomic Compositions (10^{22} at/cm³) SNEAK-2A

Elements	Zones used in k_{eff} calculations				Zones used in calculations of reaction rate distribution		Control Rods		
	R1	R2'	R2''	Blanket	R1	R2	R1	R2	
							shim- and safety rod	shim rods	safety rods
U-235	0.18762	0.25332	0.25284	0.01762	0.18759	0.25334	0.18824	0.25097	0.26007
U-238	0.65569	0.58974	0.58387	4.18400	0.65106	0.58502	0.75117	0.65643	0.68023
Cr ¹⁾	0.35649	0.31508	0.29792	0.10625	0.35808	0.31811	0.32372	0.31960	0.32375
Fe	1.21082	1.21813	1.12978	0.39570	1.21636	1.20817	1.09661	1.28188	1.09672
Ni ²⁾	0.18568	0.23092	0.21644	0.17168	0.18666	0.23602	0.16532	0.26879	0.16555
O	0.90411	1.00795	1.00316		0.90216	1.00514	0.94431	1.08294	0.94464
C	0.30030	0.24087	0.25221		0.30497	0.25287	0.20417	0.00371	0.20424
Na	0.85125	0.89763	0.49266		0.87330	0.95179	0.39706		0.39720
Al ³⁾	0.02745	0.05714	0.45239				0.58877	1.03476	0.58898
Si	0.01750	0.01546	0.01577		0.01636	0.01473	0.04264	0.02766	0.04266
Ti	0.00260	0.00184	0.00216		0.00256	0.00163	0.00471	0.00599	0.00471
H	0.00217	0.00174	0.00182		0.00221	0.00183	0.00147		0.00147

1) Mn has been assimilated to Cr 2) Co has been assimilated to Ni 3) Mg has been assimilated to Al

Table 1b

Modified atomic compositions (10^{22} at/cm³)
for the uranium-zones

Elements	Zones	
	R1	R2
U-235	0.18759	0.25334
U-238	0.65106	0.58502
Cr ¹⁾	0.35808	0.31811
Fe	1.21636	1.20817
Ni ²⁾	0.18666	0.23602
O	0.90216	1.00510
C	0.30497	0.25287
Na	0.87330	0.95179
Si	0.01636	0.01473
Ti	0.00256	0.00163
H	0.01413	0.01169

1) Mn has been assimilated to Cr

2) Co has been assimilated to Ni

Table 2

Atomic Compositions (10^{22} at/cm³)
of the SNEAK Pu-Zones

Elements	Zones	
	Z1 SNEAK	Z2 SNEAK
Pu-239	0.12756	0.16840
Pu-240	0.01146	0.01513
Pu-241	0.00104	0.00137
Pu-242	0.00005	0.00007
U-235	0.00441	0.00374
U-238	0.60224	0.50827
Cr ¹⁾	0.32340	0.39705
Fe	1.19602	1.30976
Ni ²⁾	0.22813	0.19975
O	1.25918	1.39489
C	0.00505	0.00607
Na	0.89749	0.71091
Al ³⁾	0.00056	0.24172
Ti	0.00077	0.00206
Si	0.01530	0.01920

1) Mn has been assimilated to Cr

2) Co has been assimilated to Ni

3) Mg has been assimilated to Al

Table 3a

Atomic Compositions (10^{22} at/cm³)
of the MASURCA Pu-Zones

Elements	Zones	
	Z1 MASURCA	Z2 MASURCA
Pu-239	0.12725	0.16967
Pu-240	0.01174	0.01565
Pu-241	0.00111	0.00148
Pu-242	0.00014	0.00018
U-235	0.00181	0.00125
U-238	0.62394	0.55480
Cr ¹⁾	0.34127	0.34584
Fe	1.29491	1.31997
Ni	0.17382	0.17014
O	1.22039	1.22039
Na	0.91111	0.91111

1) Mn has been assimilated to Cr

Table 3b

Atomic Compositions (10^{22} at/cm³)

Z1 MASURCA-Zone is modified

Elements	Z1 MASURCA
Pu-239	0.12104
Pu-240	0.01116
Pu-241	0.00106
Pu-242	0.00013
U-235	0.00160
U-238	0.59296
Cr ¹⁾	0.34421
Fe	1.25500
Ni	0.17644
O	1.15990
Na	0.88568

1) Mn has been assimilated to Cr

Table 4 Atomic Compositions (10^{22} at/cm³) of the storage positions and the breeder blanket in radial direction

Elements	Storage Zones		Breeder blanket
	Al	SS	
Al ¹⁾	5.63838	0.55309	0.5200
O			2.0911
C		0.01895	0.0045
Fe		5.15938	0.6300
Cr ²⁾	0.01841	1.52937	0.1824
Ni ³⁾		0.70332	0.1040
Na			0.6644
Mo		0.01725	
Si	0.04360	0.06008	0.0108
Ti	0.00005	0.02856	0.0005
U-235			0.0075
U-238			1.0297

1) Mg has been assimilated to Al

2) Mn has been assimilated to Cr

3) Co has been assimilated to Ni

Table 5

Atomic Compositions of Control Rods in SNEAK-2C and in SNR (10^{24} at/cm³)

Elements	SNEAK-2C				SNR			
	Al-Ta		Na-B ₄ C		Compens. rods		Safety rods ⁺	
	Absorber	Follower	Absorber	Follower	Absorber	Follower	Absorber	Follower
Fe	1.18-2	1.18-2	8.29-3	1.07-2	1.15-2	1.15-2	1.54-2	1.54-2
Cr	3.51-3	3.51-3	2.55-3	3.17-3	3.10-3	3.10-3	4.17-3	4.17-3
Ni	1.63-3	1.63-3	1.18-3	1.85-3	2.07-3	2.07-3	2.78-3	2.78-3
Na	--	--	--	1.66-2	1.11-2	1.77-2	1.19-2	1.19-2
Ta	1.65-2	--	--	--	1.67-2	--	--	--
B-10	--	--	9.45-3	--	--	--	1.50-2	--
B-11	--	--	3.88-2	--	--	--	1.50-2	--
C	--	--	1.21-2	--	--	--	7.51-3	--
Al	2.59-2	4.39-2	5.04-4	--	--	--	--	--

⁺ normal scram system.

Table 6

Impurities in the Chamber Deposits

Fission Chamber	FC4 20 th Century Electronics $\emptyset = 6.35$ mm			French Chambers $\emptyset = 8$ mm	
Isotope	Type	Exact isotopic contents	Deposit	Type	Exact isotopic contents
U-235	TI 500	U-235 93 % U-238 5.5 % U-234 1.25 % U-236 0.25 %	U ₃ O ₈ 1000 $\mu\text{g}/\text{cm}^2$ 4 cm^2	552 C	U-235 99.87 \pm 0.03 % U-238 0.053 \pm 0.01 % U-234 0.036 \pm 0.008 % U-236 0.039 \pm 0.008 %
U-238	UD 73	U-238 99.956% U-235 0.044%	U ₃ O ₈ 1000 $\mu\text{g}/\text{cm}^2$ 4 cm^2	871 C	U-238 99.98 % U-235 0.02 \pm 0.003 %
Pu-239	TI 536	Pu-239 99 % Pu-240 1 %	PuO ₂ 300 $\mu\text{g}/\text{cm}^2$ 4 cm^2	961 C	Pu-239 98.37 % Pu-240 1.59 % Pu-241 0.03 %
Np-237	UI 370	Np-237 99.9 % Pu-239 0.1 %	NpO ₂ 300 $\mu\text{g}/\text{cm}^2$ 4 cm^2	772 C	Np-237 99.9 % Pu-239 <0.1 %

Table 7

The 4 groups Condensation Scheme

Original 26 groups	Broad group no.
1 to 4	1
5 to 6	2
7 to 9	3
10 to 26	4

Table 8

SNEAK-2A

Results of Homogeneous Diffusion Calculations

Results with the NAPPMB - Set

	k_{eff}
2D (RZ) 4 groups ¹⁾	0.9790
Correction for cylindrisation	-0.0022
REMO correction	-0.0022
	<hr/>
	0.9746

Results with MOXTOT - Set

	k_{eff}
Result with NAP-set	0.9746
Correction NAP → MOXTOT	+0.0333
	<hr/>
	1.0079

1) With correction for condensation

Table 9

SNEAK-2A

Results of the k_{eff} calculations with corrections

	KFK-NAP-set	MOXTOT-set
homogeneous diffusion	0.9746	1.0079
heterogeneity correction	+0.0028	+0.0028
transport correction ¹⁾	+0.0072	+0.0072
	<hr/>	<hr/>
	0.9846 ²⁾	1.0179

1) In axial and radial direction

2) With MONTE CARLO PROGRAM MOCA the result of the k_{eff} calculations is:
 $k_{\text{eff}} = 0.9882.$

Table 10

SNEAK-2A

Final results with the correction of the
higher H-concentration

	KFK-NAP-set	MOXTOT-set
homogeneous diffusion (old H-concentration)	0.9768	1.0101
REMO correction	-0.0017	-0.0017
correction of the higher H-concentration	+0.0056	+0.0049
heterogeneity correction	+0.0031	+0.0031
transport correction	+0.0072	+0.0072
final results	0.9910	1.0236

Table 11

SNEAK-2A

Comparison of the calculated and measured material worths

Sample	MOXTOT			NAPPMB	
	REAC	Perturbation Theorie		Perturbation Theorie	
		one dimensional 26 groups	two dimensional 15 groups	one dimensional 26 groups	two dimensional 15 groups
C/E	C/E	C/E	C/E	C/E	
U-235	1.07	1.07	1.07	1.05	1.11
Pu-239	0.96	0.95	0.95	0.99	1.03
U-238	1.00	1.08	1.13	1.30	1.28
Pu-240	0.79	0.82	0.82	0.30	0.36
Ta	1.08	1.16	1.19	1.17	1.17
B-10	0.97	1.03	1.04	1.04	1.03
Fe	1.05	0.92	0.80	1.07	0.89
Cr		0.64		0.73	
Ni	1.23	1.25		1.29	
Na ¹⁾	0.41	0.47	0.31	0.43	0.35
Na ²⁾	1.23	1.40	0.97	1.30	1.02

1) measured in the center

2) obtained by extrapolation of the axial traverse in the center

Table 12

SNEAK-2A

Influence of the higher H-concentration on the results of the material worth calculations

Sample	MOXTOT-set	NAPPMB-set
	$\frac{\text{corrected values}}{\text{uncorrected values}}$	$\frac{\text{corrected values}}{\text{uncorrected values}}$
U-235	0.996	0.993
U-238	1.014	1.020
Pu-239	0.988	0.987
Pu-240	0.921	0.693
Ta	1.124	1.124
B-10	1.054	1.054
Fe	0.963	1.058
Cr	0.860	0.960
Ni	1.014	1.011
Na	0.883	0.899

Table 13

Results of the Substitution Experiment
(SNEAK-2A → SNEAK-2B)

Substitution step	k_{eff}	Δk_{eff}
Ref. core SNEAK-2A	1.000433	
Step 1	1.001077	0.000644
Step 2	1.001338	0.000261
Step 3	1.001559	0.000221
Step 4	1.001741	0.000182
Step 5	1.001893	0.000152
Step 6	1.002022	0.000129
Step 7 a)	1.002321	0.001304
4 edge elements replaced by blanket	1.000868	-0.001453
Step 8	1.001820	0.000952

$\Delta k_{1 \rightarrow 7}^{b)}$

a) Between Step 6 and 7 the radial blanket was decreased causing reactivity decrease of 0.006 %

b) $\Delta k_{7 \rightarrow 1}$ is the reactivity difference between Step 1 and 7 corrected for reactivity change mentioned under a).

Table 14

Results of the k_{eff} calculations for SNEAK-2B

	MOXTOT-set	NAPPMB-set
2D (RZ) 26 groups homogeneous diffusion	0.9903	
1D 26 groups MOXTOT → NAPPMB		0.9821
correction of cylindrisation	-0.0022	-0.0022
REMO-correction	+0.0039	+0.0091
correction of heterogeneity	+0.0007	+0.0009
transport correction	+0.0058	+0.0058
final results	<u>0.9985</u>	<u>0.9957</u>

Table 15 Results of the k_{eff} -calculations for SNEAK-2C

	k_{eff}		k_{eff}
2D (RZ) diffusion		2D (XY) diffusion	0.9811
right side	0.9858		
left side	0.9819		
average	0.9839		
correction for group condensation	-0.0001		-0.0001
cylindrisation correction	-0.0024		
transport correction	+0.0074		+0.0074
			<hr/>
final results	0.9888		0.9884

Table 16

Relative deviations $\frac{C-E}{E}$ [%] of calculated (C) and experimental (E) fission rate and power density traverses in SNEAK-2C

		Blanket			Al or Steel	Storage Position
		R = 70 cm	85 cm	100 cm		
R ₂ /Al	U-235	-3.4	-19.7	-44.9	-60.7	-65.1
	U-238	-5.0	-20.7	-54.2	-60.4	-65.5
	Pu-239	-6.0	-20.5	-48.4	-63.8	-63.6
	Power	-4.7	-19.9	-48.8	--	-65.1
Al/Al	U-235	-3.4	-19.7	-44.9	-57.2	-75.7
	U-238	-5.0	-20.7	-41.8	-71.1	-66.6
	Pu-239	-6.0	-20.5	-48.4	-62.9	-73.7
	Power	-4.7	-19.9	-43.0	--	--
SS/SS	U-235	-5.1	-11.7	-27.3	-42.1	-26.7
	U-238	-10.2	-22.8	-55.0	-62.5	-37.0
	Pu-239	-7.5	-10.8	-21.9	-40.5	-12.1
	Power	-8.6	-17.0	-35.2	--	--
R ₂ /SS	U-235	-5.1	-11.7	-27.3	-39.0	-44.8
	U-238	-10.2	-22.8	-45.9	-56.1	-46.2
	Pu-239	-7.5	-10.8	-21.9	-33.3	-38.4
	Power	-8.6	-17.0	-34.0	--	-33.8

Table 17

SNEAK-2C

Axial sodium-void-reactivity-traverse

Step Nr.	Exp. in ϵ	Ratios of calculated over experimental values C/E				
		Two dimensions (R-Z)		One dimension (slab geometry)		
		MOXTOT HET C/E	NAPPMB HOM C/E	MOXTOT HET C/E	MOXTOT HOM C/E	NAPPMB HOM C/E
1	1.25	0.97	1.37	0.97	1.17	1.26
2	1.75	0.88	1.34	0.88	1.13	1.24
3	1.61	0.80	1.43	0.80	1.17	1.34
4	0.25	-2.5	1.64	-2.7	0.48	2.16

Table 18

SNEAK-2C

Radial sodium-void-reactivity-traverse

Zone	Step Nr.	Exp. in ϕ	Ratios of calculated over experimental values C/E			
			Two dimensions (R-Z)		One dimension (cylindrical geometry)	
			NAPPMB HOM C/E	MOXTOT HET C/E	MOXTOT HOM C/E	NAPPMB HOM C/E
Z1	1	1.25	1.37	0.97	1.17	1.26
	2	1.25	1.36	0.95	1.15	1.27
	3	1.23	1.33	0.91	1.13	1.22
	4	1.17	1.30	0.89	1.10	1.20
	5	1.04	1.32	0.88	1.12	1.20
	6	0.92	1.27	0.85	1.12	1.22
	7	0.71	1.32	0.84	1.17	1.28
	8	0.46	1.45	0.96	1.28	1.43
Z2	9	0.11	--	1.09	1.73	1.91
	10	-0.36	0.96	0.97	0.58	0.58
	11	-1.01	0.89	0.83	0.70	0.69
	12	-1.50	0.90	0.83	0.72	0.71
	13	-1.43	--	0.78	0.73	0.78
B1	14	-0.19	0.75	0.87	0.87	0.87

Table 19

SNEAK-2C, control rod experiments
measurements performed

Reactivity measurements ⁺	Fission rate traverses ⁺⁺⁺⁺		
	Radial	Axial	Azimuthal
<u>Core 1</u> (476 core elements) ⁺⁺ Ref., (Na) ₁ , (Al) ₁		Ref. (Z2)	
<u>Core 2</u> (494 core elements) (Al) ₁ , (Na) ₁ , (Al-Ta) ₁ , (Na-B ₄ C) ₁ , (Ta) ₁ (Na) ₅ , (Al) ₅	(Ta) ₁ (Na) ₅	Ref. (Z1) (Ta) ₁	(Ta) ₁
<u>Core 3</u> (509 core elements) (Al) ₅ , (Al-Ta) ₅ , (Na-B ₄ C) ₅ , (Ta) ₅ ⁺⁺⁺ , (Ta) ₅ void ₅ (B ₄ C) ₁ , (B ₄ C) _{1a} , (B ₄ C) _{1b} (Na) _{1,2,3} charact. curve (B ₄ C) ₄ for (Na) _{1,2,3}	(Ta) ₅ (B ₄ C) ₁	void ₅ (Na-B ₄ C) ₁ , (B ₄ C) ₁	(B ₄ C) ₁
<u>Core 4</u> (539 core elements) (B ₄ C) ₅ (Na-B ₄ C) _{2,3} and (B ₄ C) _{2c, 3c} with: 1) (Na) ₁ 2) (Na-B ₄ C) ₁ 3) (B ₄ C) ₁ charact. curve (B ₄ C) ₄ for (B ₄ C) _{1,2,3}	(B ₄ C) ₅ (Na-B ₄ C) _{1,2,3}	(Na-B ₄ C) _{1,2,3}	(Na-B ₄ C) _{1,2,3}
<u>Core 5</u> (561 core elements) (B ₄ C) _{2,3} , (B ₄ C) _{2a, 3a} and (B ₄ C) _{2b, 3b} with: 1) (Na) ₁ 2) (Na-B ₄ C) ₁ 3) (B ₄ C) ₁	(B ₄ C) _{1,2,3}	(B ₄ C) _{1,2,3}	(B ₄ C) _{1,2,3}

Table 19 *a*

- + The indices designate the location of the rods:
- 1 : outer position, typical of the SNR shim rods;
 - 1a and 1b are the position 1 displaced inwards of, respectively, 1 and 2 SNEAK elements;
 - 2,3: neighbouring outer positions (shadowing experiment);
 - 2a, 2b, 2c, 3a, 3b, 3c are the positions 2 and 3 displaced azimuthally;
 - 4 : off-center position in the central zone (one SNEAK element large);
 - 5 : central position;
- See Fig.32 for the exact positions on the core lay-out.
- ++ With some slight simplifications the main core configurations reduce to 5;
- +++ Ta' : modified version of Ta, in which the 4 central thin Ta rodlets are replaced by Al
- ++++ -The fission rate traverses were measured using the following techniques: (see description in Chapter 1);
- Fission chambers (U^{235} , U^{238} , Pu^{239}); all the radial traverses, the axial traverses except for $(B_4C)_1$ and $(B_4C)_{1,2,3}$;
 - Detector foils (U at two enrichment stages); the axial traverse $(Ta)_1$ and $(B_4C)_1$, the azimuthal traverses $(Ta)_1$, $(Na-B_4C)_{1,2,3}$ and $(B_4C)_{1,2,3}$.
 - Activation of normal UO_2 - PuO_2 platelets: the axial traverse $(Ta)_1$, $(B_4C)_1$ and $(B_4C)_{1,2,3}$, the azimuthal traverses $(Ta)_1$, $(B_4C)_1$, $(Na-B_4C)_{1,2,3}$ and $(B_4C)_{1,2,3}$.

Table 20a

SNEAK-2C

Reactivity changes with a single control rod.

Calculations (2D, XY and 3D, XY/Z) compared with experiments.

Fuel replaced by Na, Na-B₄C, B₄C, Al, Al-Ta or Ta.

Fuel replaced by	Experimental values		Ratios C/E of calculated over experimental values obtained with diffusion theory	
	directly obtained	converted in Δk	2D (XY)	3D (XY/Z)
	in ϵ	(10 ⁻⁵)		
<u>Position 5 (center)</u>				
Na	98	506	1.39	1.24
Na-B ₄ C	297	1527	--	.98
B ₄ C	440	2271	.99	.99
Al	101	523	1.11	1.08
Al-Ta	188	967	--	1.03
Ta	260	1337	1.04	1.05
Ta ⁺	247	1273	1.02	1.02
<u>Position 1b (R=38.1 cm)</u>				
B ₄ C	308	1590	1.03	1.00
<u>Position 1a (R=43.5 cm)</u>				
B ₄ C	278	1431	1.04	1.01
<u>Position 1 (R=49.0 cm)</u>				
Na	84	434	1.20	1.07
Na-B ₄ C	166	858	--	1.01
B ₄ C	244	1251	1.05	1.01
Al	82	421	1.08	1.02
Al-Ta	117	605	--	1.05
Ta	148	765	1.09	1.05

⁺ see footnote ⁺⁺⁺ of Table 19

Table 20b

(continued)

Half or full insertion of an absorber into a follower
(SNR-simulation)

Changes	Experimental values		Ratios C/E of calculated (diffusion theory) over experimental values	
	directly obtained in ϕ	converted in 10 ⁻⁵ Δk	2D (XY)	3D (XY/Z)
<u>Position 5</u> (center)				
Na-NaB ₄ C	199	1021	--	.85
NaB ₄ C-B ₄ C	143	744	--	1.02
Na-B ₄ C	342	1765	.89	.92
Al-AlTa	87	444	--	.98
AlTa-Ta	72	370	--	1.09
Al-Ta	159	814	1.00	1.03
<u>Position 1</u> (R=49.0 cm)				
Na-NaB ₄ C	82	424	--	.95
NaB ₄ C-B ₄ C	78	393	--	1.01
Na-B ₄ C	160	817	.96	.98
Al-AlTa	35.5	184	--	1.10
AlTa-Ta	30.7	160	--	1.08
Al-Ta	66.2	344	1.10	1.09

Table 21

SNEAK-2C

Reactivity changes with three control rods (shadowing experiment).
Calculations (2D, XY and 3D, XY/Z) compared with experiments.

Neighboring rods at distances (cm) (center-to-center)	Changes in position 1 O. = full out (Na) H.I. = half in (Na-B ₄ C) I. = full in (B ₄ C)	Experimental values		Ratios C/E of calculated over experimental values obtained with diffusion	
		directly obtained in ϕ	converted in $10^{-5} \Delta k$	2D (XY)	3D (XY/Z)
∞ a)	O. - H.I.	82	424	--	.95
	H.I. - I.	78	393	--	1.01
	O. - I.	160	817	.96	.98
52	O. - H.I.	65	358	--	.87
	H.I. - I.	45	248	--	.94
	O. - I.	110	806	.87	.89
37	O. - H.I.	43.6	242	--	.86
	H.I. - I.	30.2	169	--	.96
	O. - I.	73.8	411	.87	.90
29.5	O. - H.I.	37.0	205	--	.80
	H.I. - I.	25.0	140	--	.98
	O. - I.	62.0	345	.91	.87
11	O. - H.I.	16.3	89	--	.79
	H.I. - I.	14.2	78	--	.95
	O. - I.	30.5	167	.85	.86

a) The distance ∞ indicates the case of no neighboring rods present.

Table 22

SNEAK-2C

Power density traverses

Relative deviations of the power density ratios $\frac{C-E}{E}$ (%)

Part A : Radial traverses								
Distance (cm) to central axis	0	10.9	21.5	32.6	43.5	54.4	65.3	
<u>Reference</u>	+0.4	+0.6	+0.8	+0.9	+0.4	-1.2	--	
<u>One central rod</u>								
(Na) ₅	--	-2.0	-0.3	+1.3	+1.6	+0.3	--	
(Ta) ₅	--	-2.4	-0.2	+0.4	+1.2	+1.3	-0.1	
(B ₄ C) ₅	--	+0.4	+1.2	+1.9	+2.2	+0.8	-1.3	
<u>One outer rod</u>								
(Ta) ₁	+1.0	+1.7	+2.4	+1.4	--	-0.3	--	
(B ₄ C) ₁	-0.9	-0.8	-0.7	-0.4	--	+1.5	--	
<u>Three outer rods</u>								
(B ₄ C) _{1,1,3} full in	+0.7	+0.5	+0.5	-0.2	--	-0.2	-1.8	
(B ₄ C) _{1,2,3} half in	+2.5	+1.7	+2.0	+3.4	--	+0.1	-0.7	
Part B : Axial traverses (maximum)								
Reference in Z1							+1.2	
Reference in Z2							+0.9	
One outer rod (B ₄ C) ₁ (full in)							+1.0	
One outer rod (B ₄ C) ₁ (half in)							+2.8	
Three outer rods B ₄ C (full in)							0	
Three outer rods B ₄ C (half in)							+1.6	
Part C : Azimuthal traverses (maximum)								
One outer rod (B ₄ C) ₁							+1.4	
One outer rod Ta ₁							+0.8	
Three outer rods B ₄ C full in							+1.3	
Three outer rods B ₄ C half in above core midplane (B ₄ C) below core midplane (Na)							+0.3 -0.8	

Table 23

SNEAK-2C

Sodium void reactivity effect with control rods [¢]

	Distance from the centre [cm]	Experiment		Calculation	Experiment without B ₄ C	Zone
		voiding	reloading			
B ₄ C in Position 1,2,3	0	+0.90	+0.88	+0.89 ^{+))}	+1.25	Z1
	27.20	-0.23	-0.18	-0.01	+0.92	
	38.08	-0.41	-0.39	-0.39	+0.46	
	59.84	+0.04	--	+0.03	-1.50	Z2
	65.28	-0.05	-0.15	-0.04	-1.43	
B ₄ C in 1, 2c, 3c	38.08	-1.14	-1.11	--	+0.46	Z1
	59.84	+0.11	+0.10	--	-1.50	Z2

+) Central value fitted on the measurements.

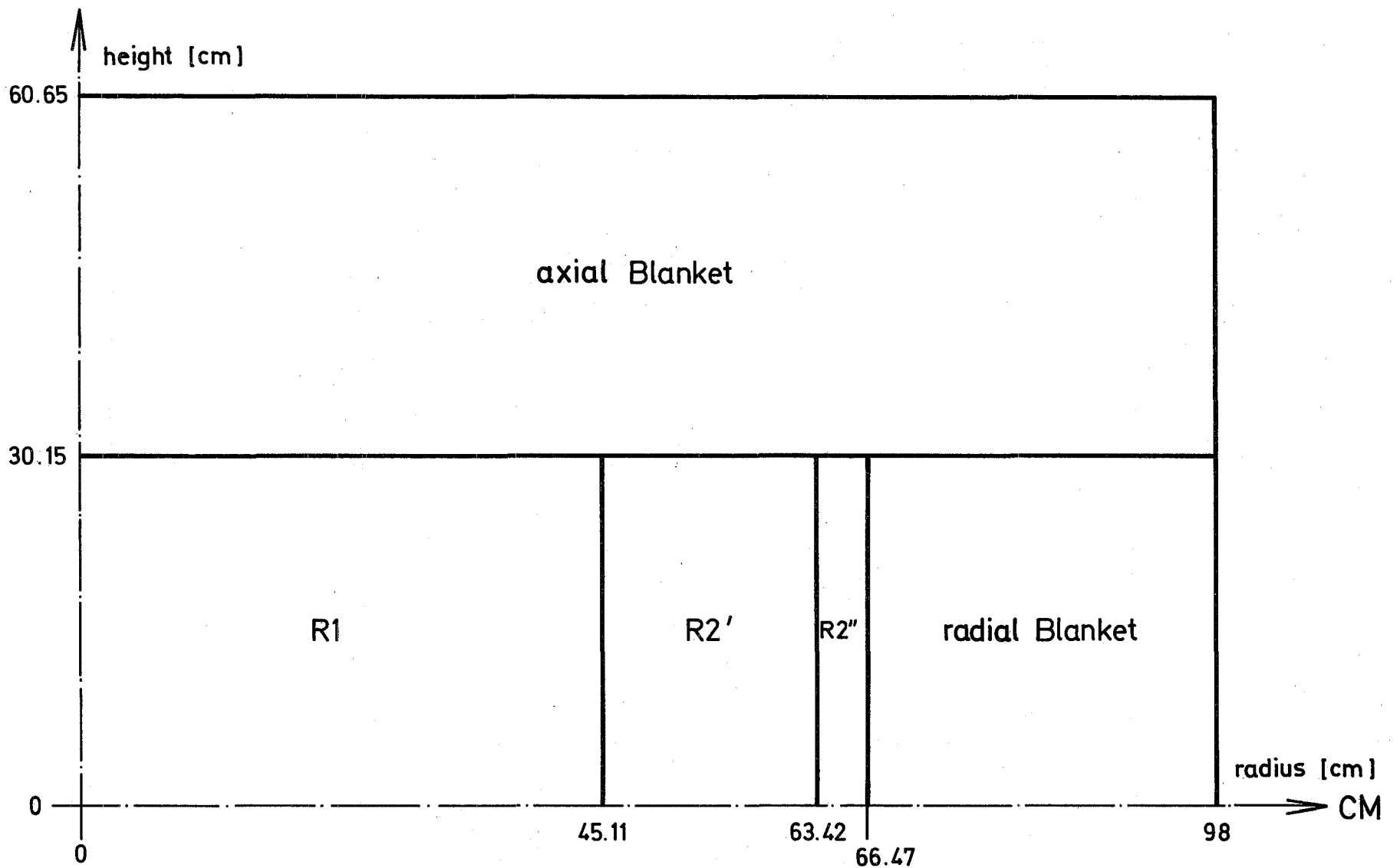


Fig. 1a Axial Cut through a Quarter of the critical Core
SNEAK - 2A

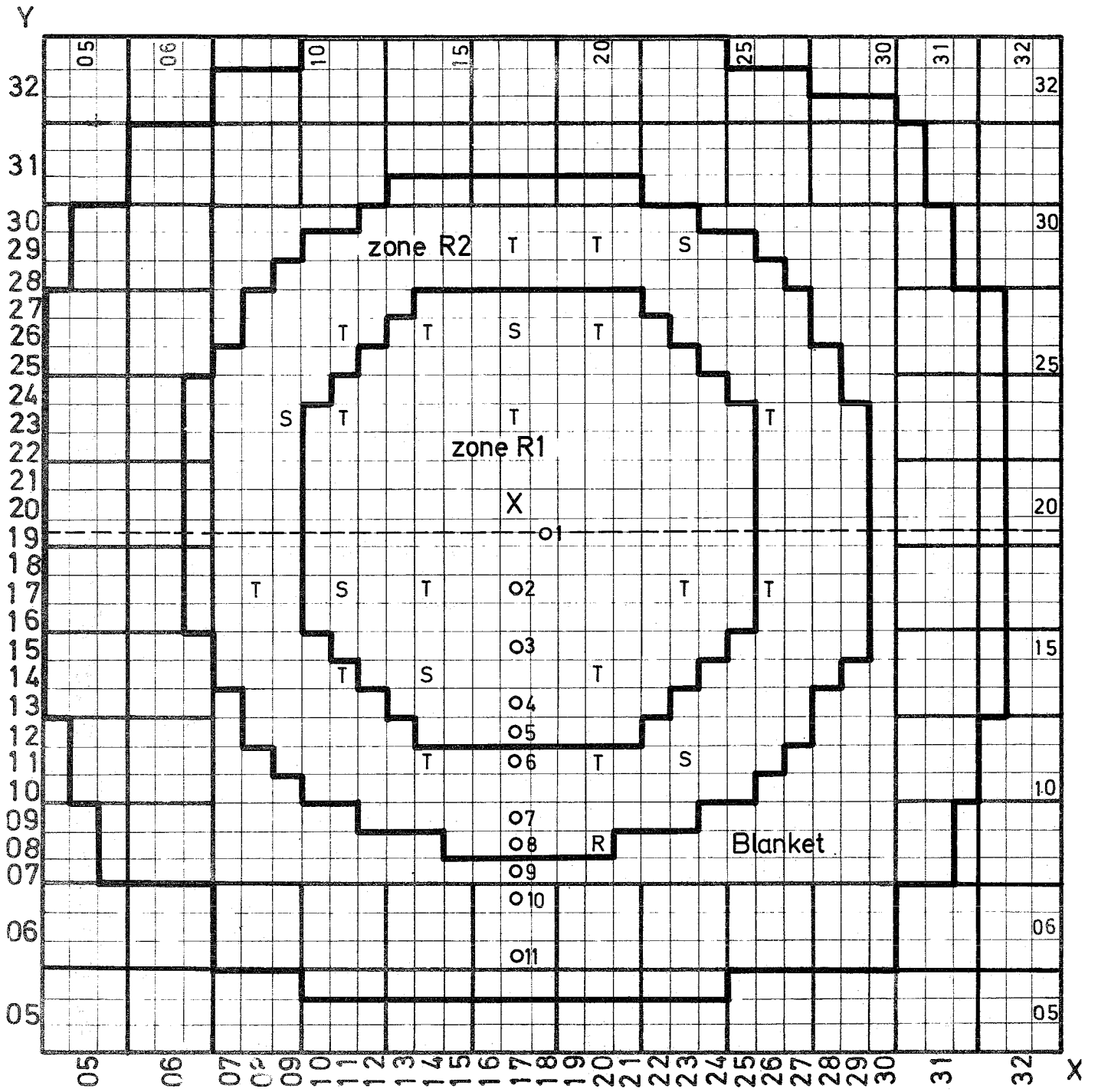
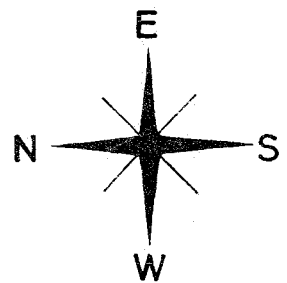
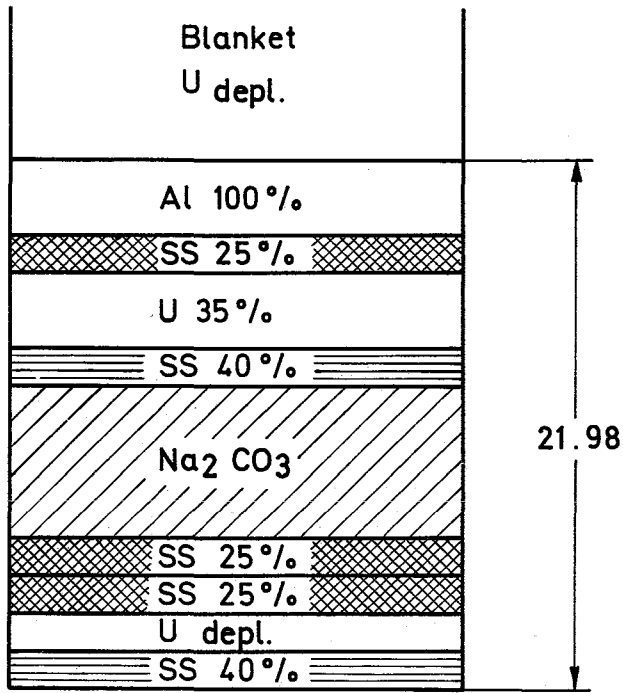


Fig.1b Cross Section of SNEAK-2A

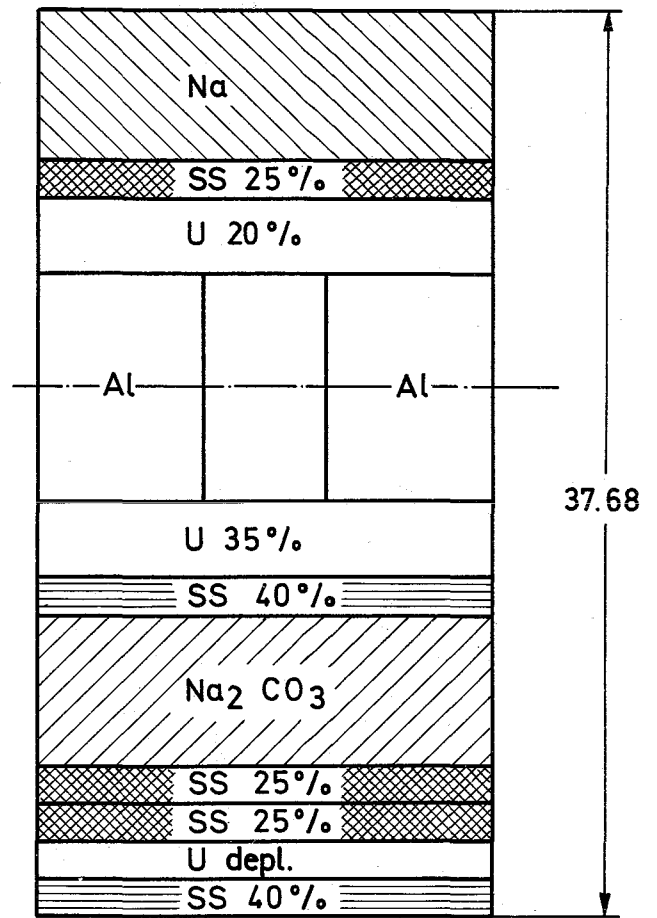
- o radial foil traverse
- radial chamber traverse
- X axial traverse
- T SNEAK shim rod
- S SNEAK safety rod
- R SNEAK control rod



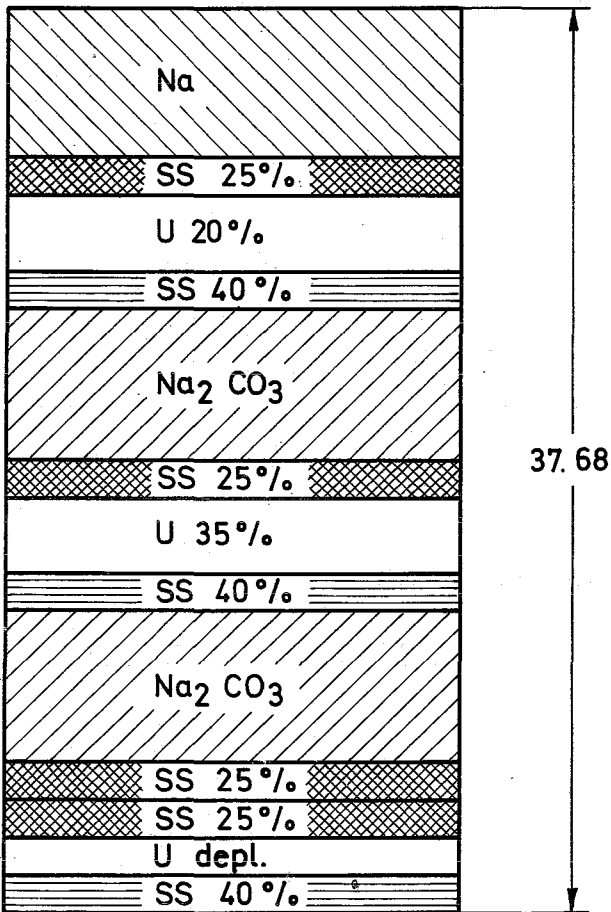
scale 1:10



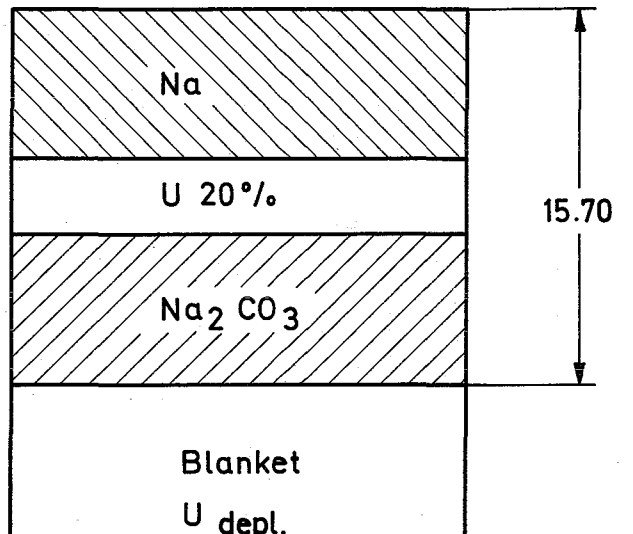
upper rest cell



window cell

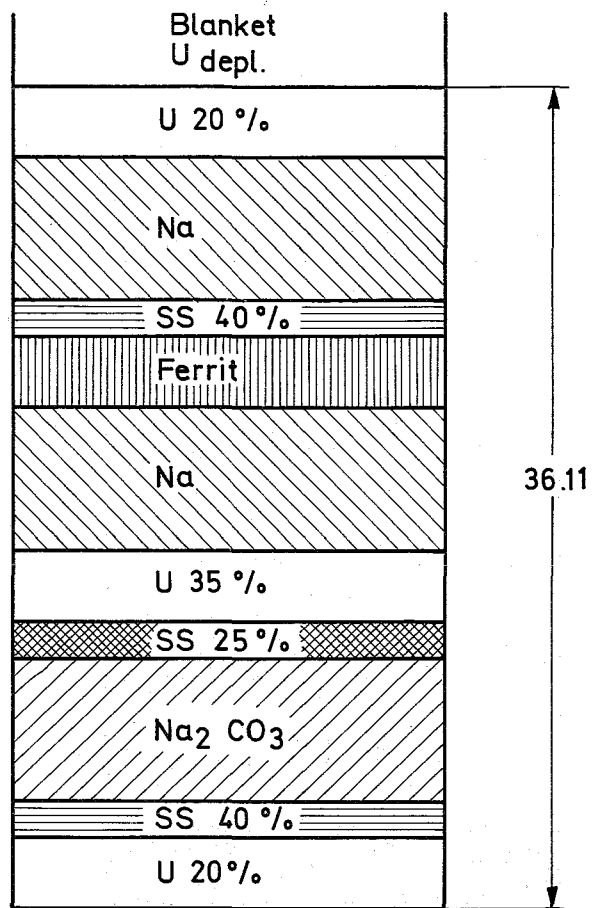


normal cell

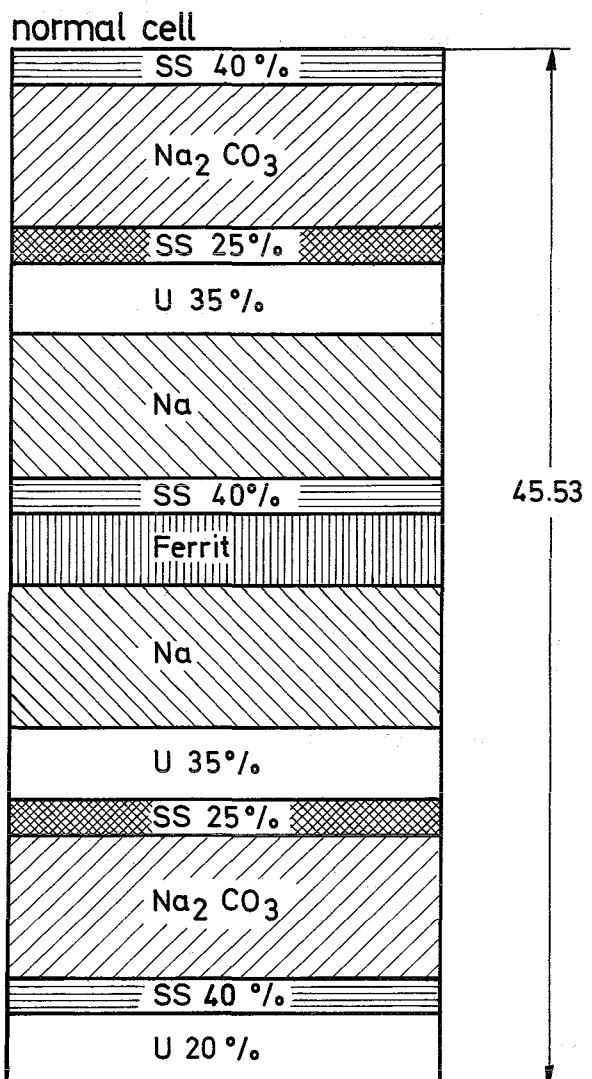


lower rest cell

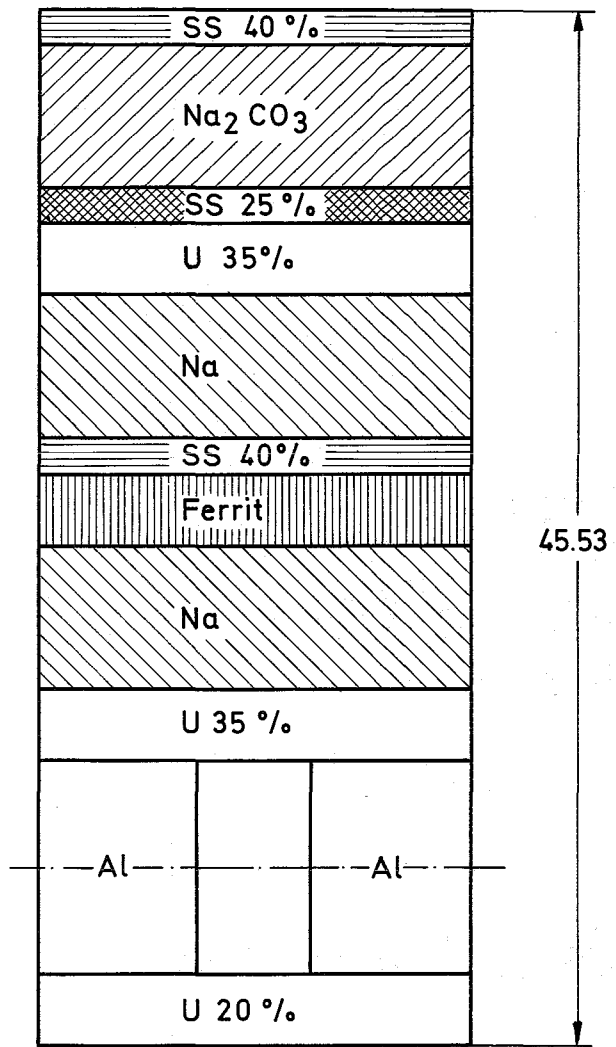
Fig. 2a Cells of the zone R1



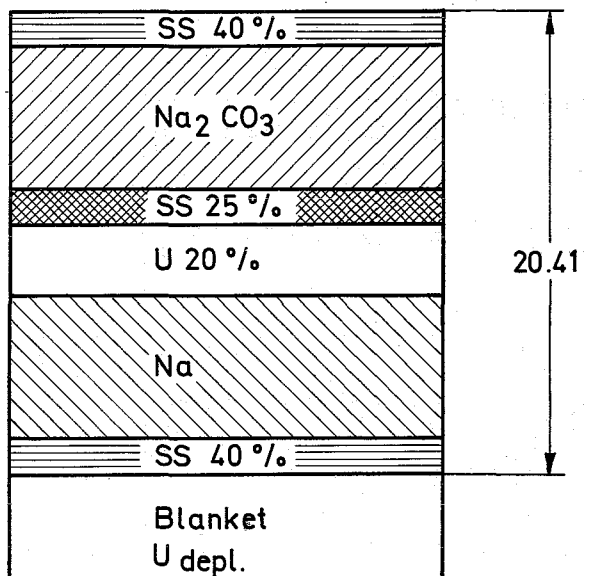
upper rest cell



normal cell



window cell



lower rest cell

Fig. 2b
Cells of the zone R2

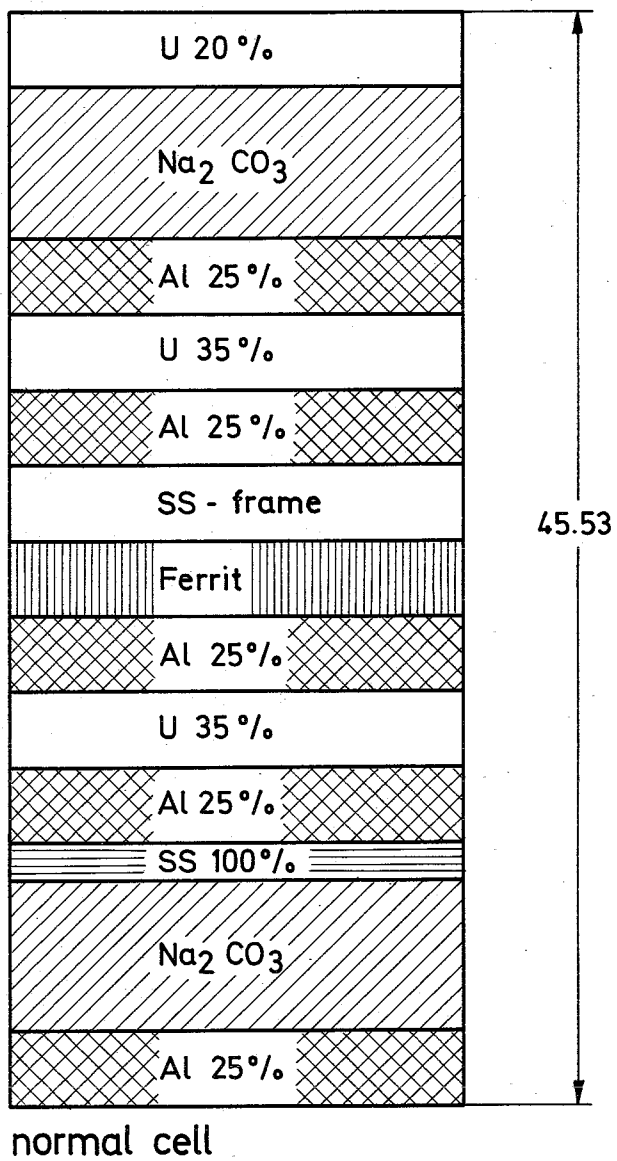
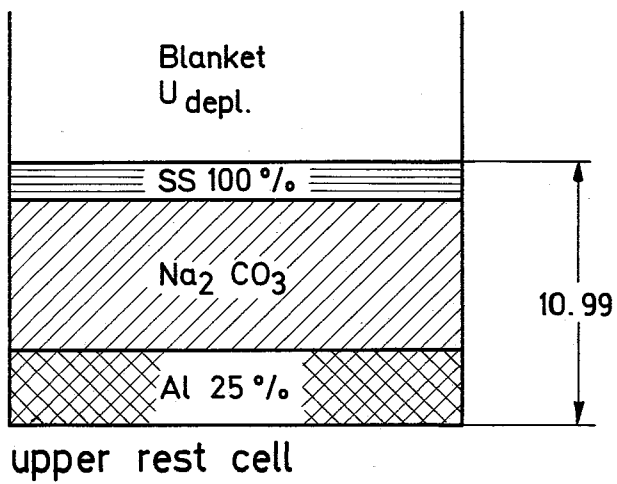
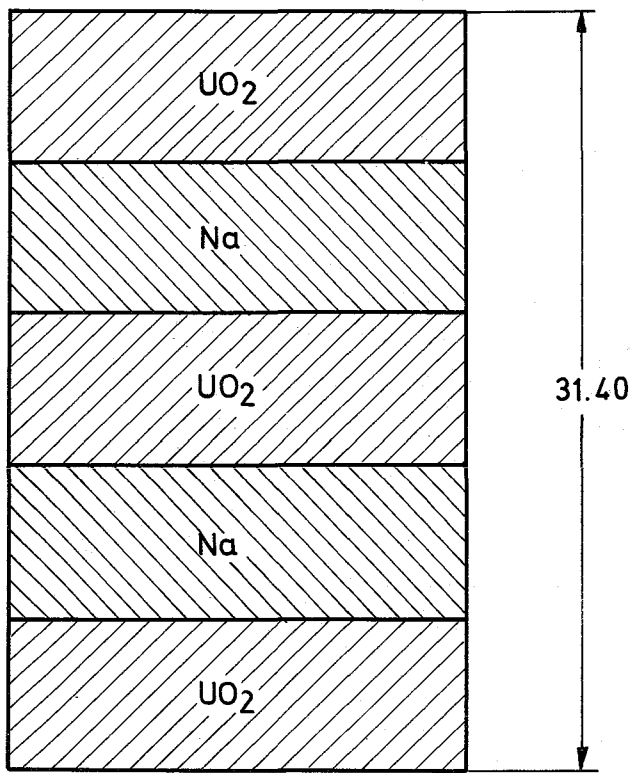
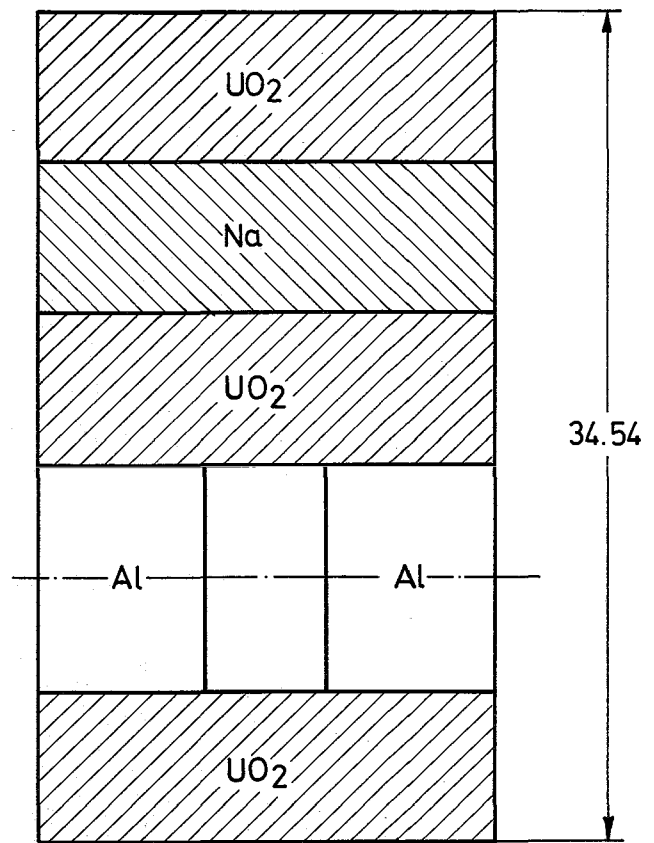


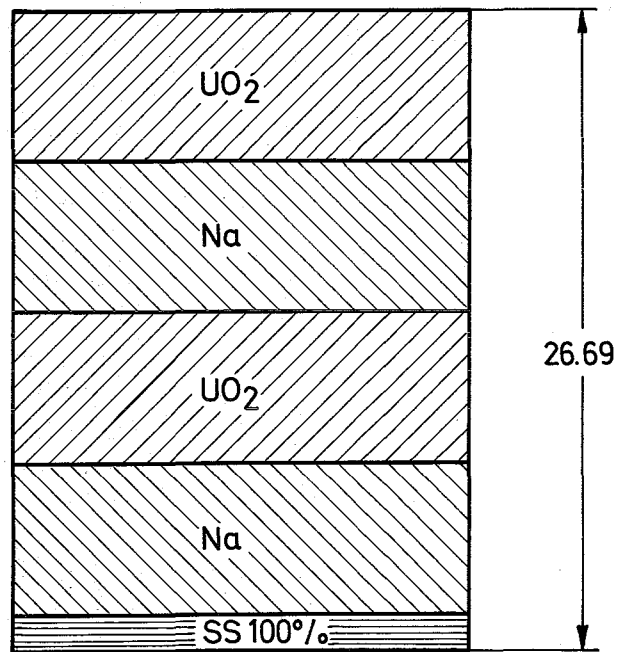
Fig.2c Cell of the Zone R2"



normal cell

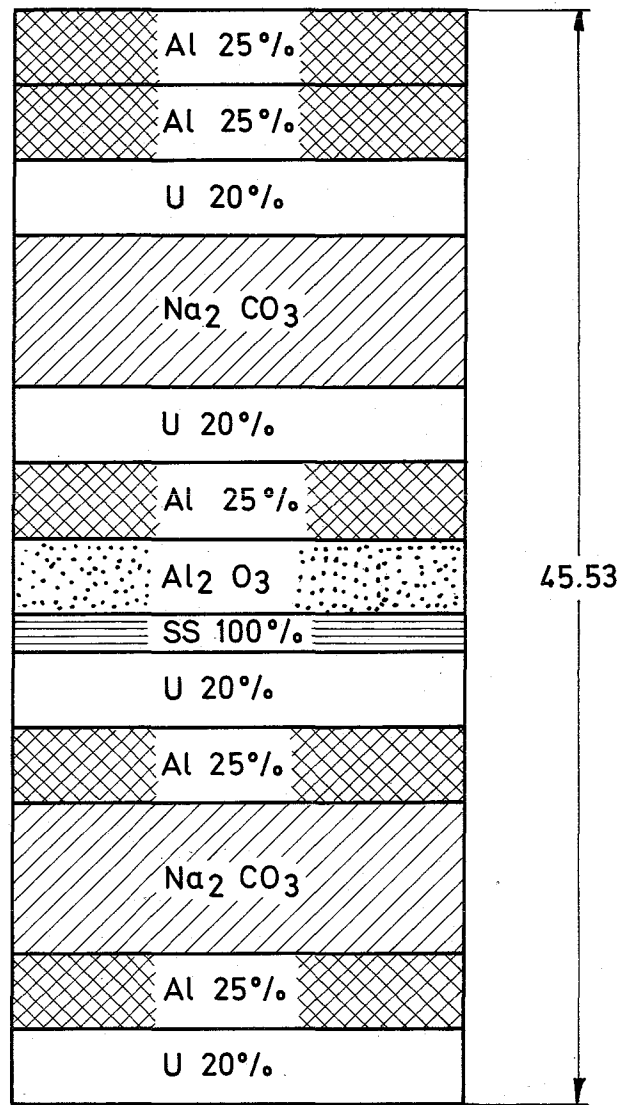


window cell

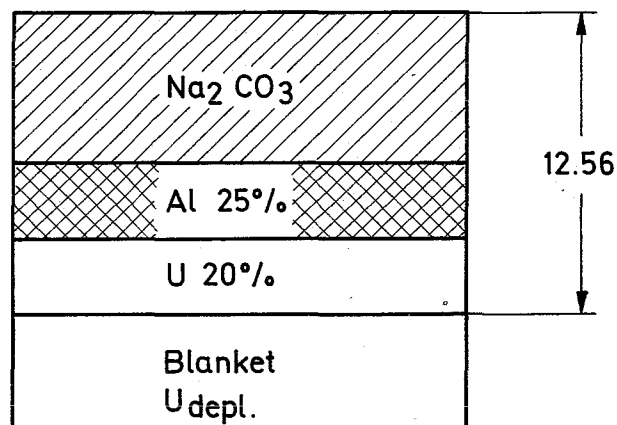


upper rest cell

Fig.2d Cells for Breeder Blanket

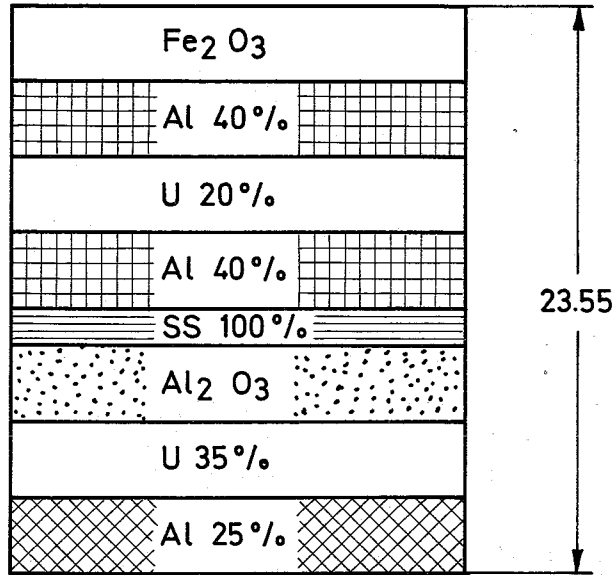


normal cell

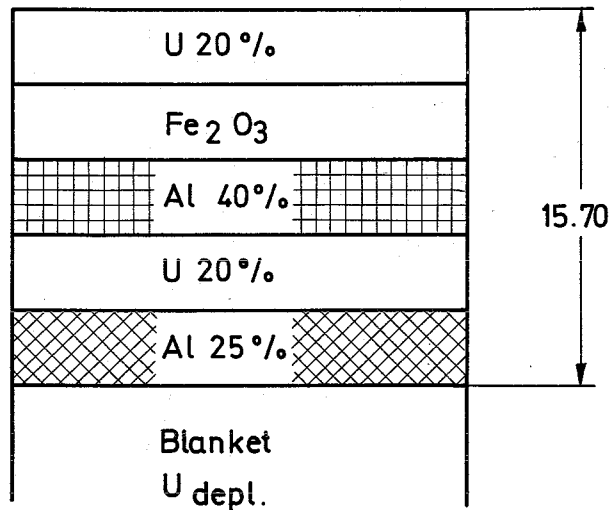


lower rest cell

Fig.3a Cells for SNEAK Safety - and Shim Rods in Zone R1 and Z1

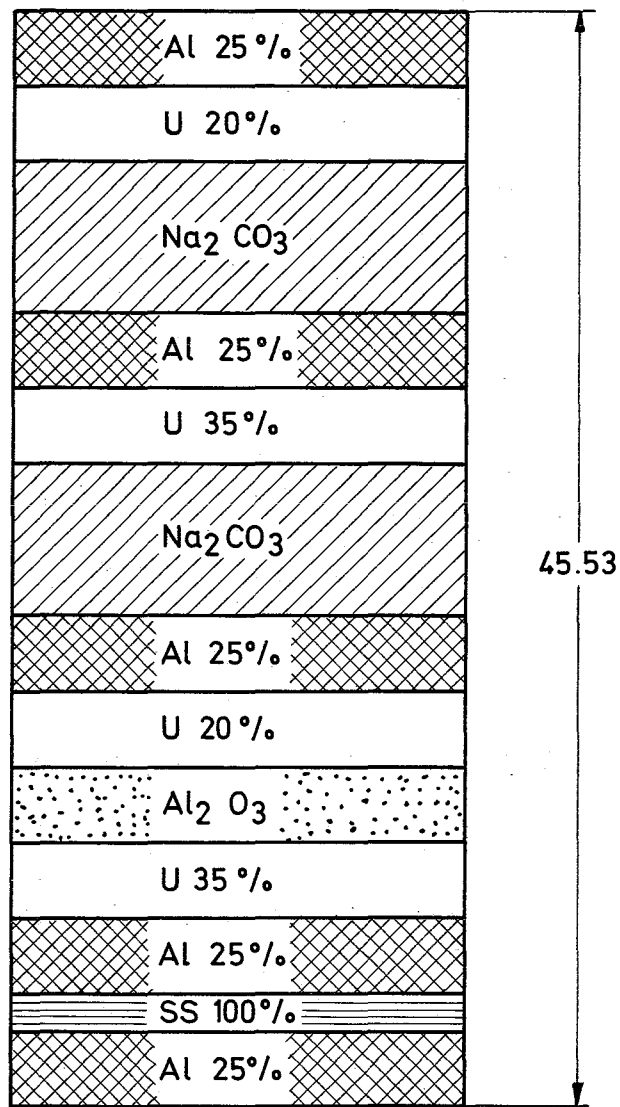


normal cell



lower rest cell

Fig.3b Cells for SNEAK Shim Rod in Zone R2 and Z2



normal cell

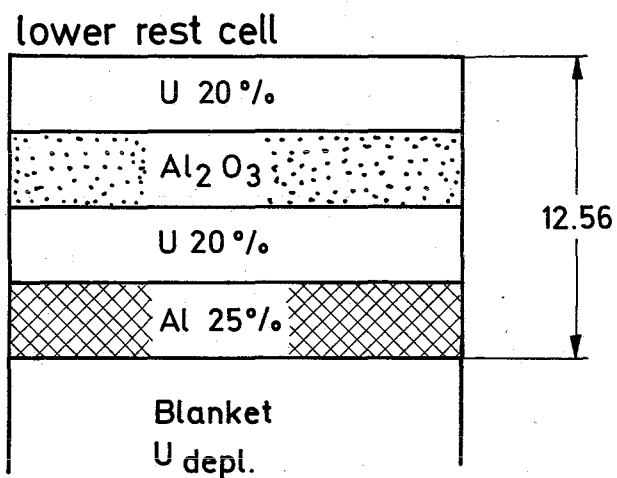


Fig.3c Cells for SNEAK Safety Rod in Zone R2 and Z2

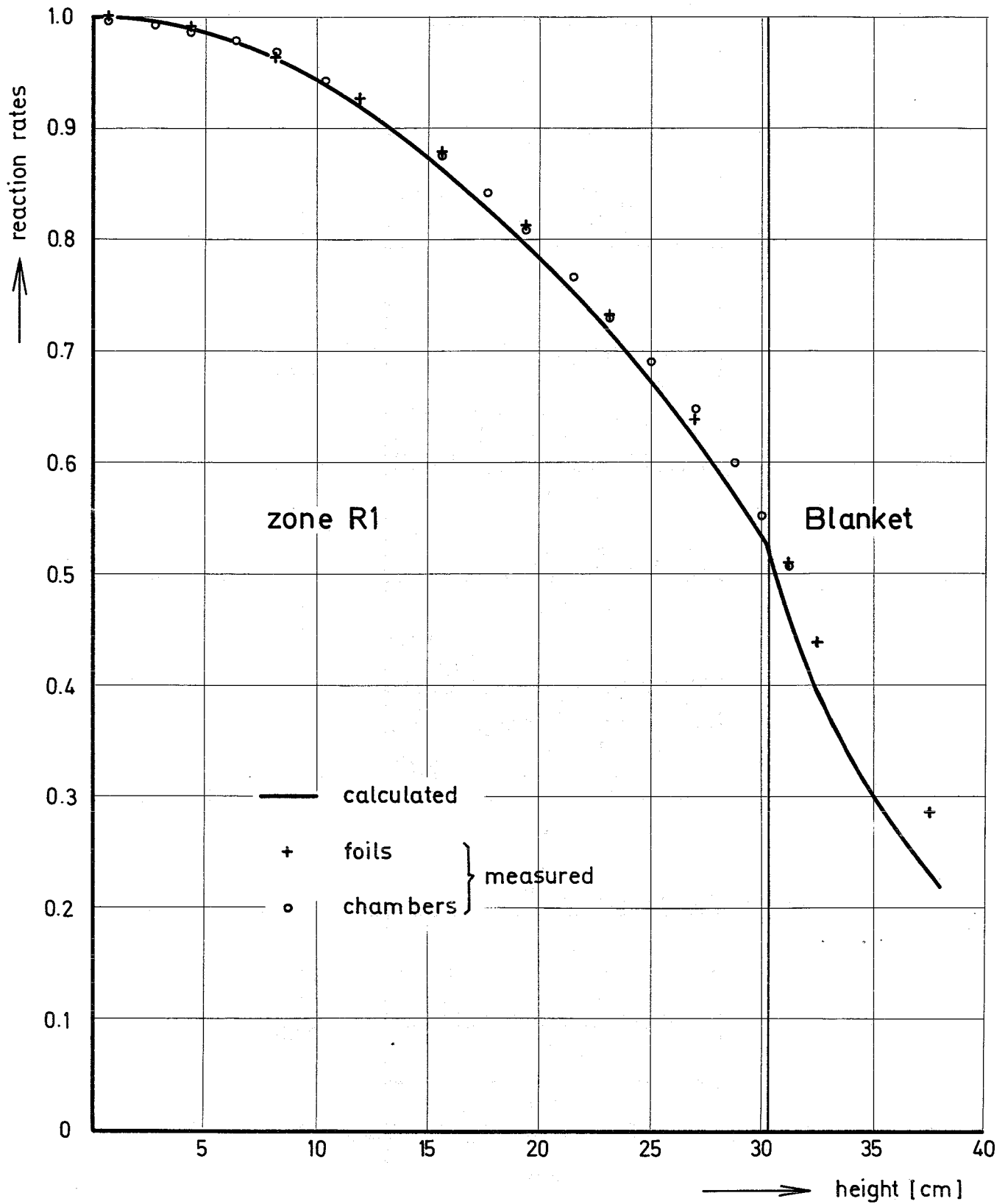


Fig. 4 SNEAK - 2A
 Axial Fission Rate Traverse for U235

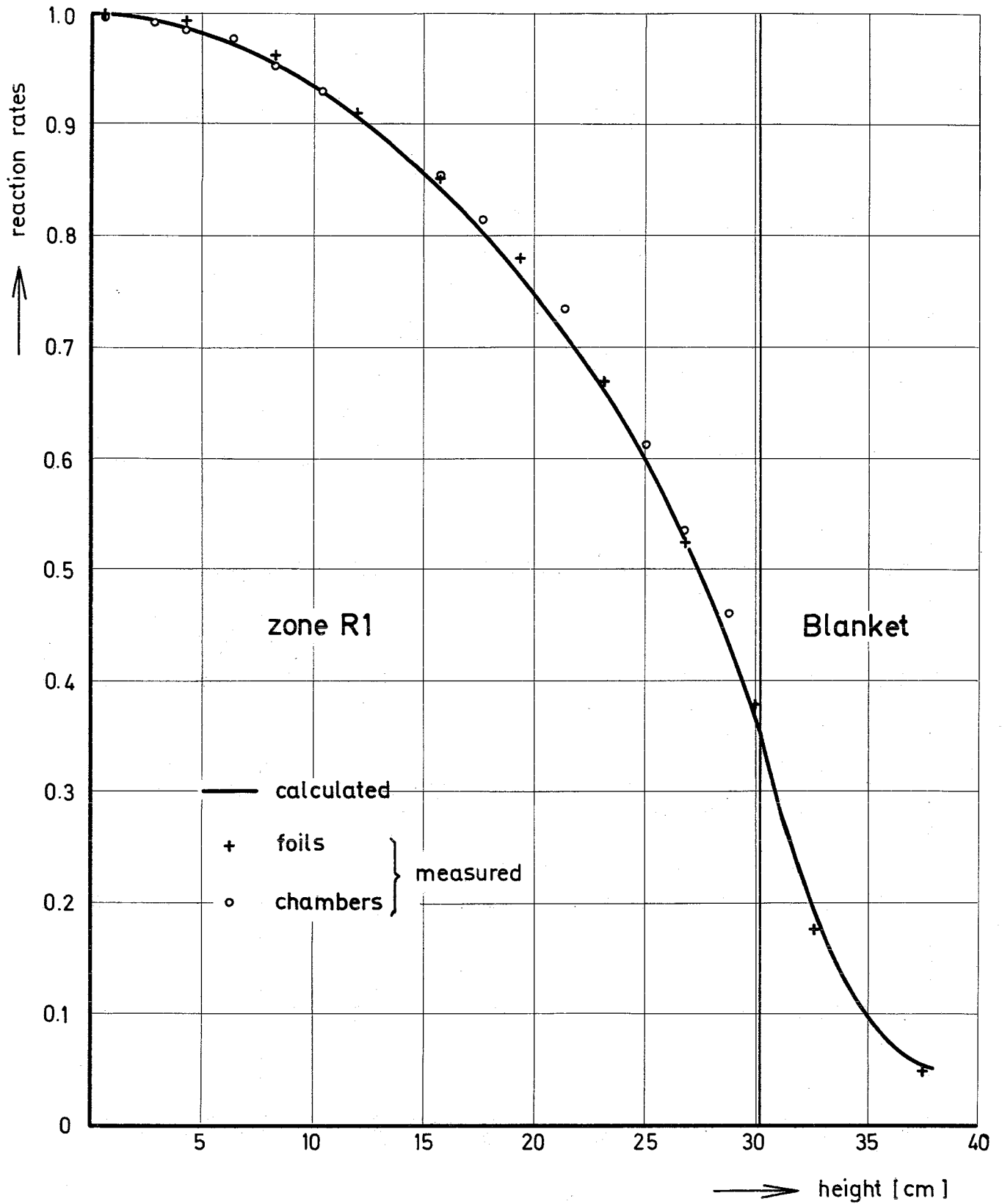


Fig.5 SNEAK - 2A
 Axial Fission Rate Traverse for U238

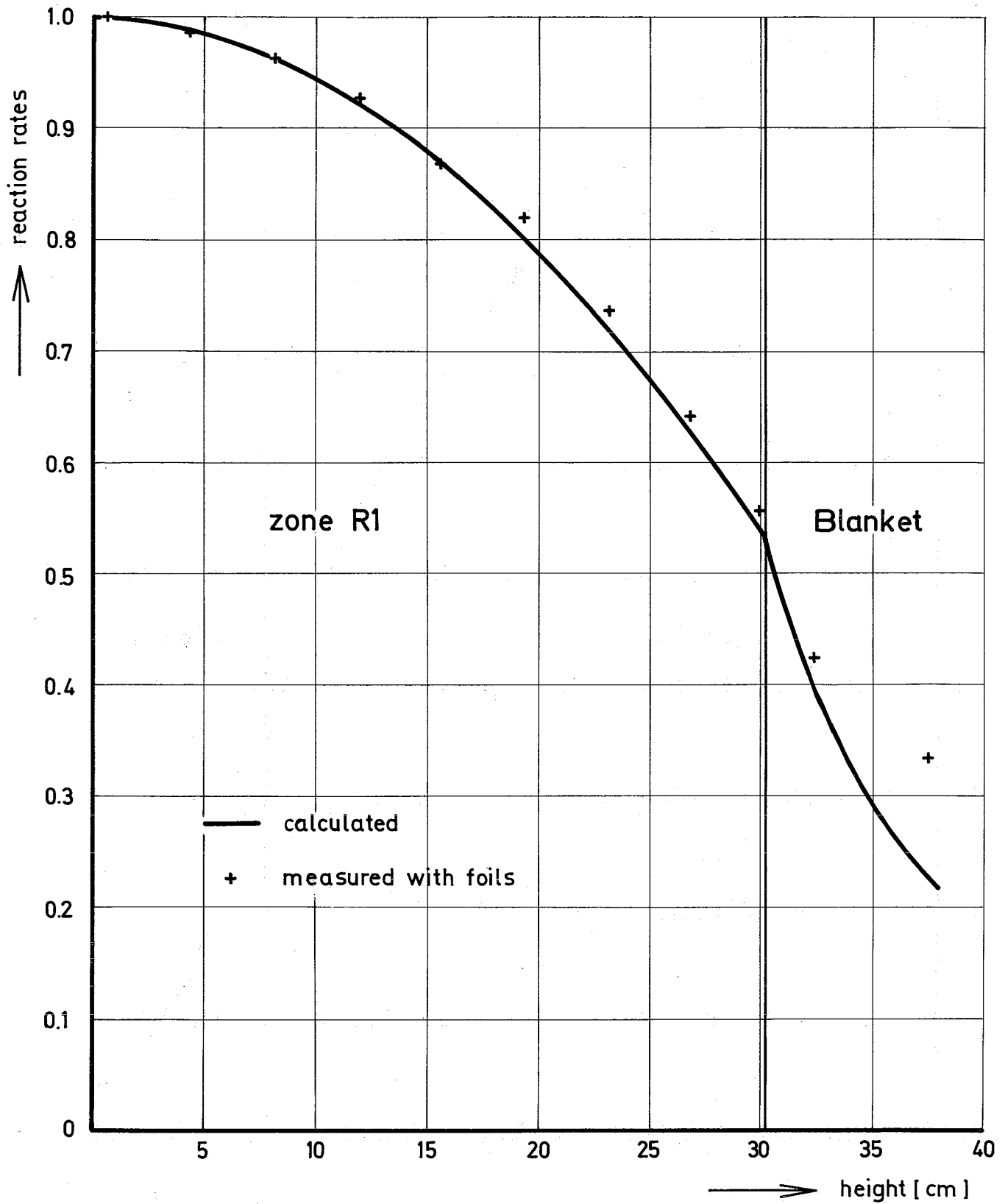
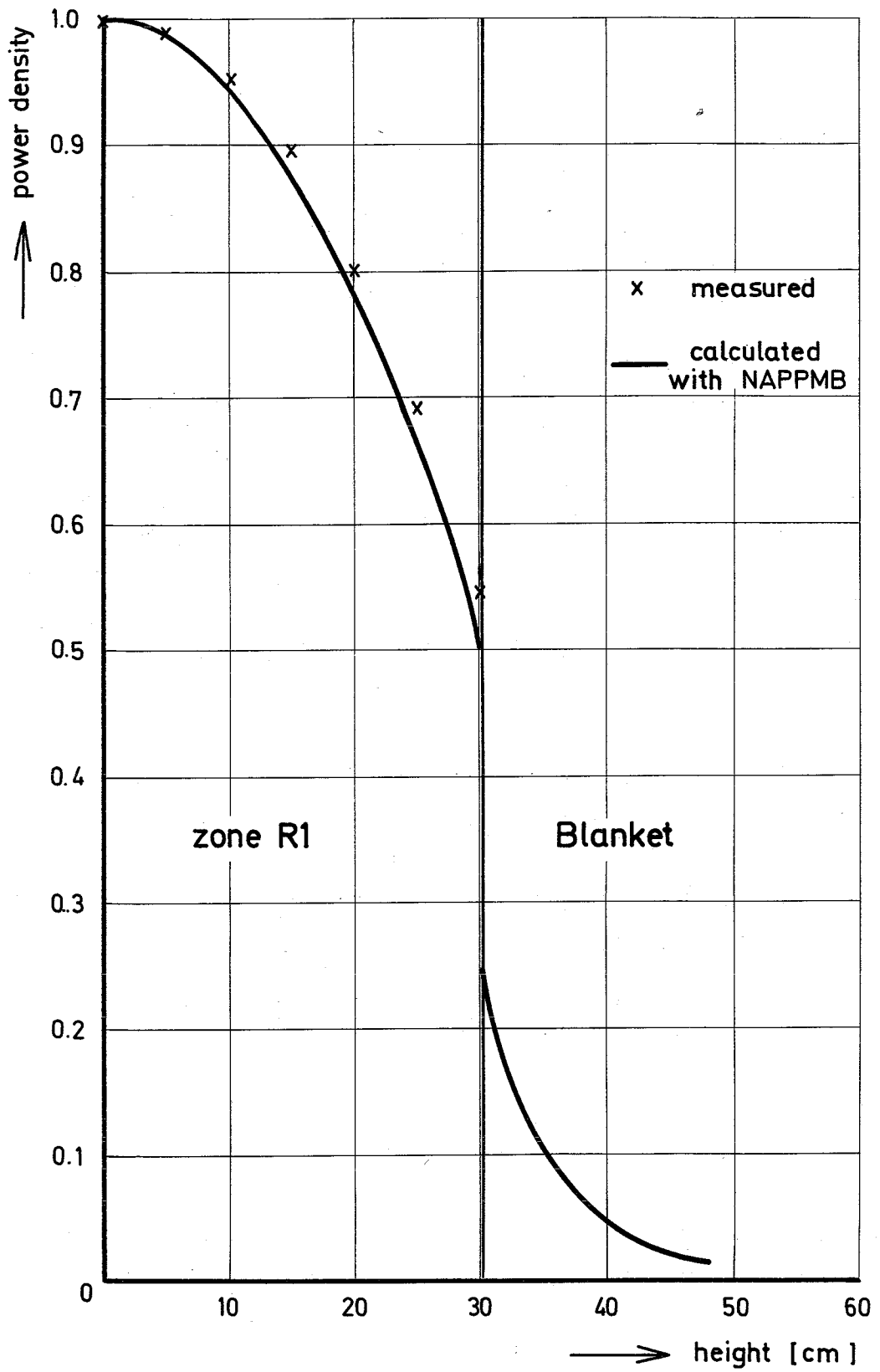


Fig.6 SNEAK - 2A
 Axial Capture Rate Traverse for U238



**Fig.7 SNEAK - 2A
Axial Power Distribution**

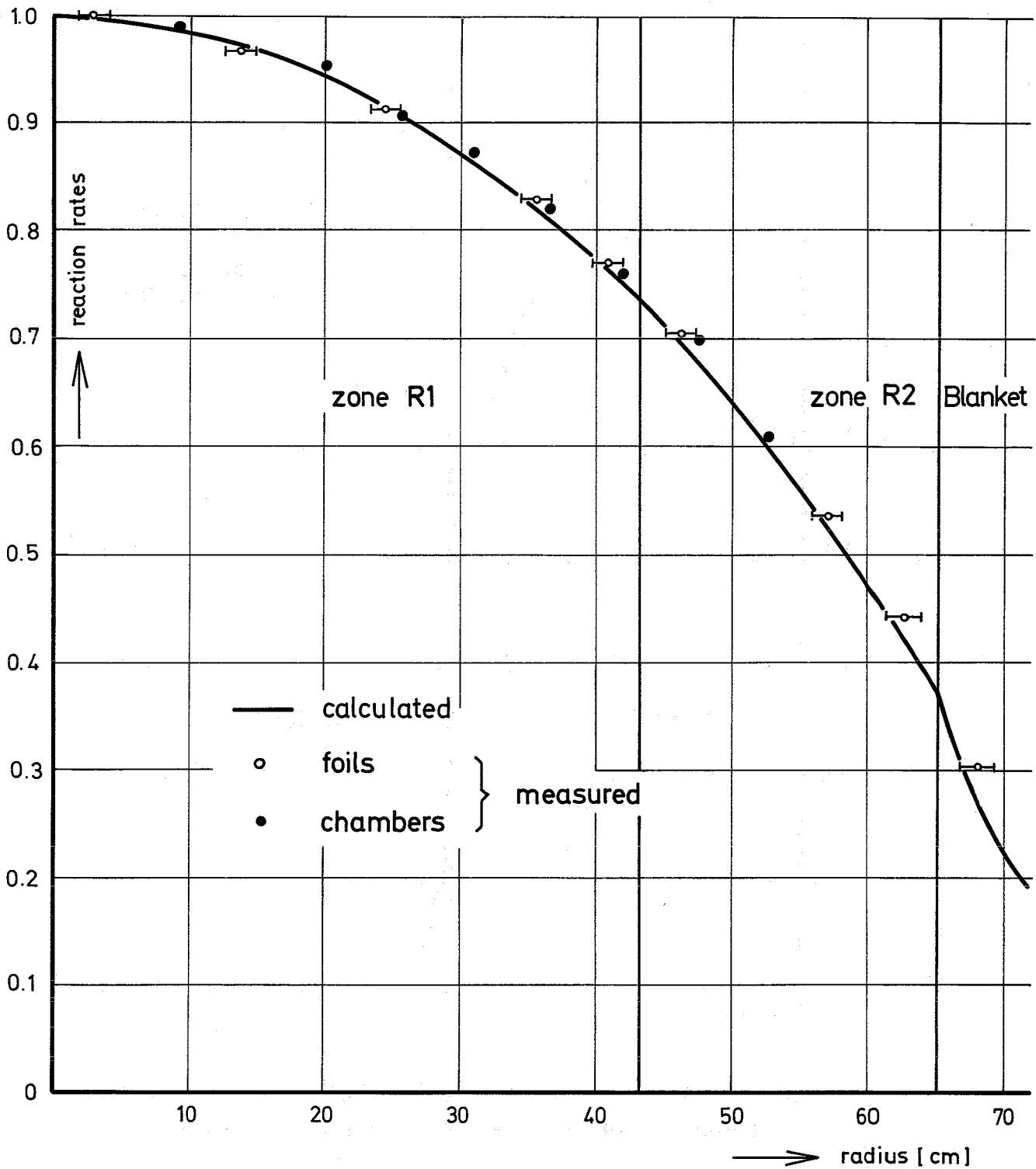


Fig. 8 SNEAK - 2A
Radial Fission Rate Traverse for U235

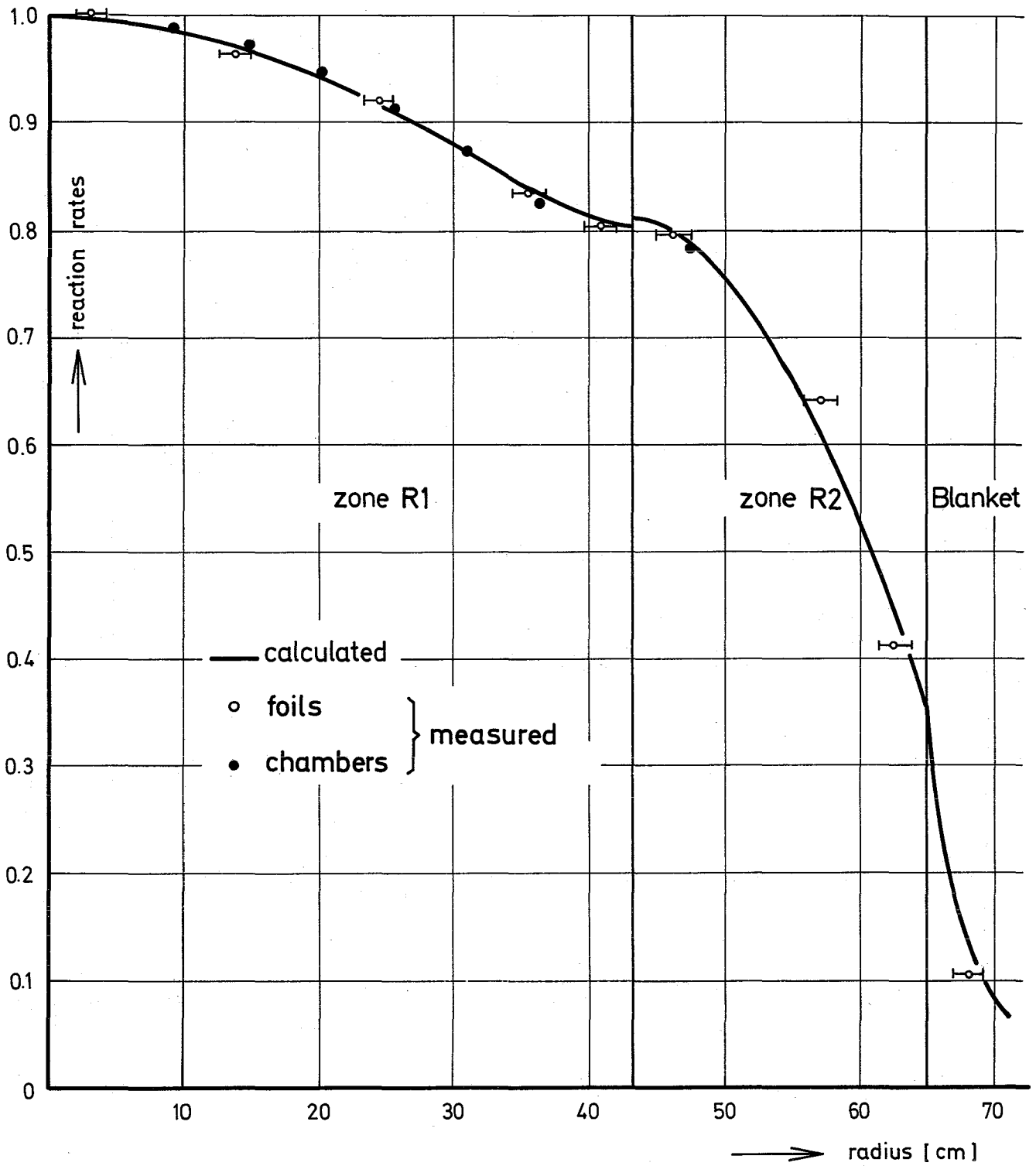


Fig. 9 SNEAK - 2A
Radial Fission Rate Traverse for U238

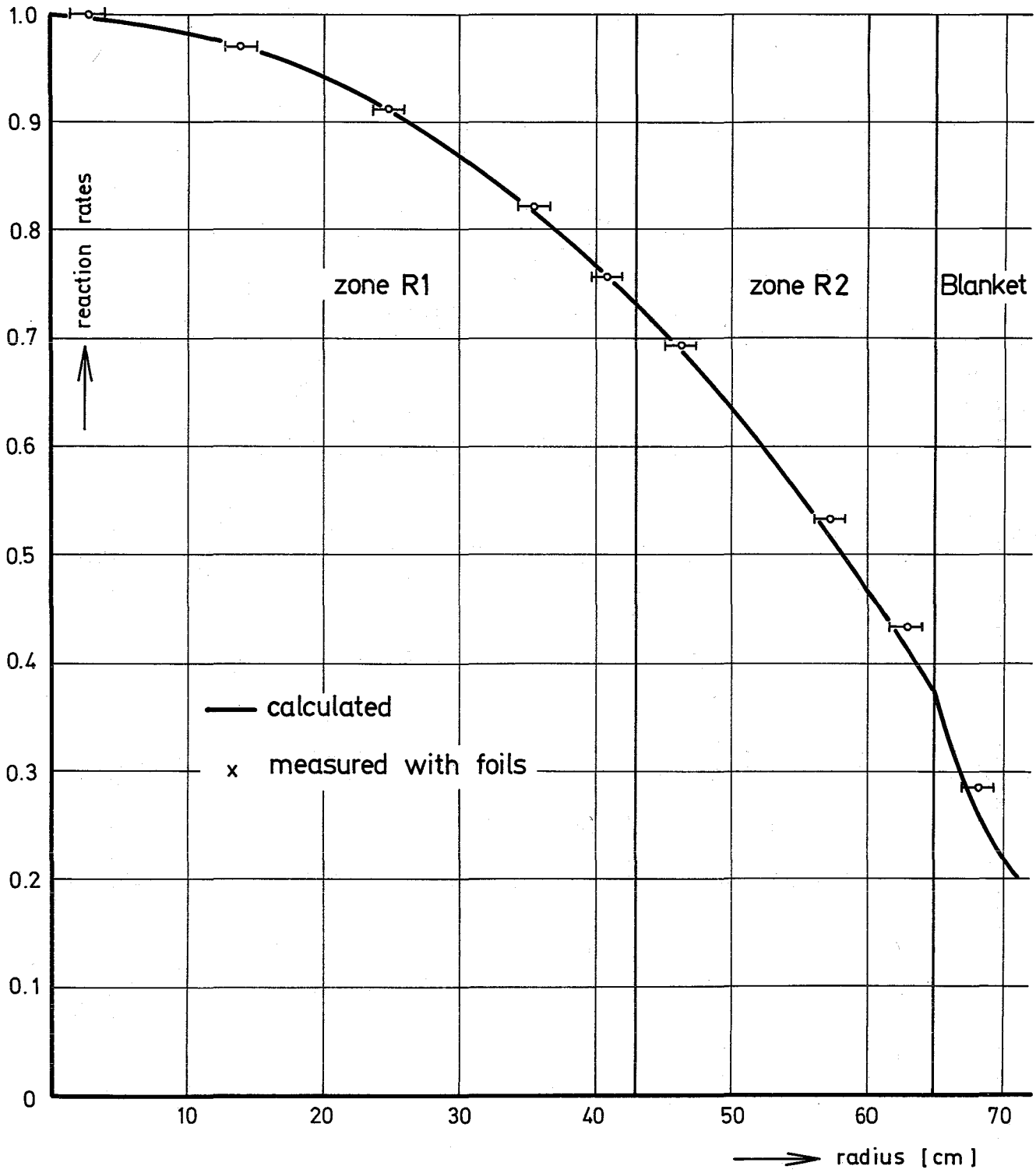


Fig. 10 SNEAK - 2A
Radial Capture Rate Traverse for U238

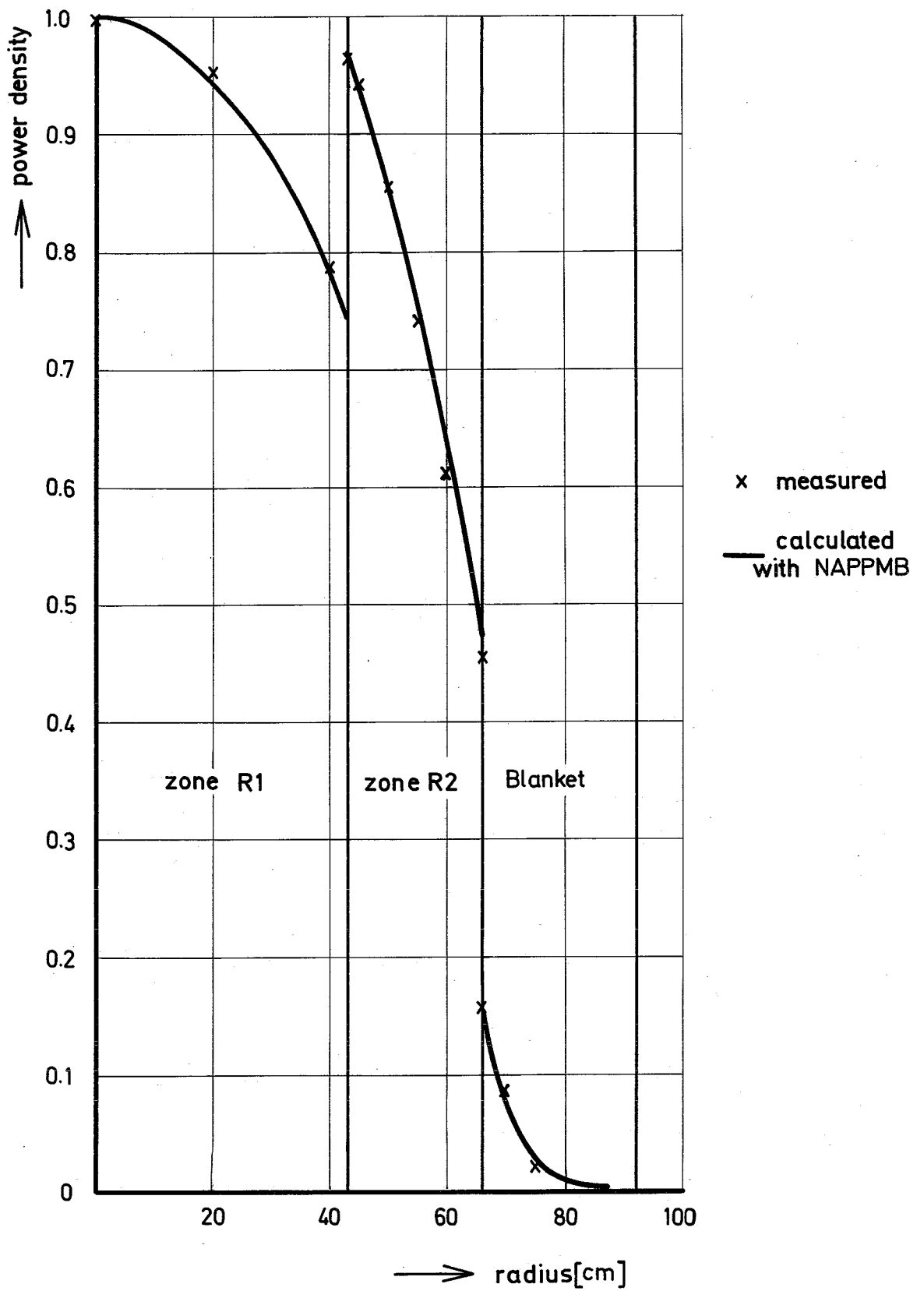


Fig.11 SNEAK - 2A
Radial Power Distribution

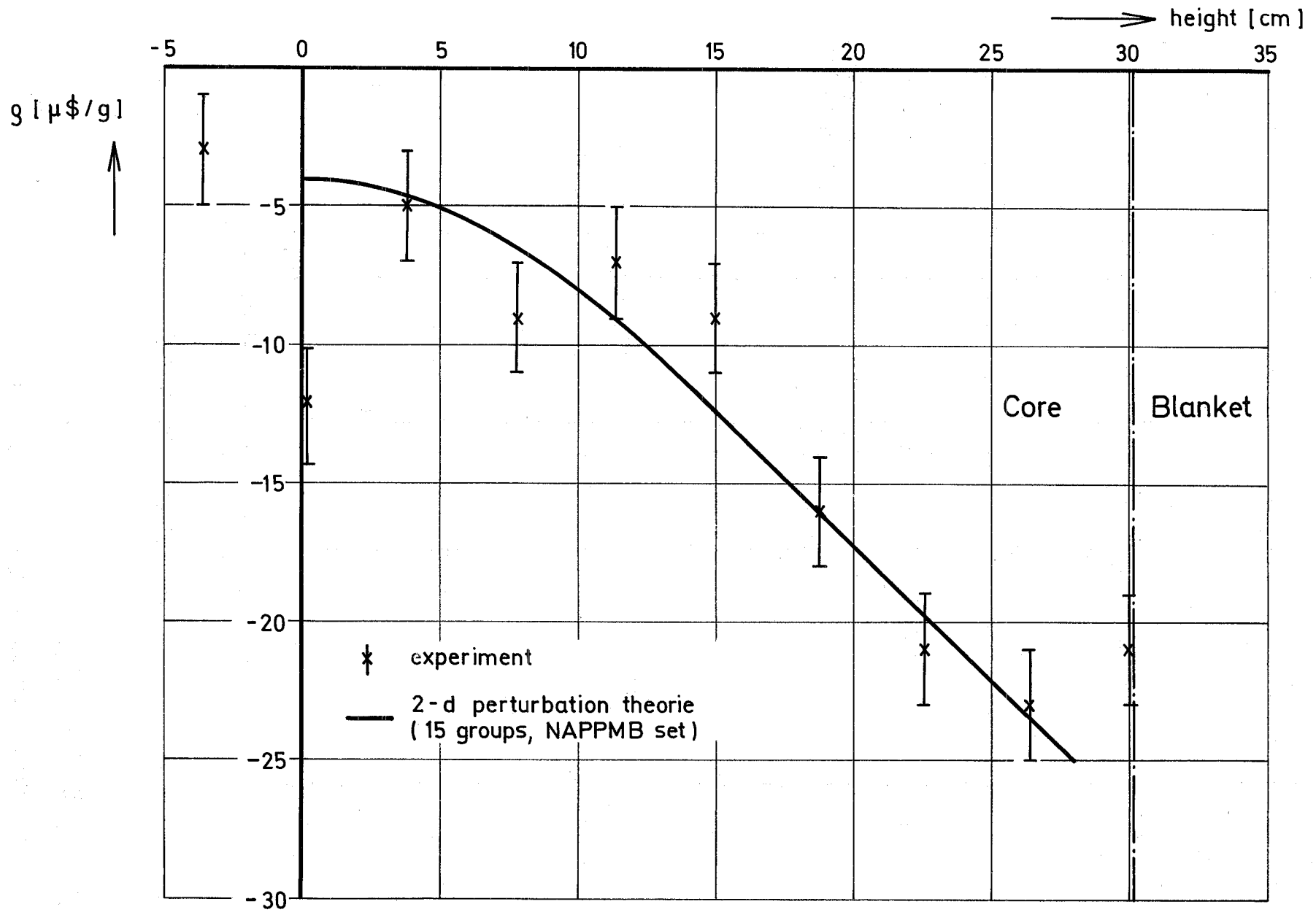
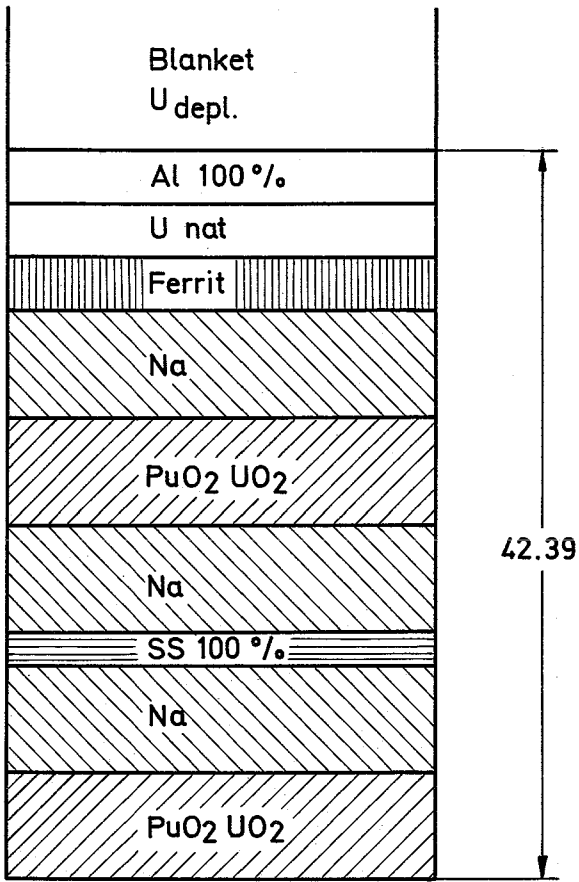
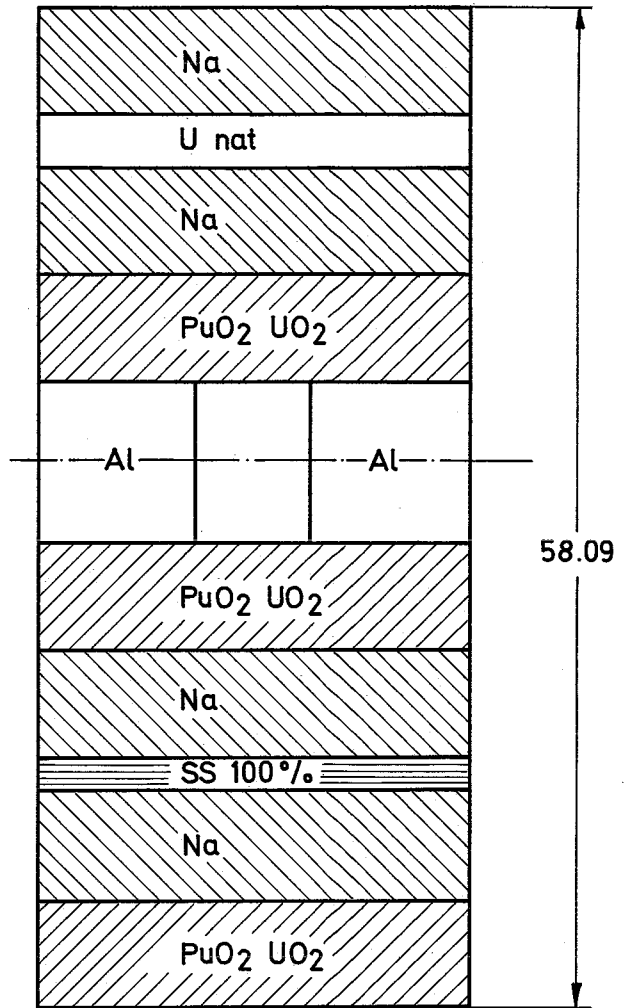


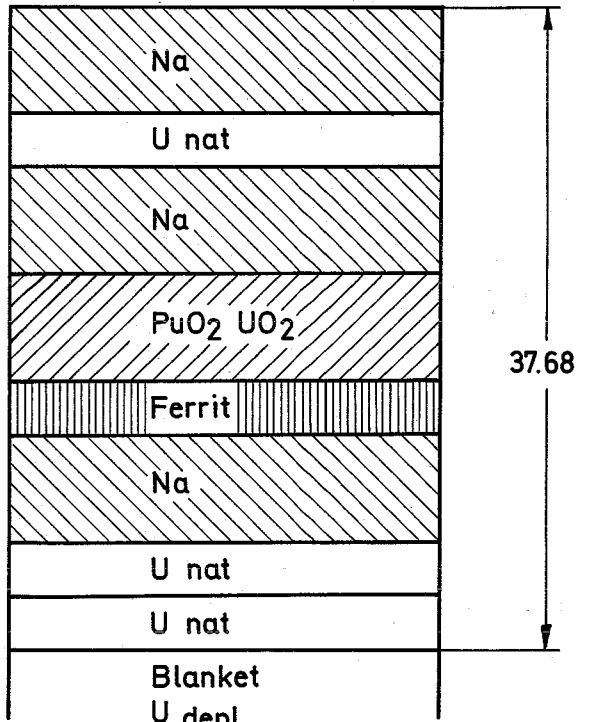
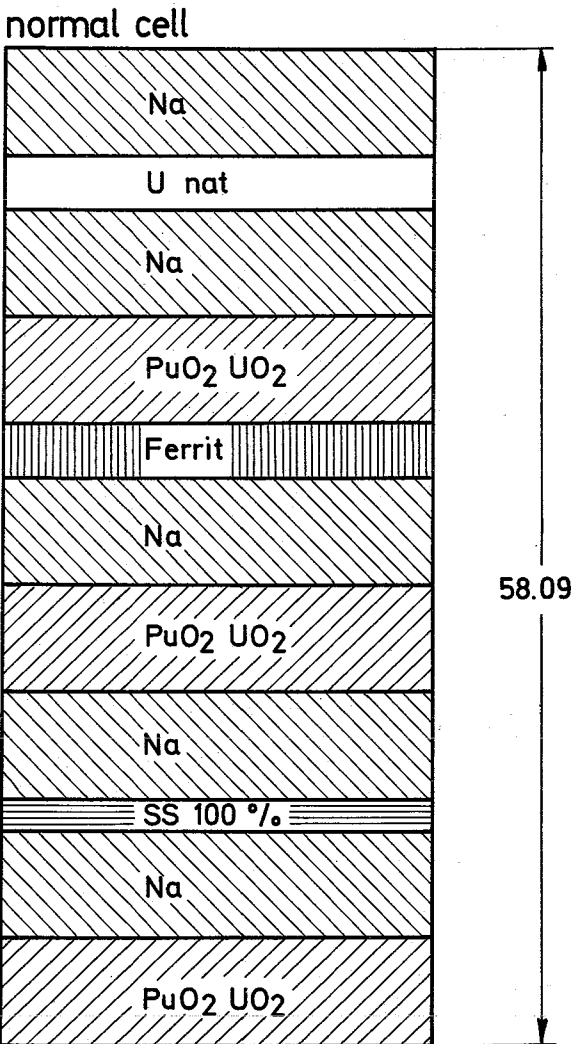
Fig. 12 SNEAK-2A Axial Na-Void Traverse



upper rest cell

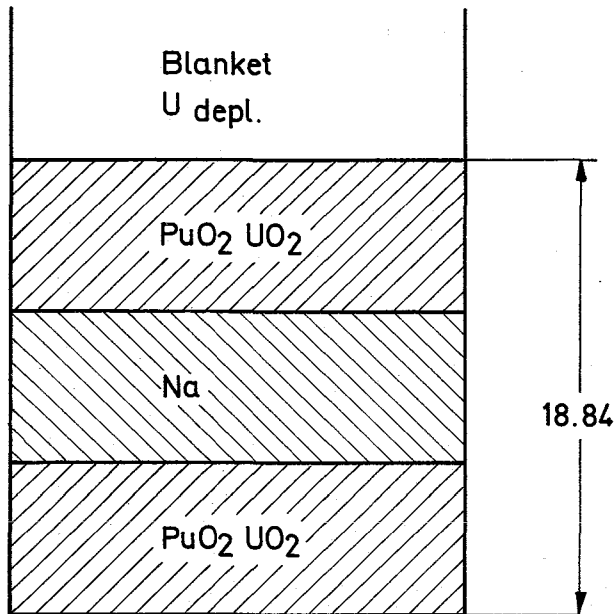


window cell

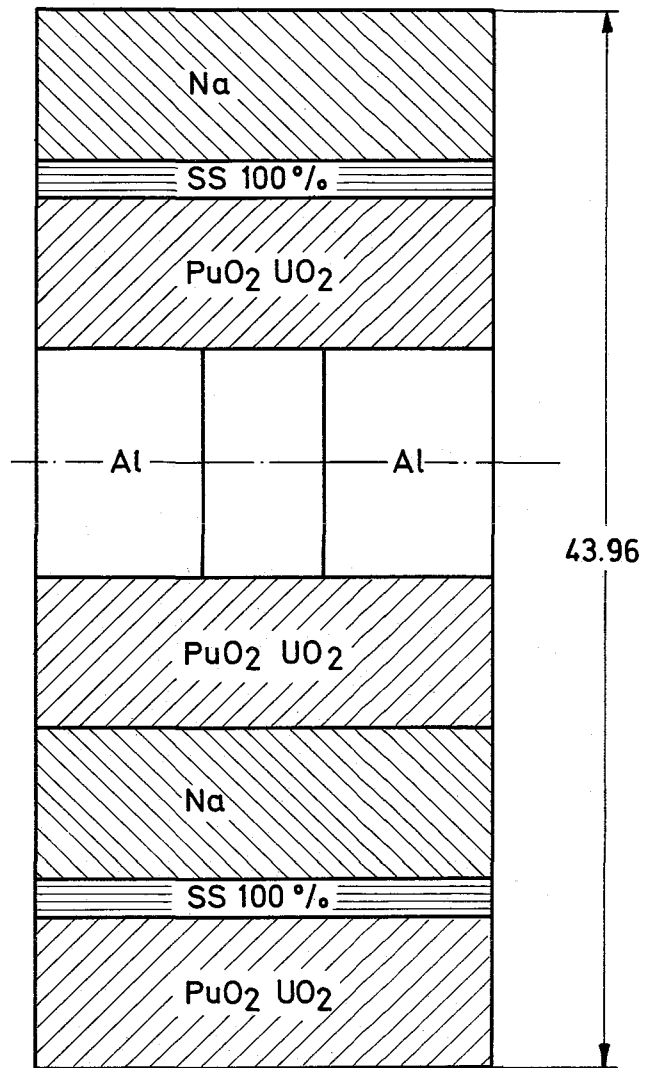


lower rest cell

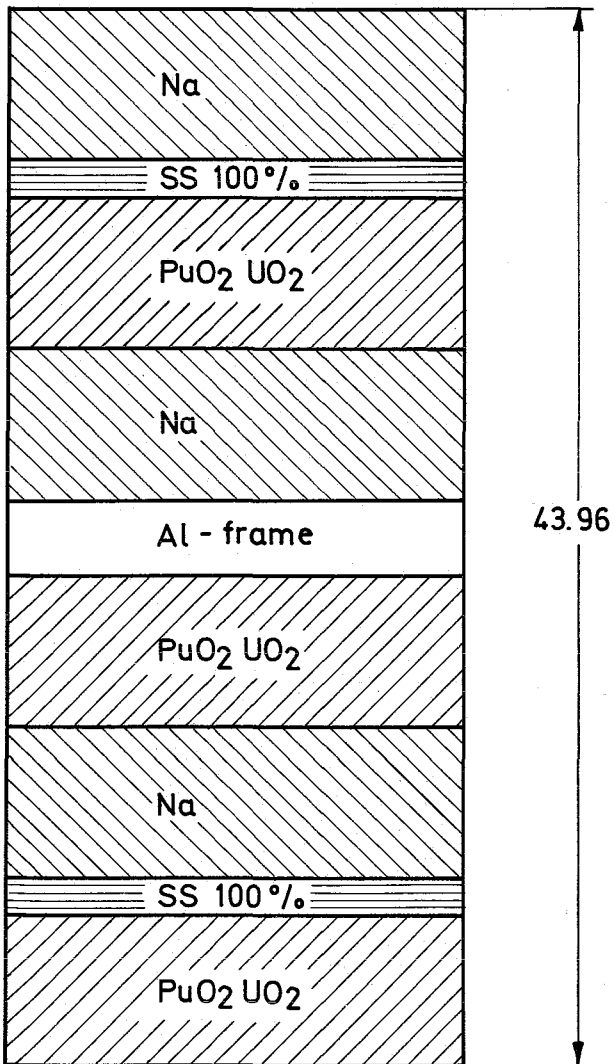
Fig. 13 a
Cells of the Zone Z1



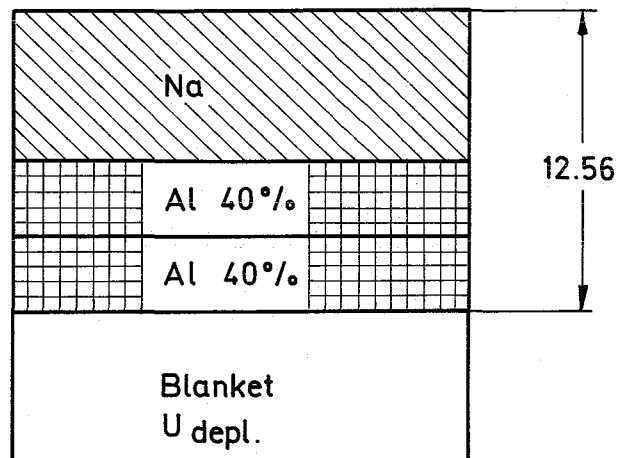
upper rest cell



window cell

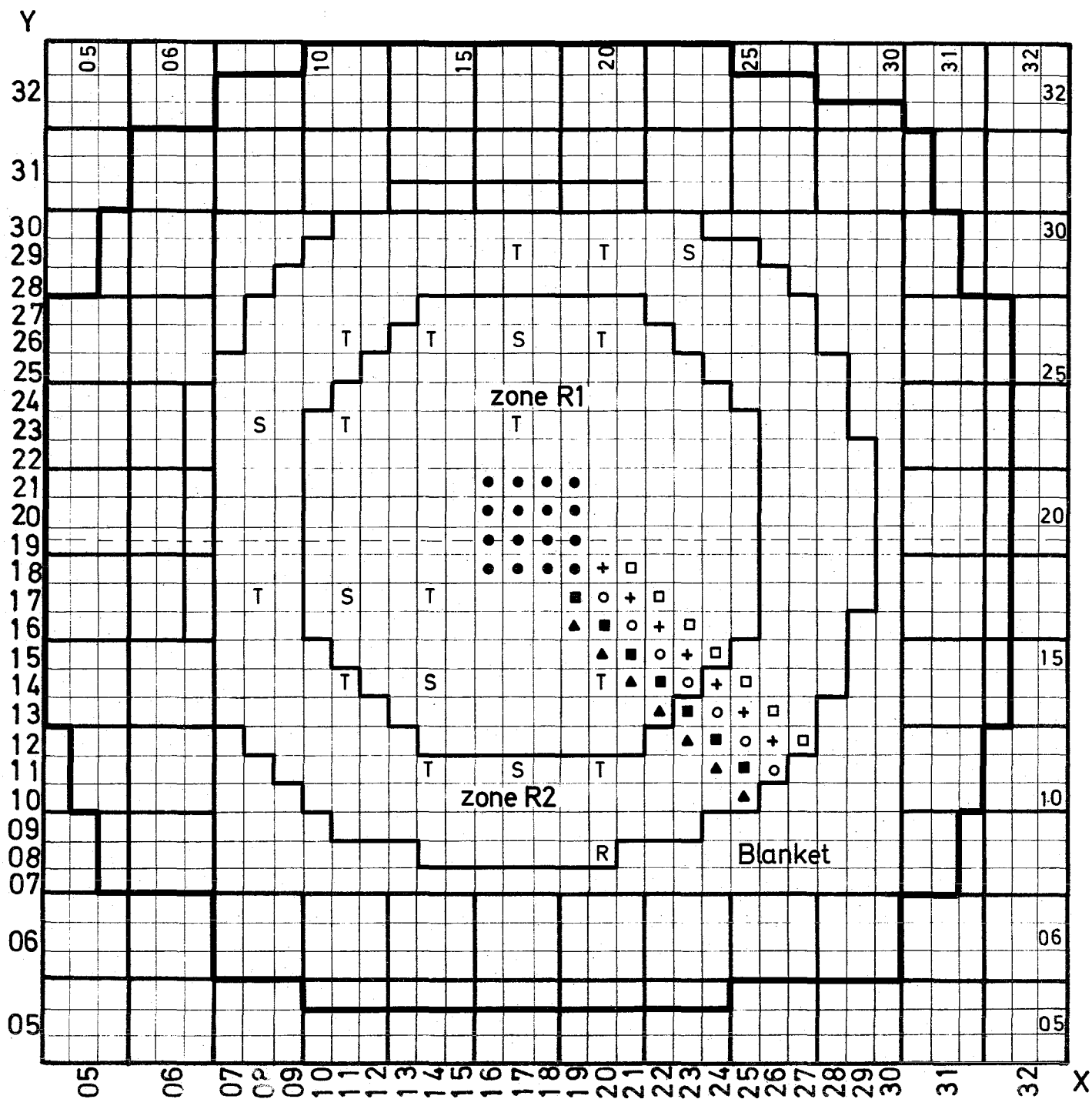


normal cell



lower rest cell

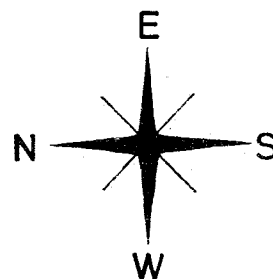
Fig.13b Cells of the Zone Z2



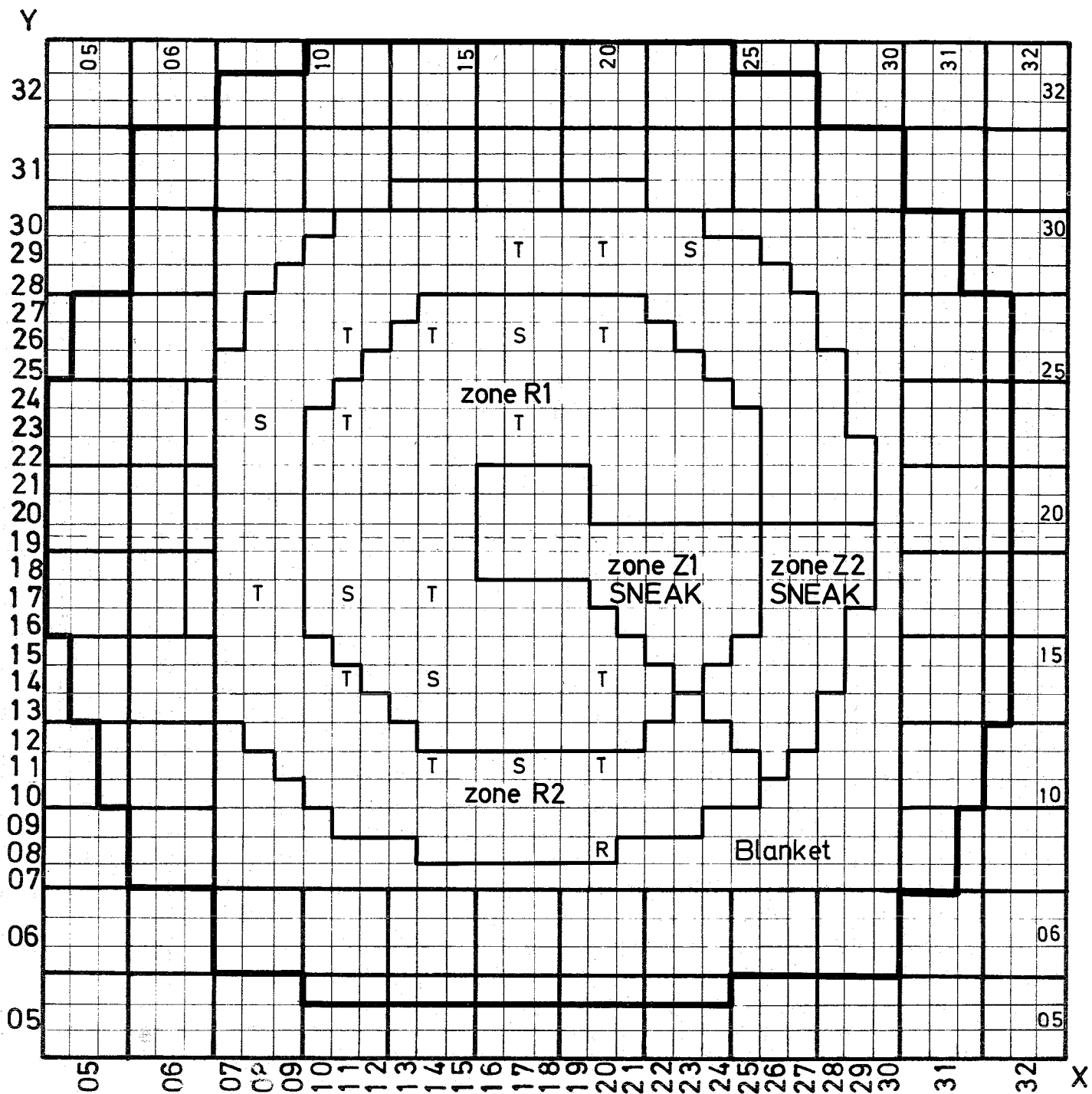
Substitution
 SNEAK-2A → SNEAK-2B

- | | | |
|------|---|---|
| step | 1 | ● |
| " | 2 | ○ |
| " | 3 | + |
| " | 4 | ■ |
| " | 5 | □ |
| " | 6 | ▲ |

Fig. 14



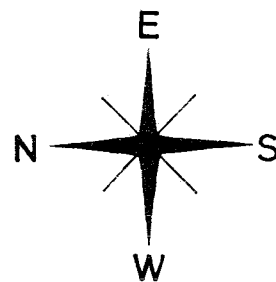
scale 1:10



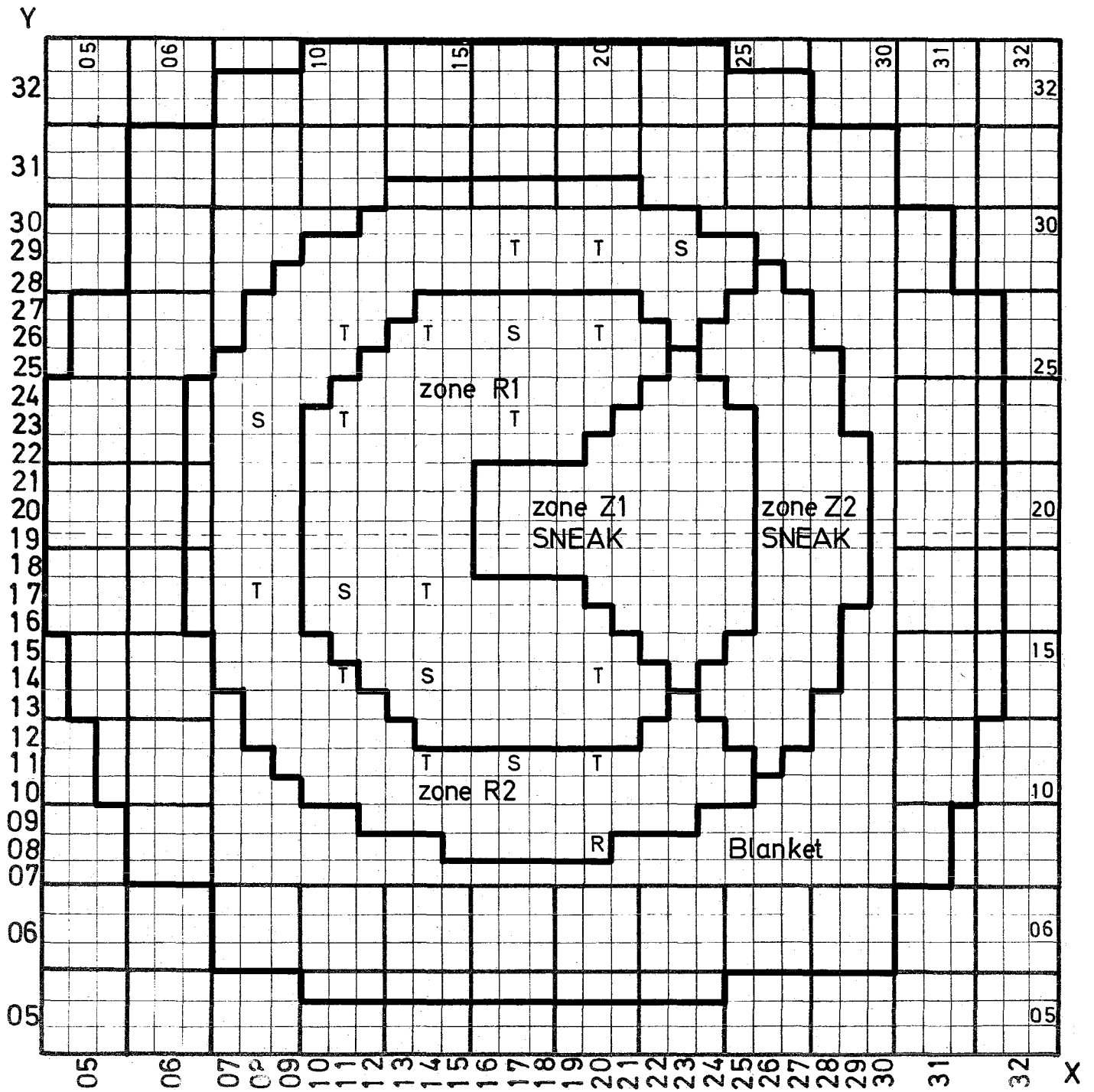
Substitution
 SNEAK-2A → SNEAK-2B

step 7

Fig. 15



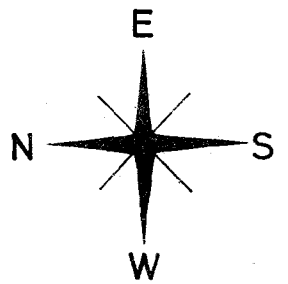
scale 1:10



SNEAK- 2B

(Final Configuration of Substitution Experiment)

Fig. 16



scale 1:10

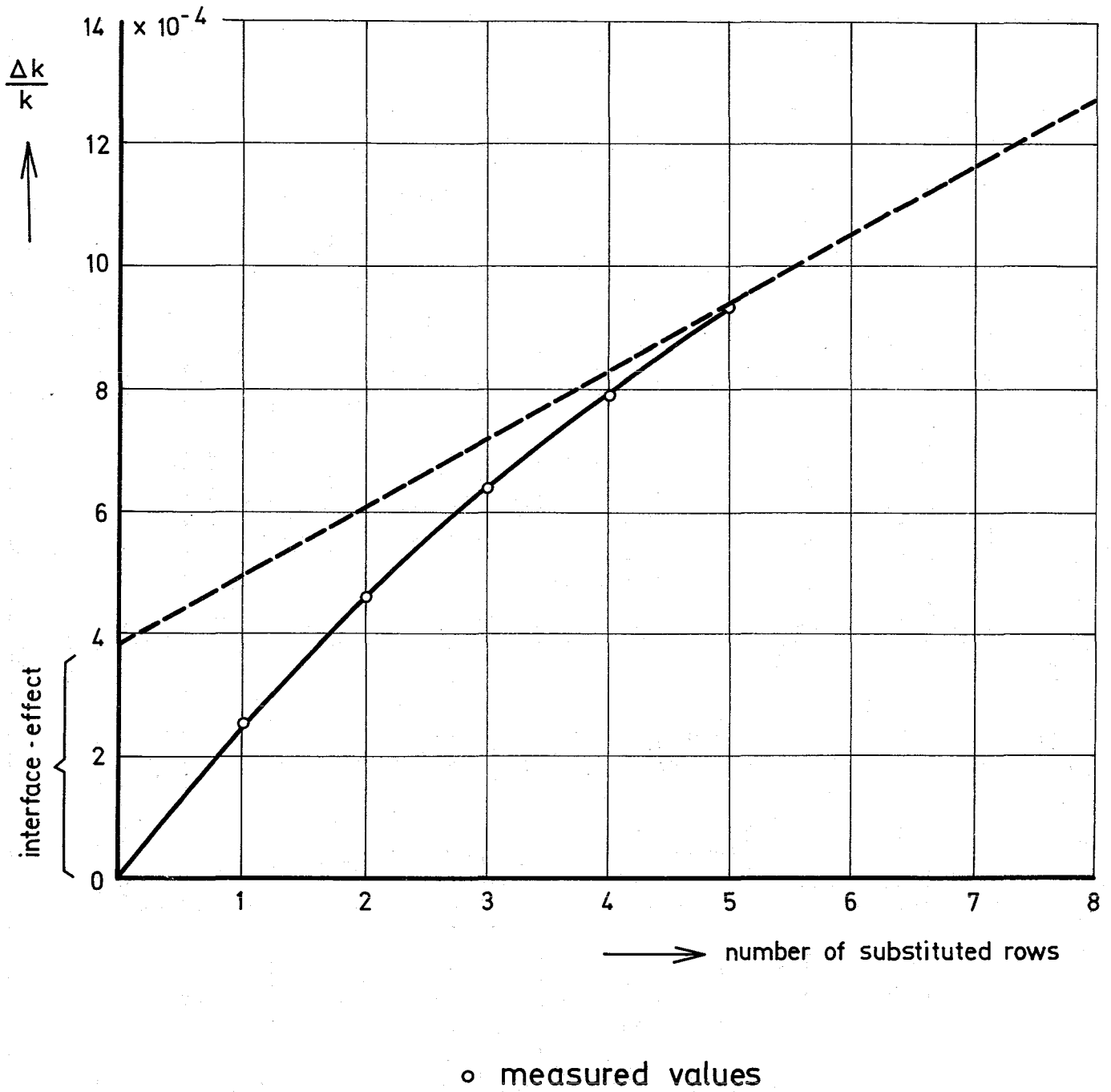
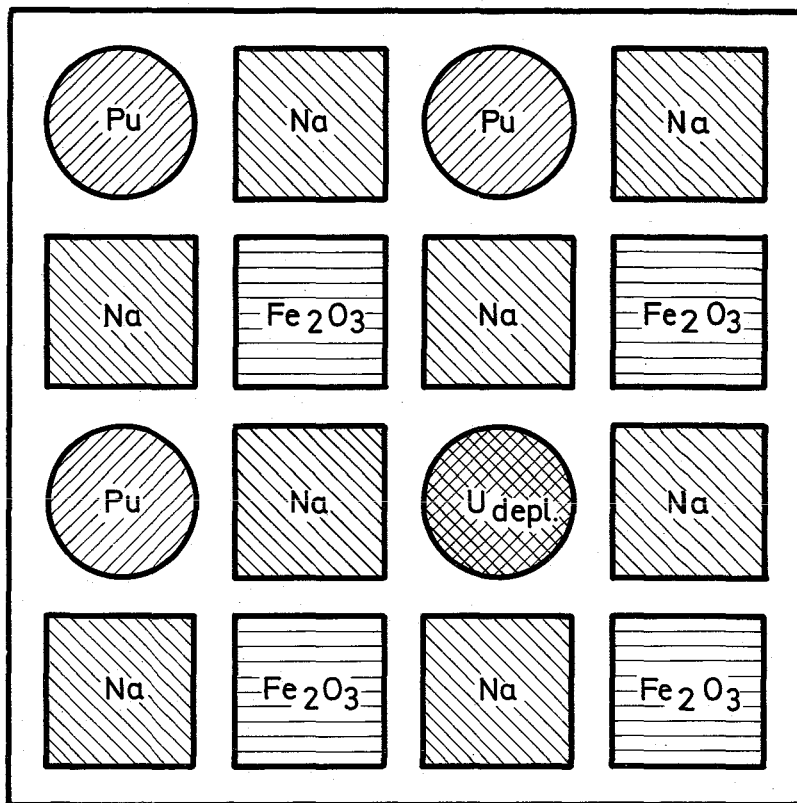


Fig.17 Substitution SNEAK-2A \longrightarrow SNEAK-2B



Cross Section Normal Cell Zone Z1 (MAS.)

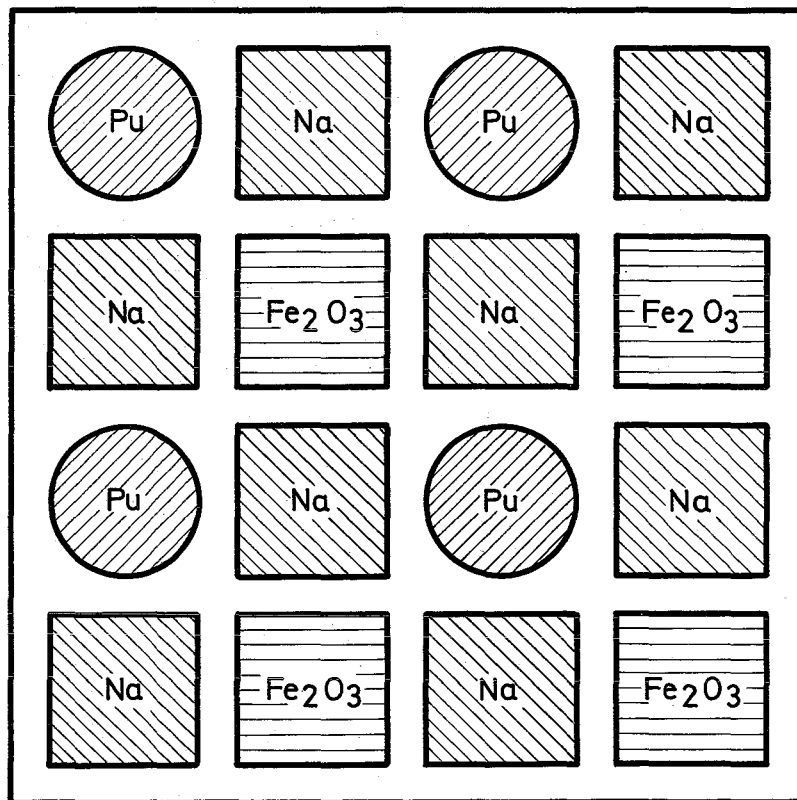
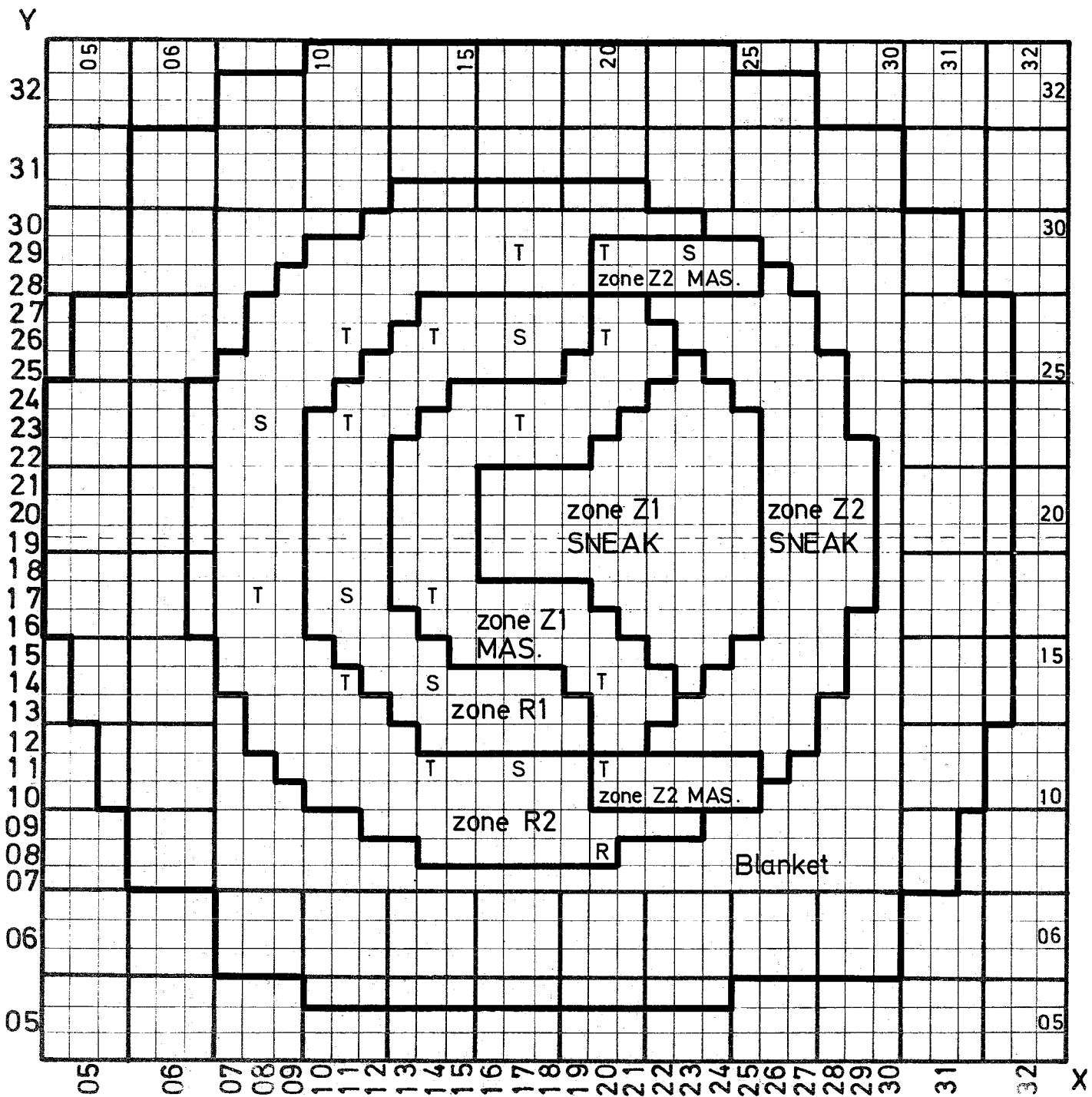
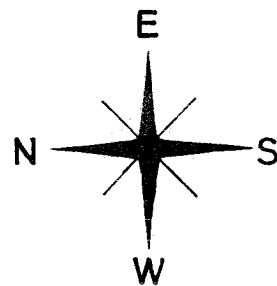


Fig. 18 Cross Section Normal Cell Zone Z2 (MAS.)

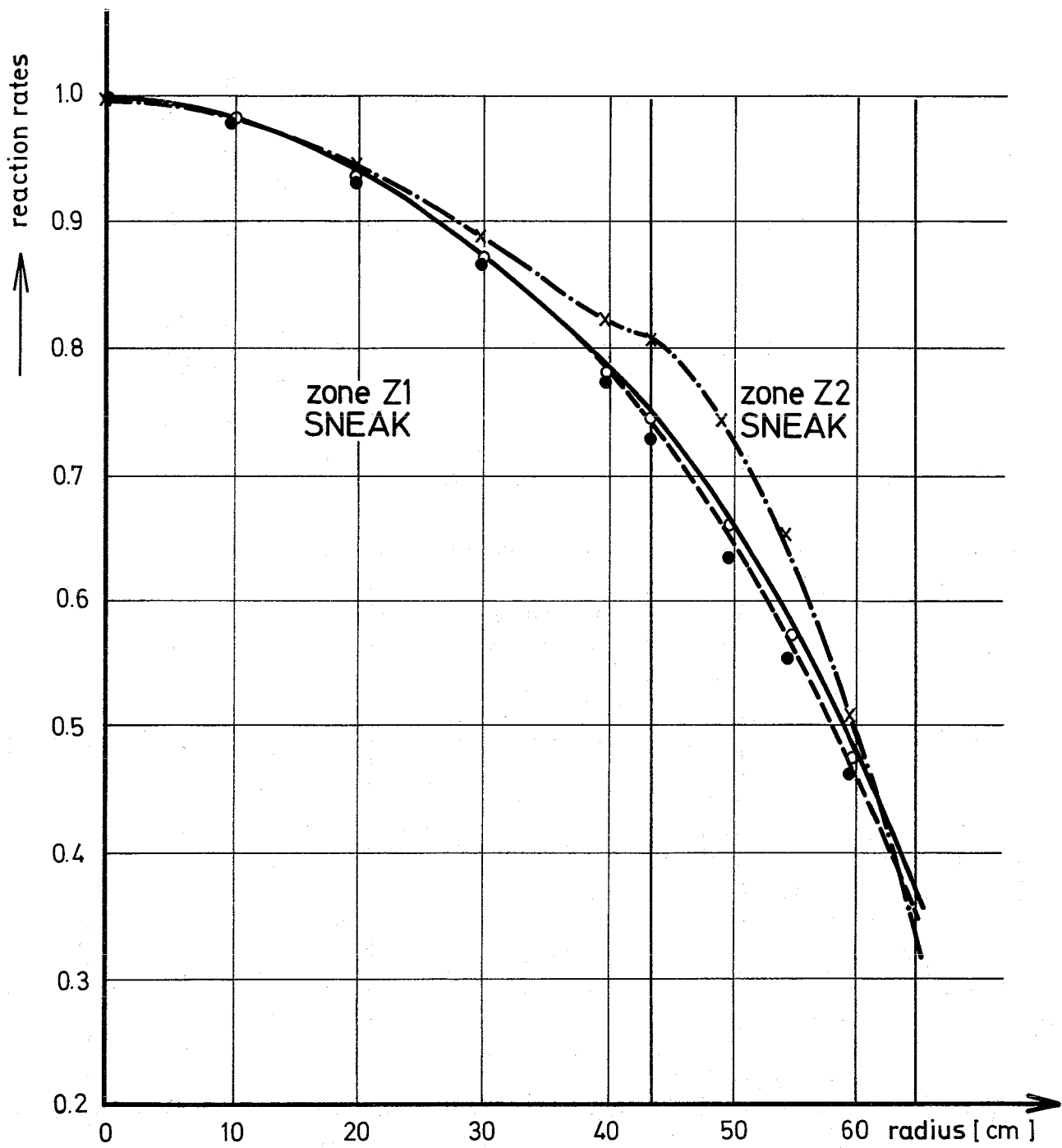


Cross Section of SNEAK - 2C
(Reference Core)

Fig. 19



scale 1:10



	U238 f	Pu239	U235
Theory	— · —	—	- - -
Exp.	x	o	•

Fig. 20 Radial Rate Traverses through SNEAK-2C, Core Region

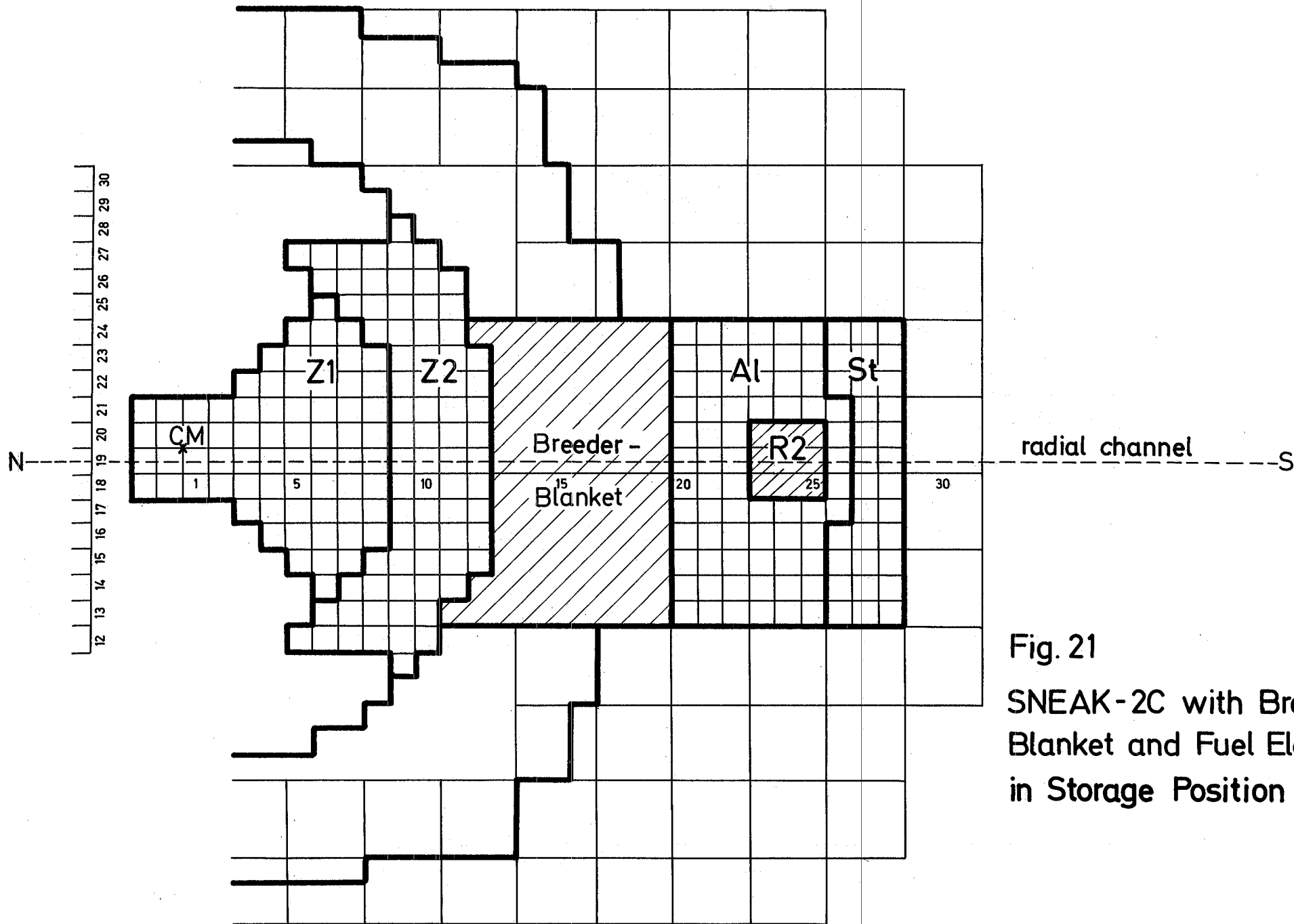


Fig. 21
 SNEAK-2C with Breeder
 Blanket and Fuel Element
 in Storage Position

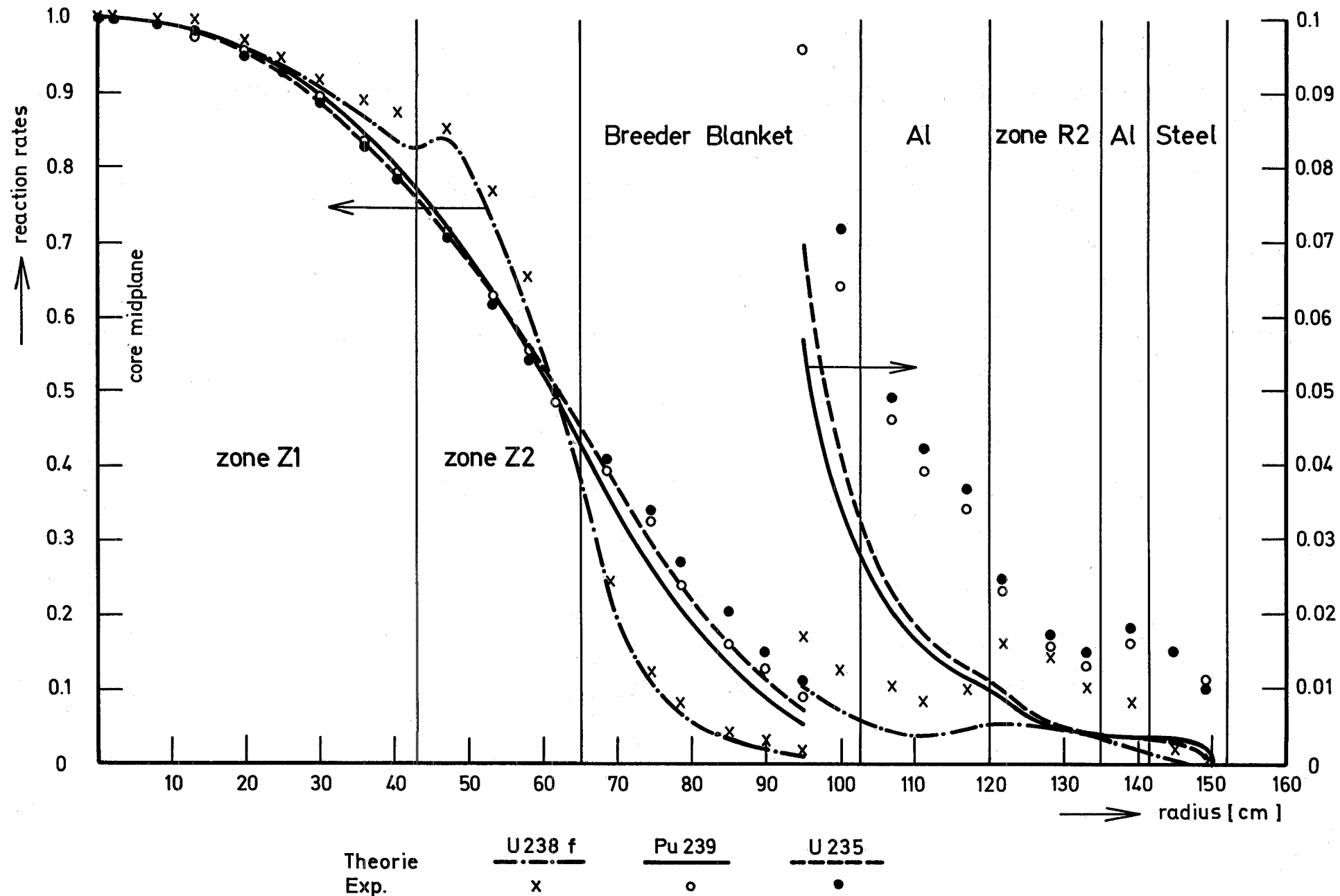


Fig. 22 Radial Rate Traverses through SNEAK-2C including Breeder Blanket and Storage Position

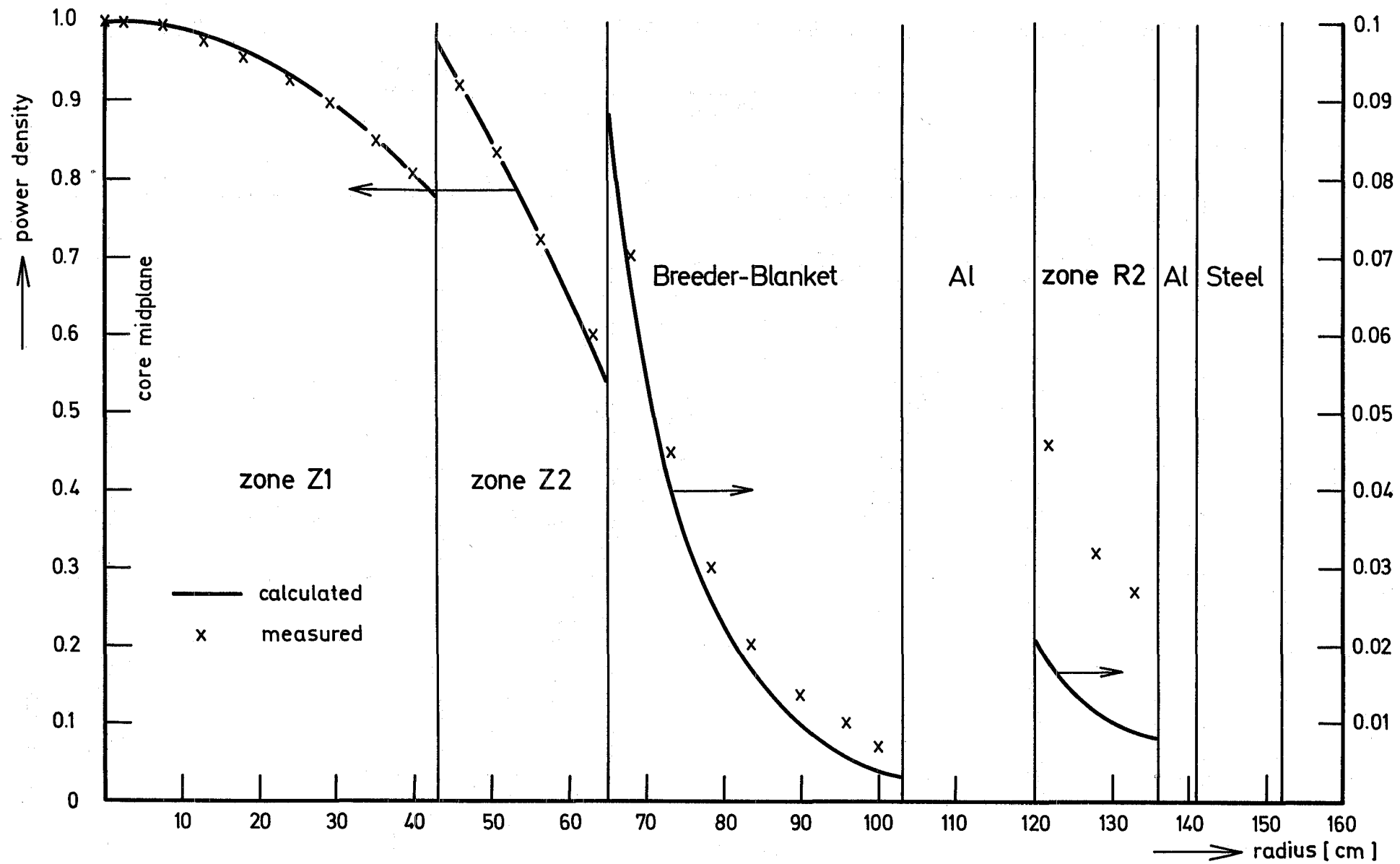


Fig.23 Radial Power Distribution through SNEAK-2C including Breeder Blanket and Storage Position

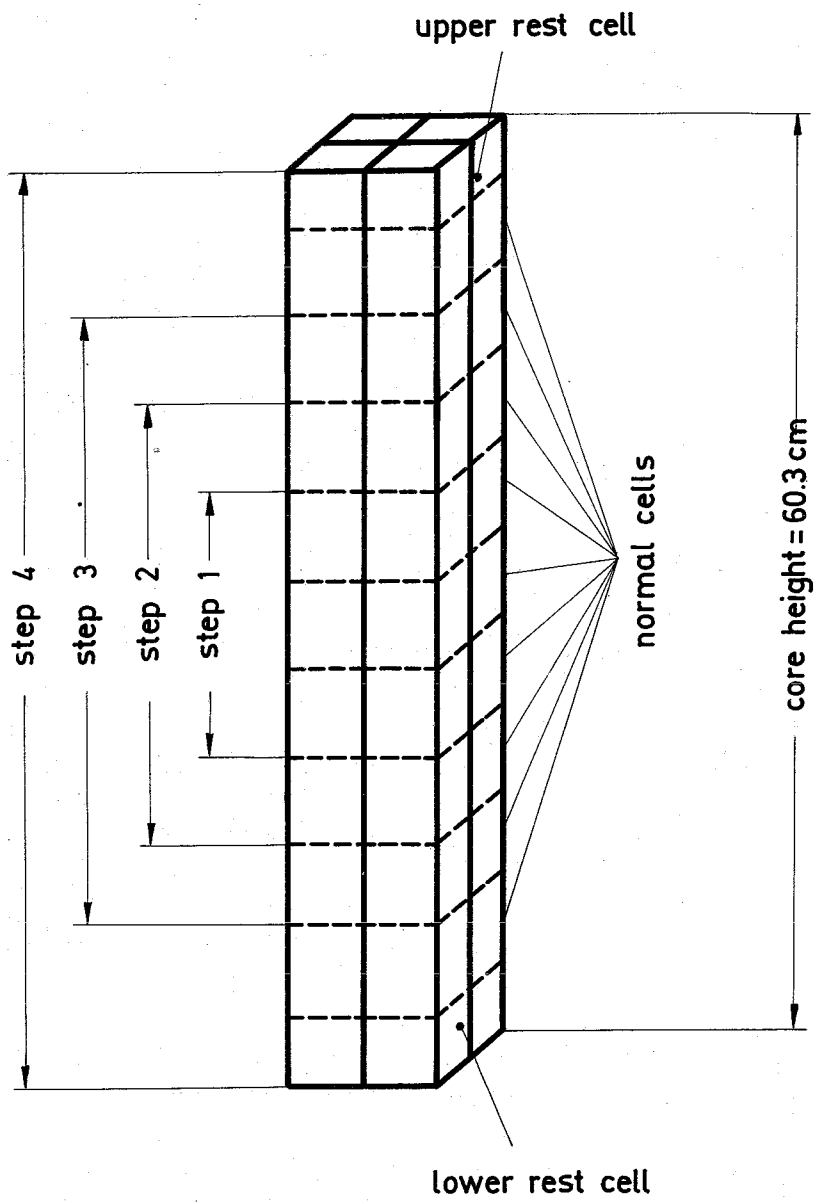
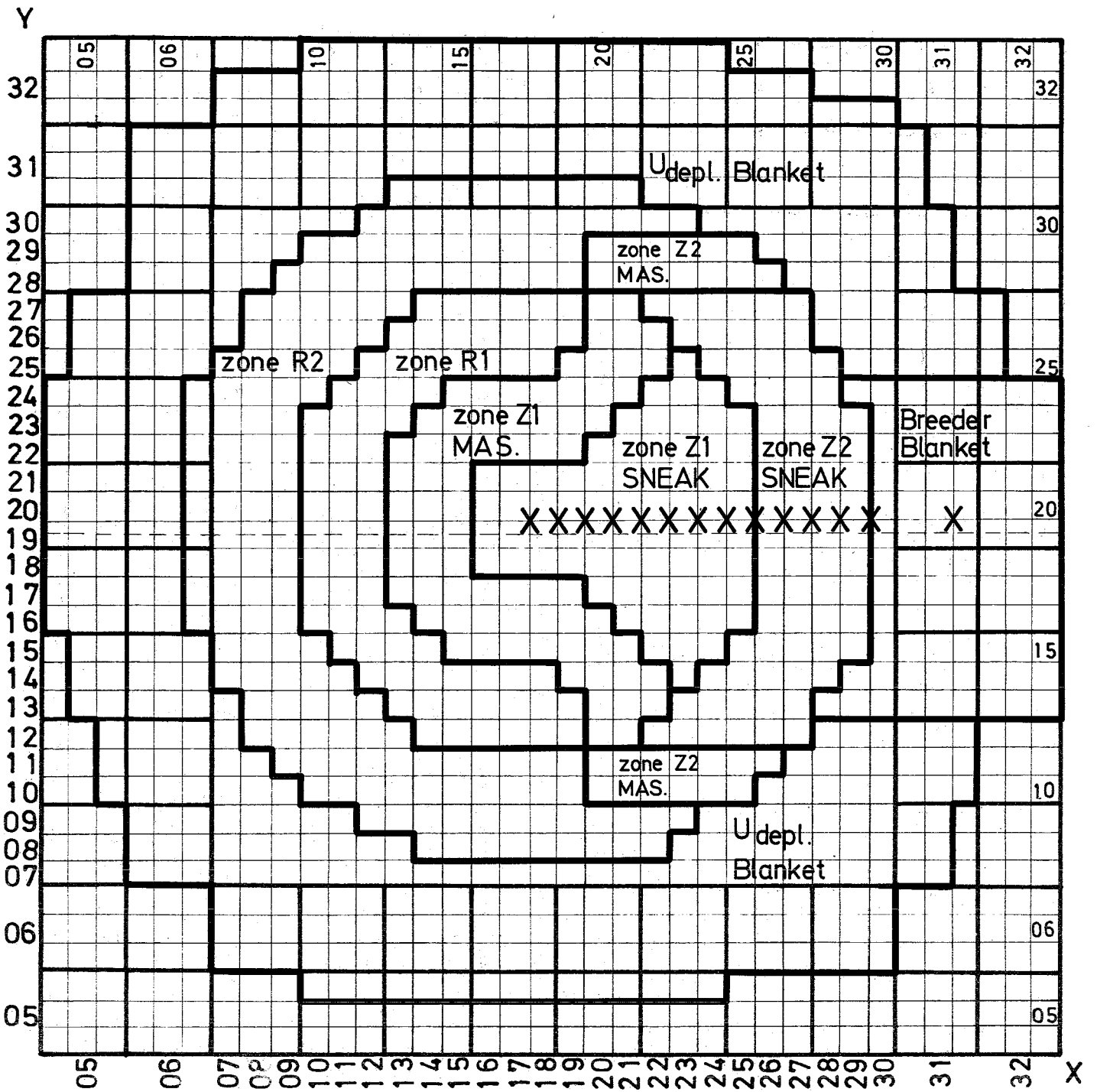
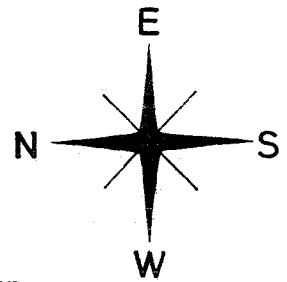


Fig. 24 **Geometry of the axial Void Traverse**



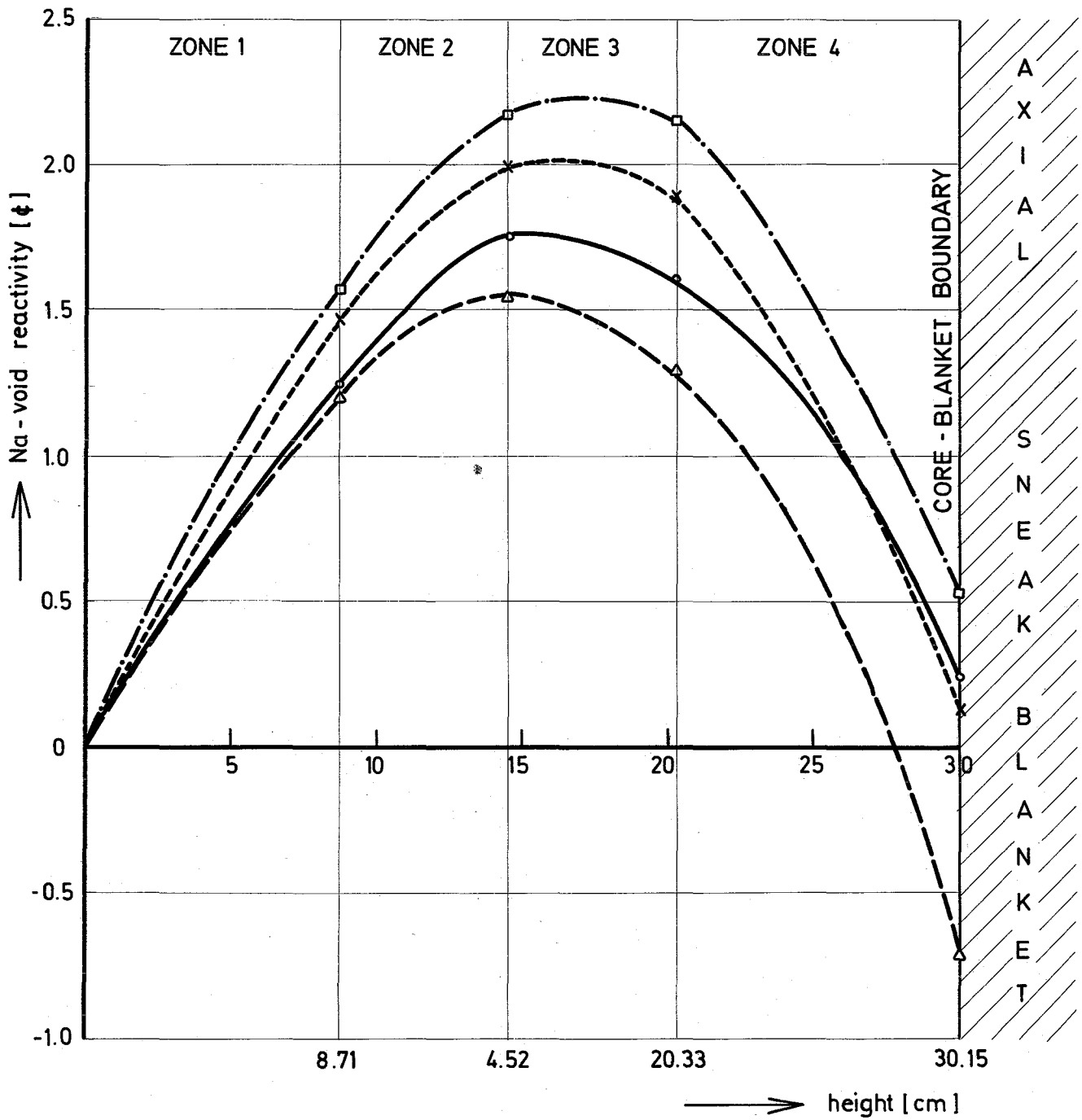
SNEAK- 2C

Fig.25 Geometry of the radial Na-Void Traverse



designates the 4 elements for one void configuration

scale 1:10



- NAPPMB HOM. — · — ·
- △ MOXTOT HET. - - - -
- x MOXTOT HOM. · · · ·
- MEASUREMENT — — — —

Fig.26 Axial Na - Void (integral Values)

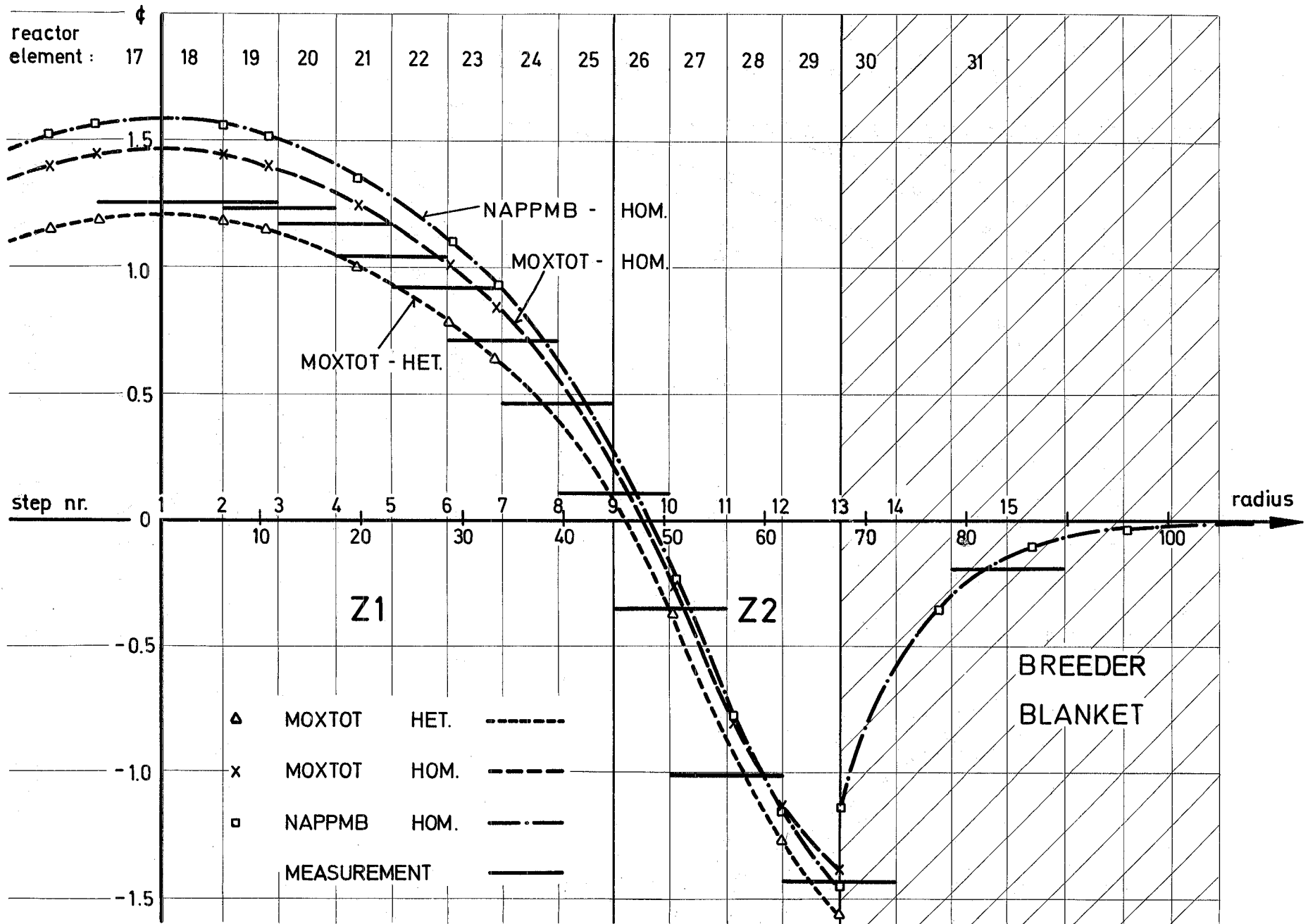


Fig.27 Radial Na - Void Traverse

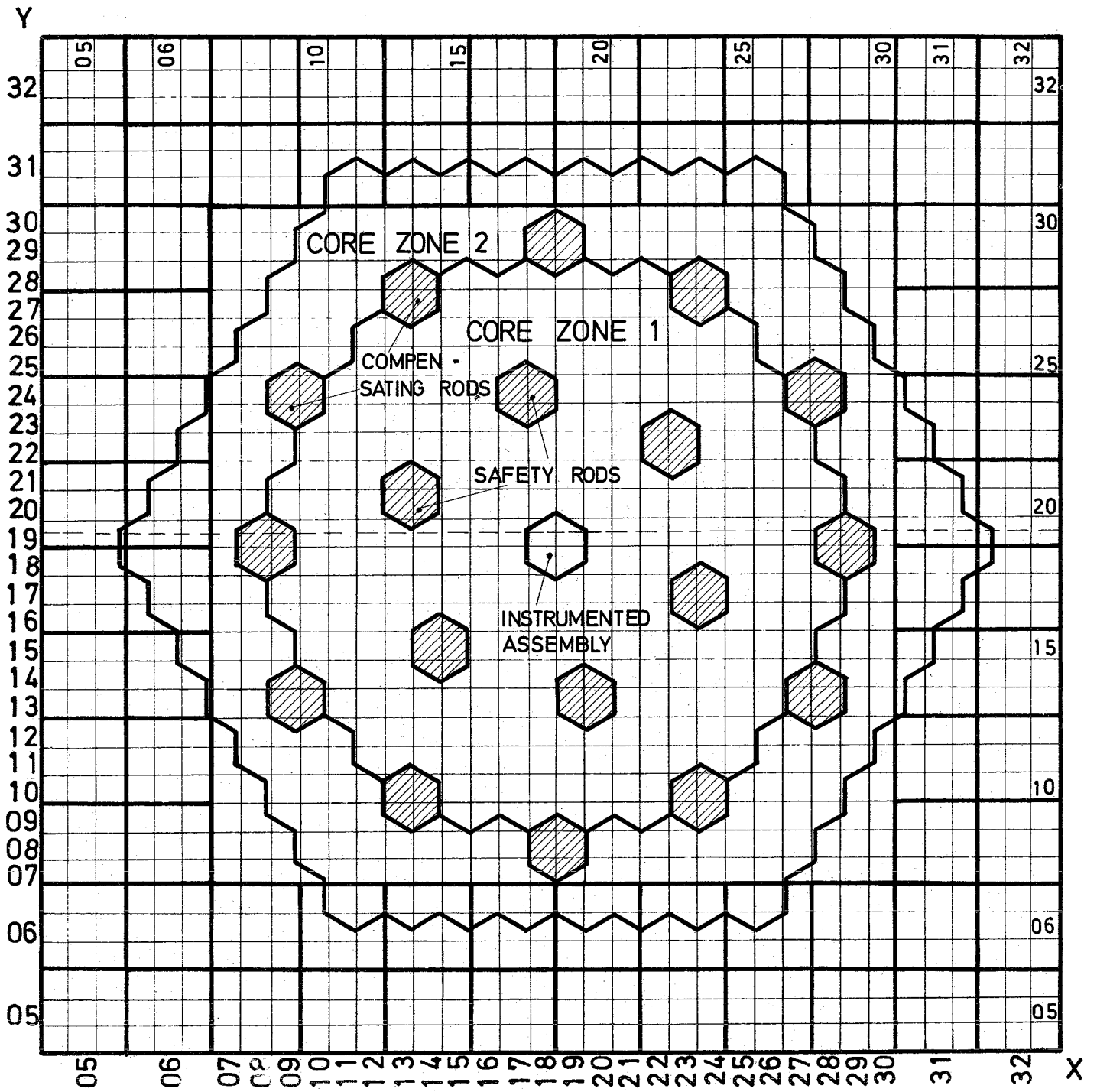
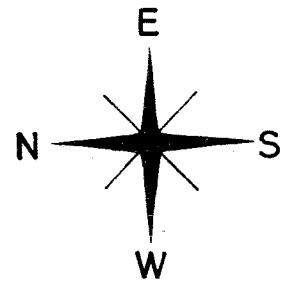


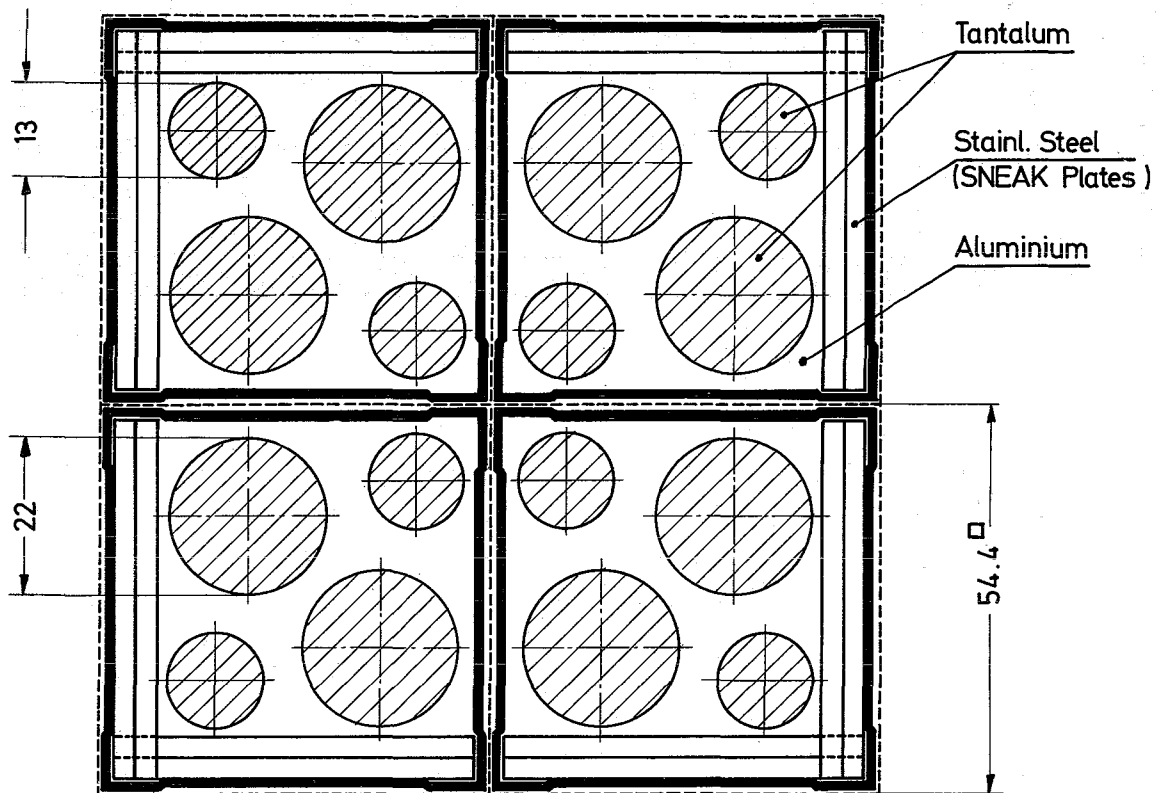
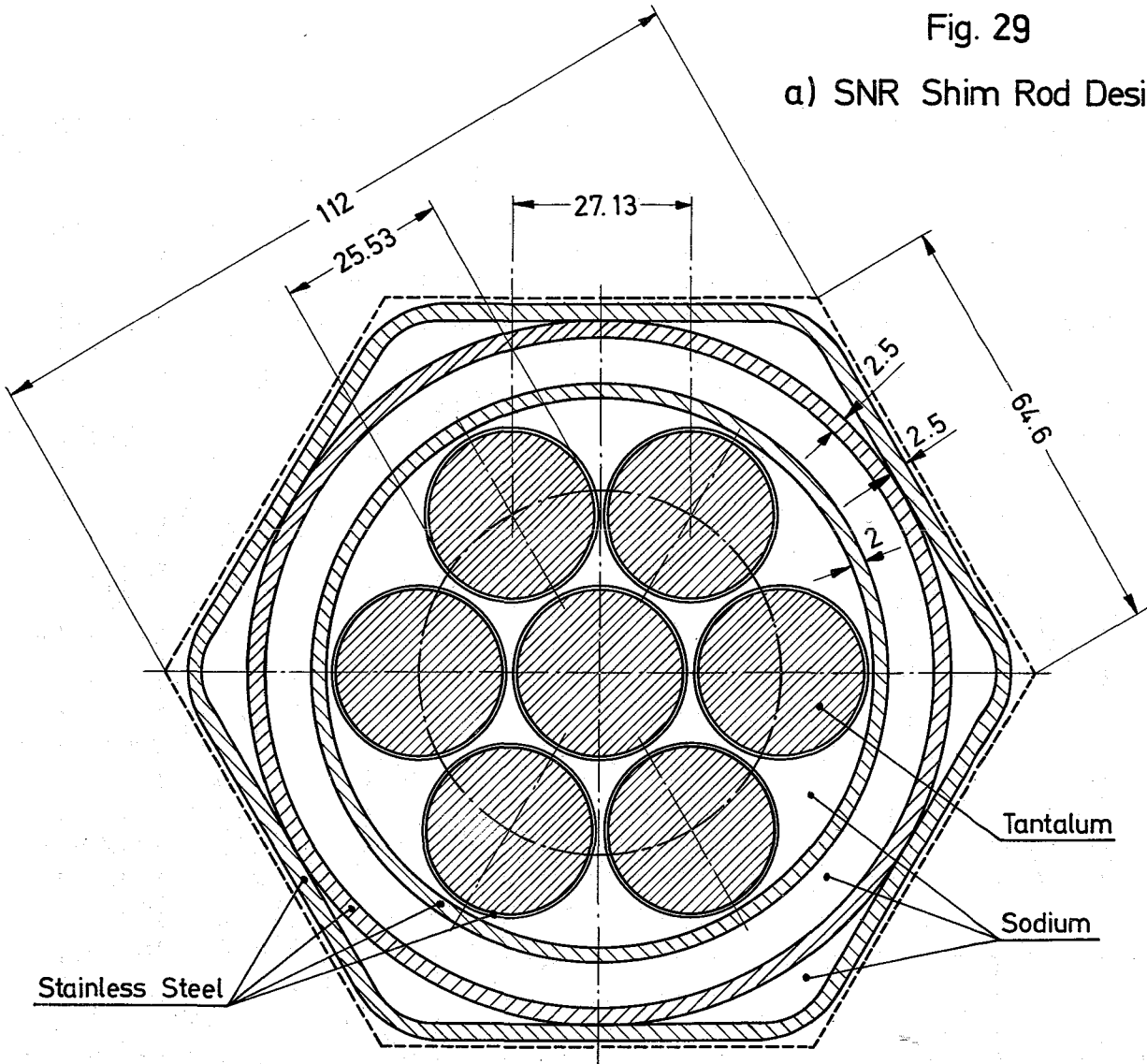
FIG. 28 SNR CORE



scale 1:10

Fig. 29

a) SNR Shim Rod Design



b) Mock - up in SNEAK

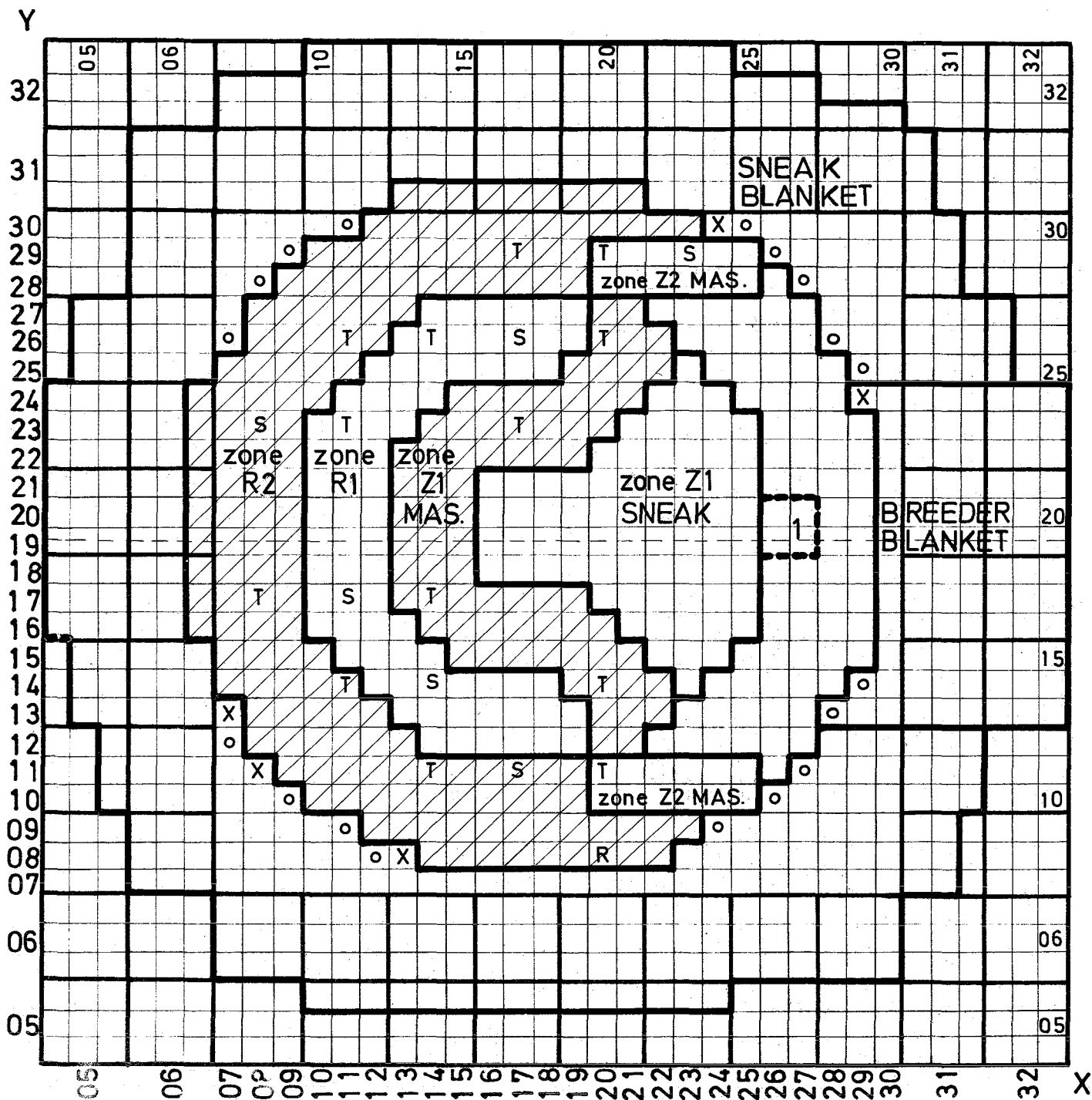

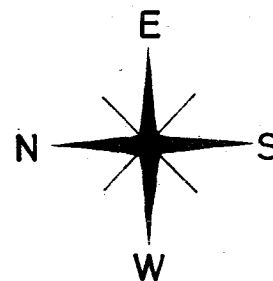


Fig.30 SNEAK-2C Control Rod Experiments

start-up Core : solid line
 group 1 of edge elements : X
 group 2 of edge elements : O

 = Position 1 for absorber or follower rod

T = SNEAK shim rod R = control rod
 S = SNEAK safety rod



scale 1:10

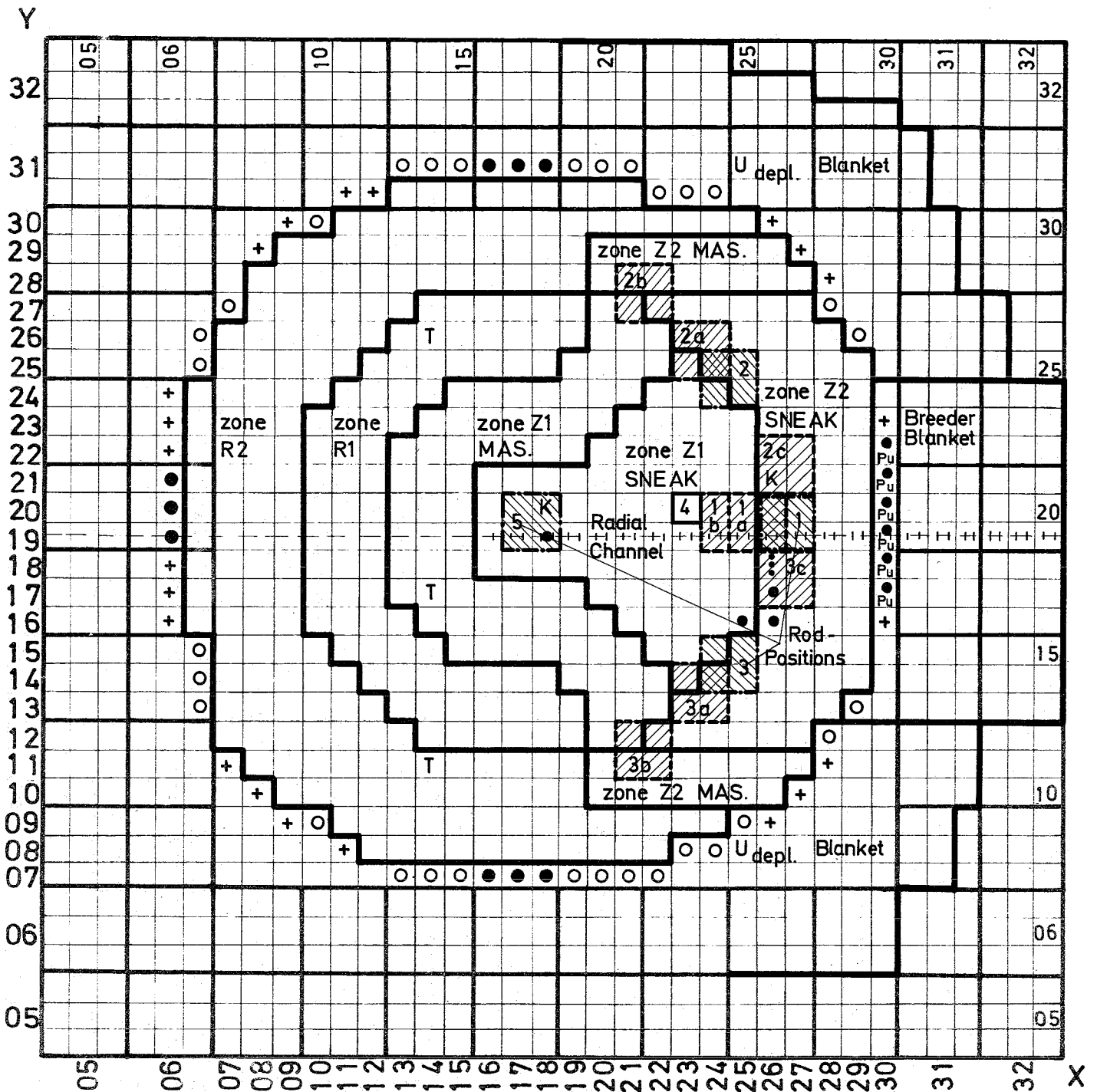


Fig.31 SNEAK-2C Second Part of the Control Rod Experiments
Core Configurations

groups of edge elements

group nr.	number of elements	designation
3	15	●
4	30	○
5	22	+

●●●●● Pos. for azimuthal traverses
(foils and platelets)

K = Pos. for axial chamber traverses

⊞ Pos. for radial chamber traverses

scale 1:10

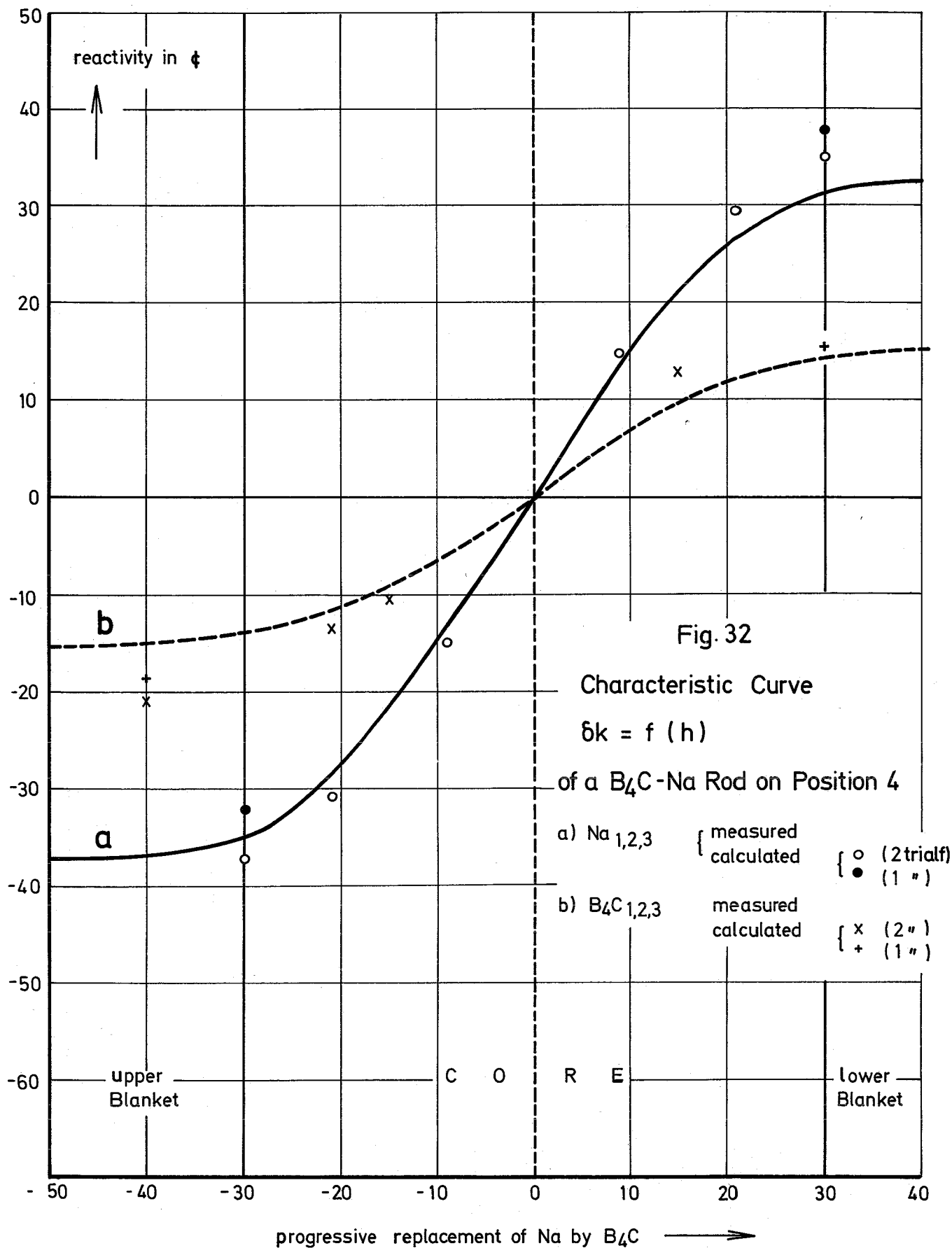
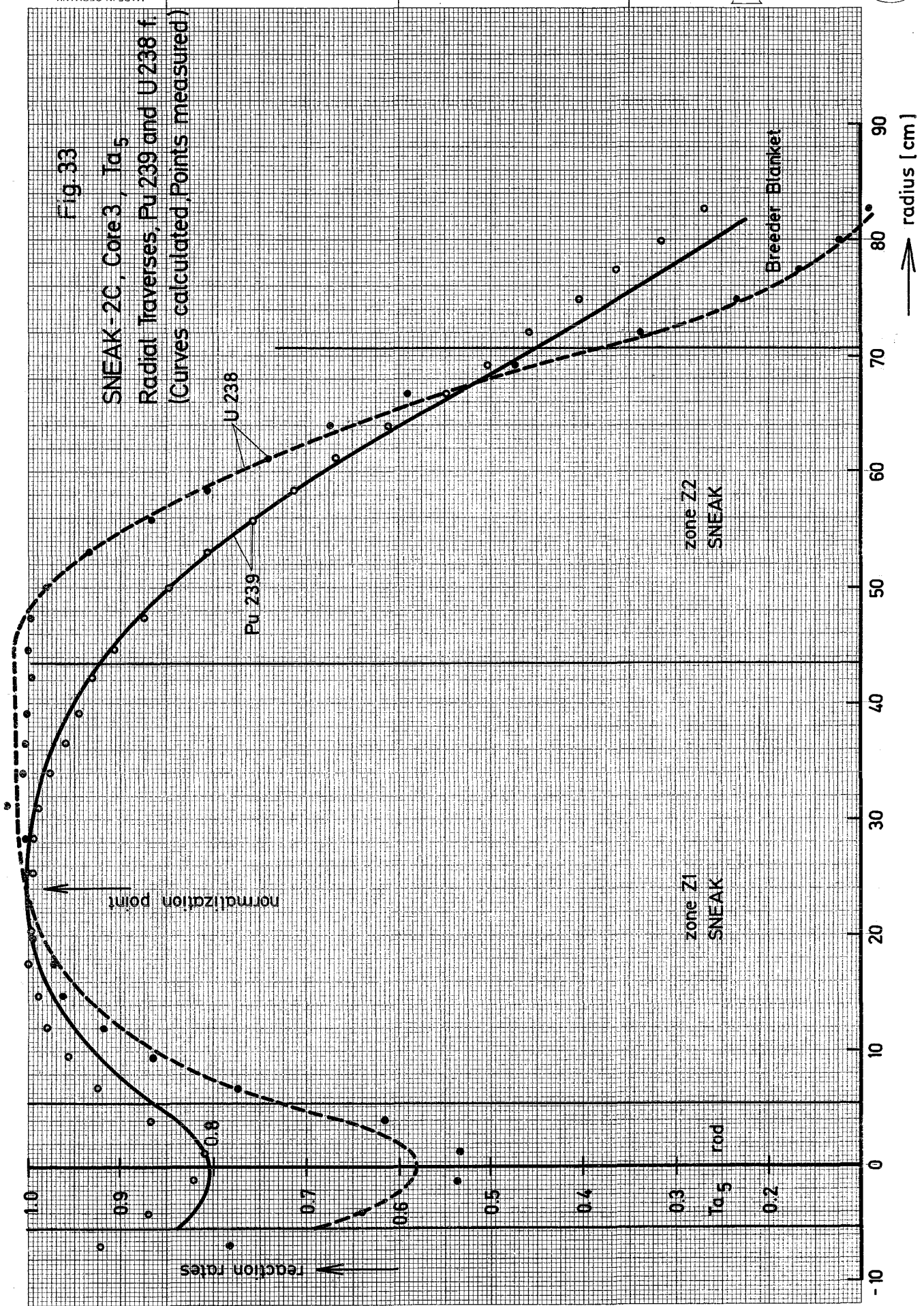


Fig. 33

SNEAK-2C, Core 3, Ta_5
 Radial Traverses, Pu 239 and U 238 f.
 (Curves calculated, Points measured)



reaction rates

Ta_5 rad

zone Z1
SNEAK

zone Z2
SNEAK

Breeder Blanket

radius [cm]



Fig. 34

SNEAK-2C, Core 3, B₄C₁
Radial Traverses, Pu239 and U238f.
(Curves calculated, Points measured)

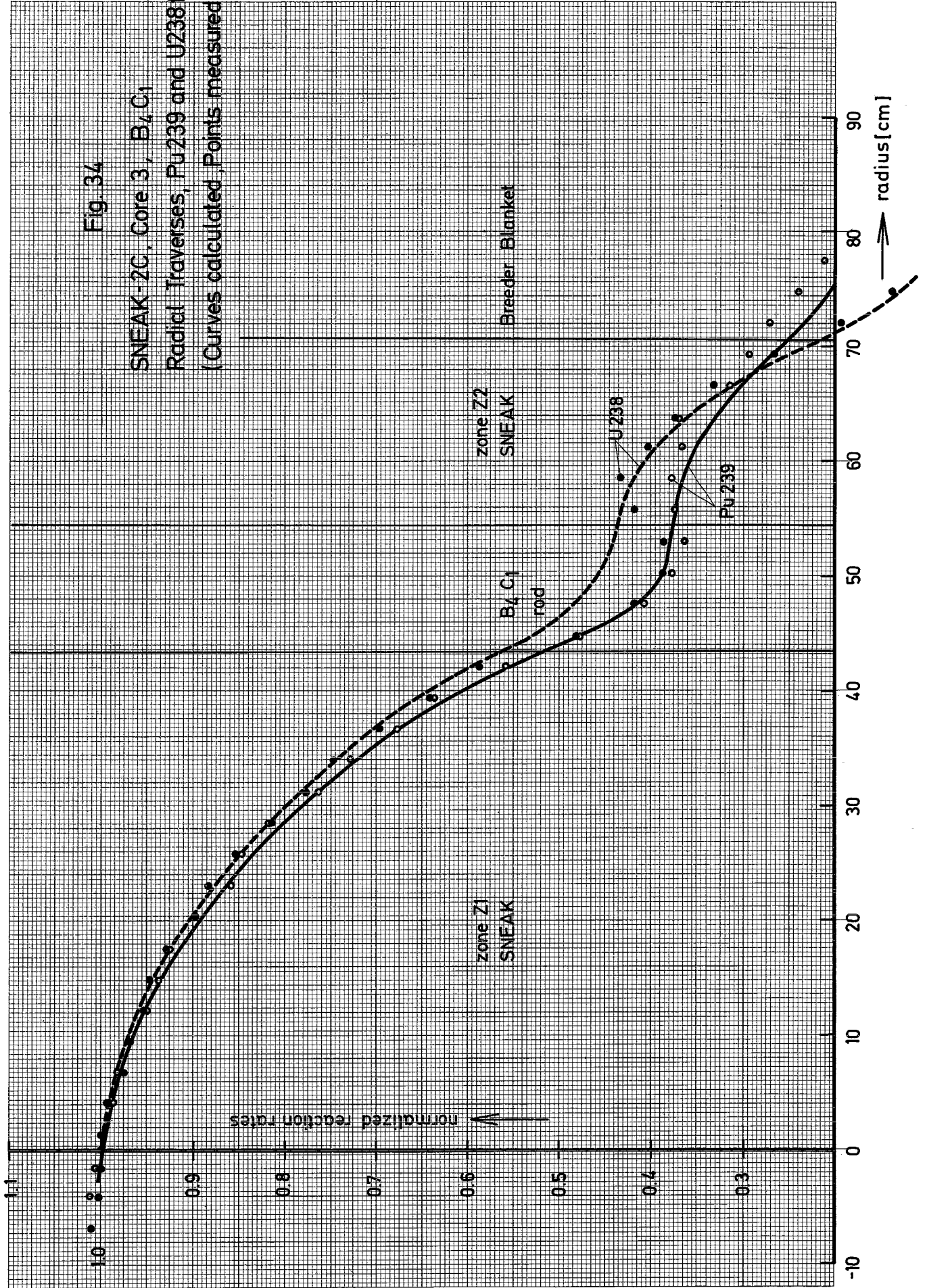


Fig. 35

SNEAK-20, Core 3, Na-B₄C,
Axial Traverses, Pu 239 and U 238 f
(Curves calculated, Points measured)

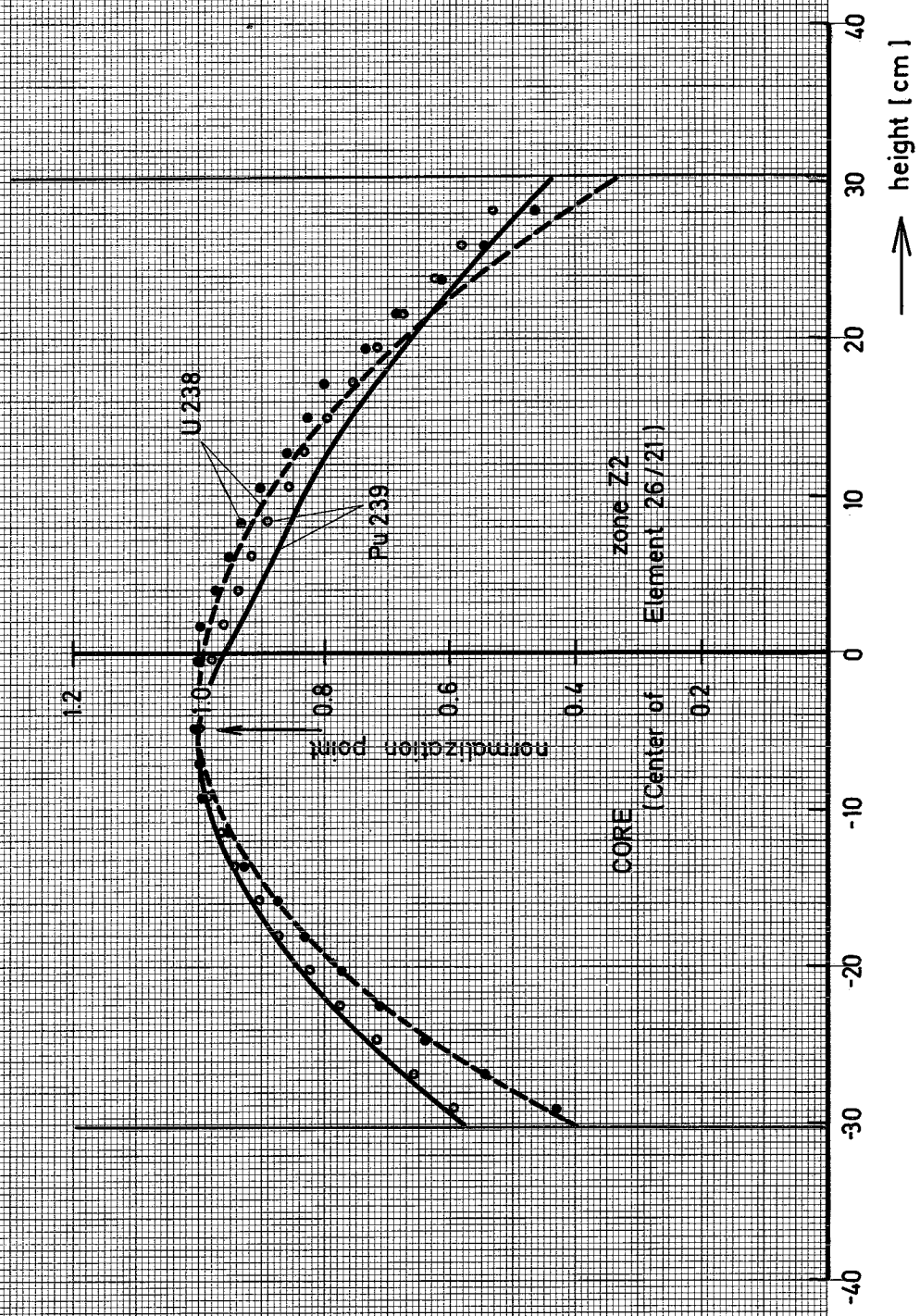




Fig. 36

SNEAK-2C, Core 4, B₄C₅

Radial Traverse, Power Density

(Curve calculated, Points measured)

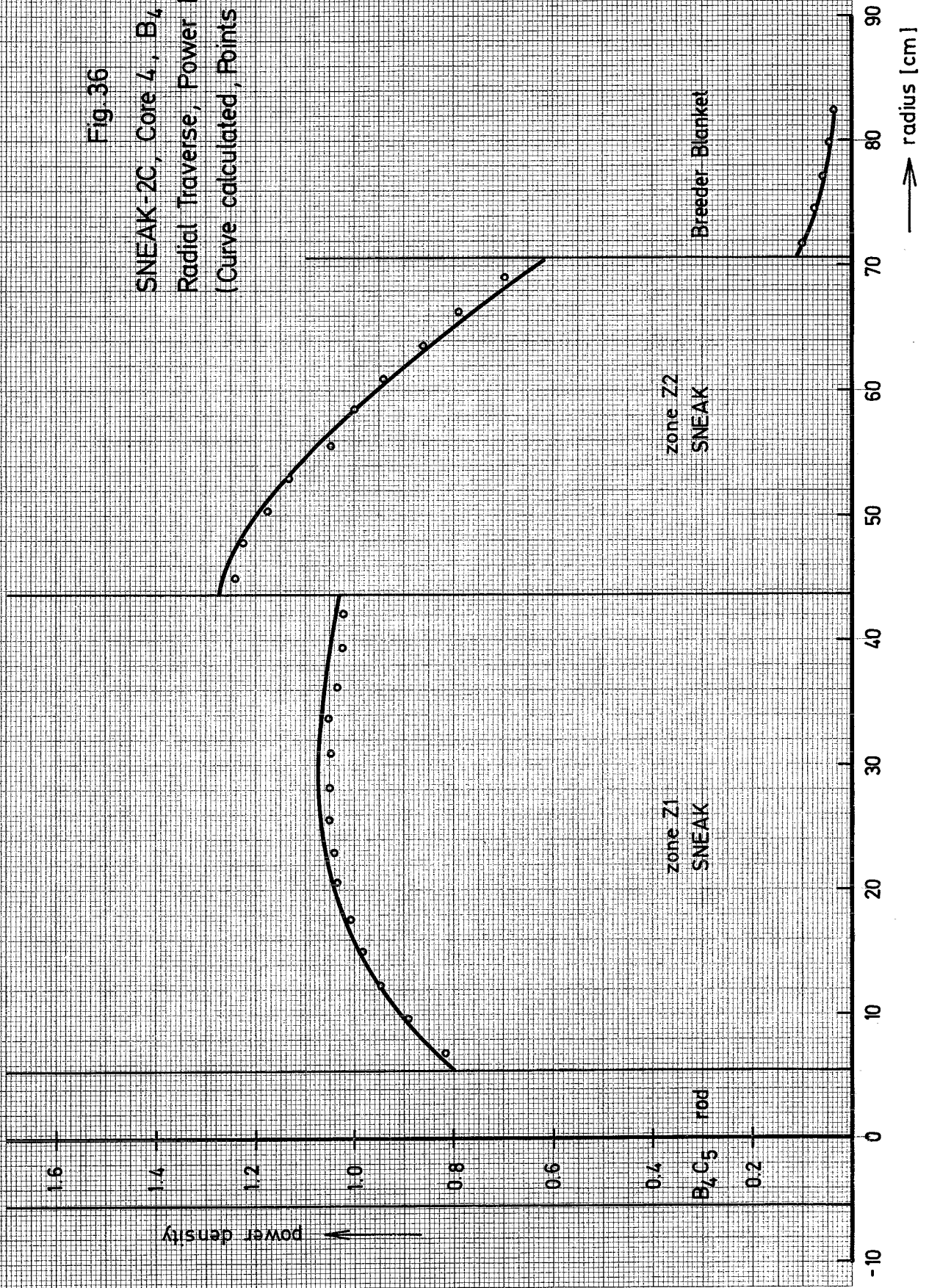




Fig. 37

SNEAK-2C, Core 3, B₄C-1
Radial Traverse, Power Density
(Curve calculated, Points measured)

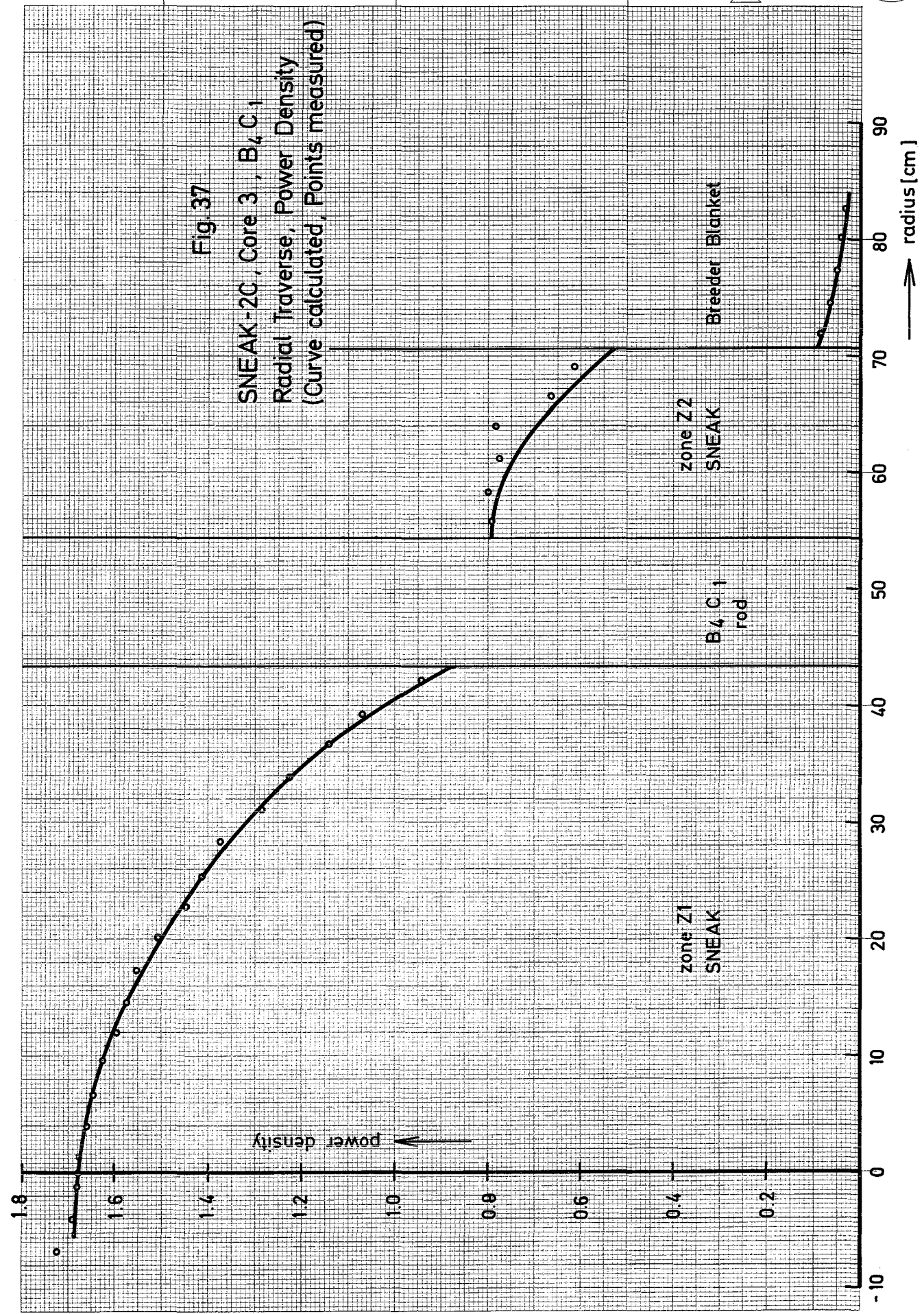


Fig. 38

SNEAK-2C, Core 1, Reference (Z2)
Axial Traverse, Power Density
(Curve calculated, Points measured)

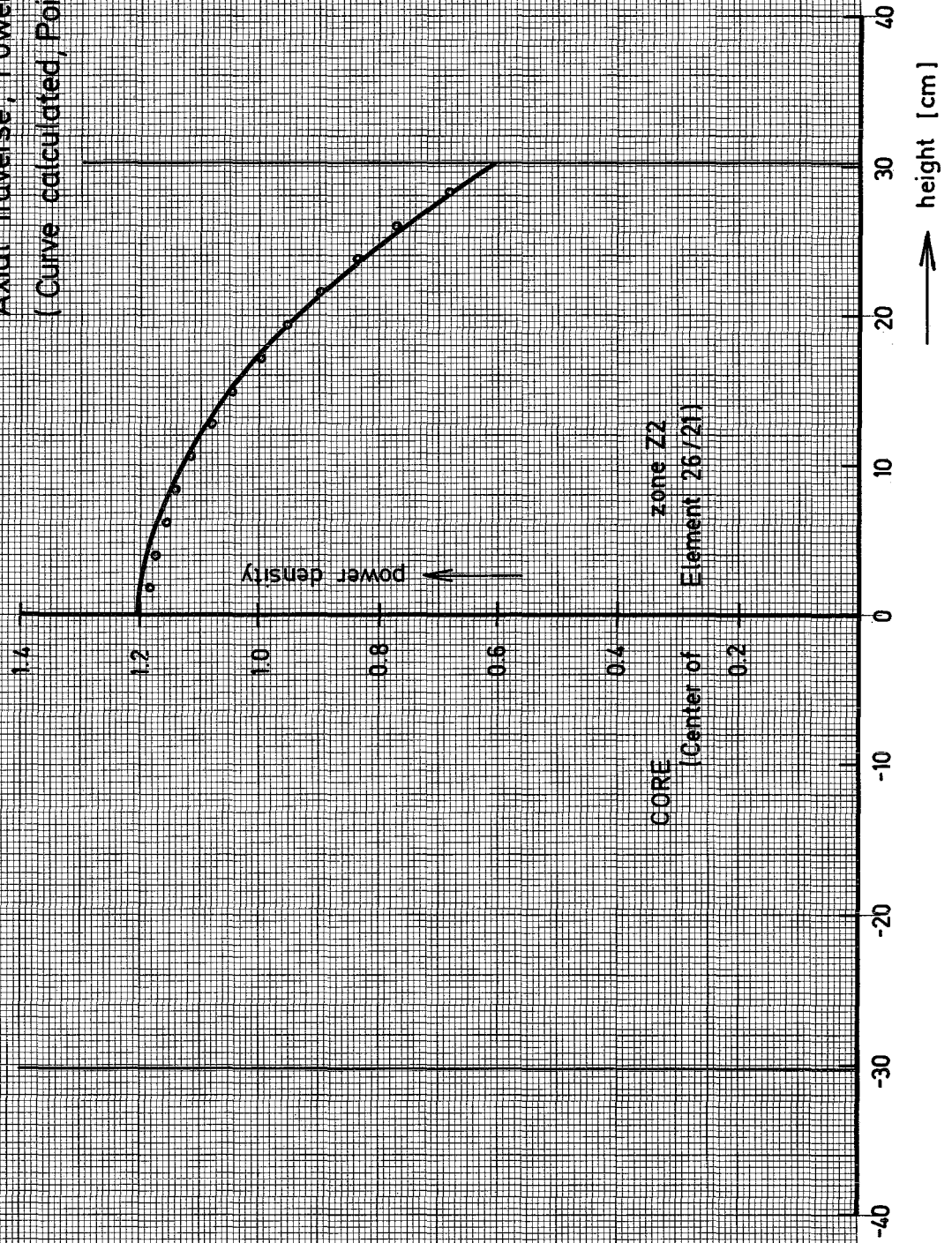


Fig. 39

SNEAK -2C, Core 3, B₄C₁
Azimuthal Traverse, Power Density
(Curve calculated, Points measured)

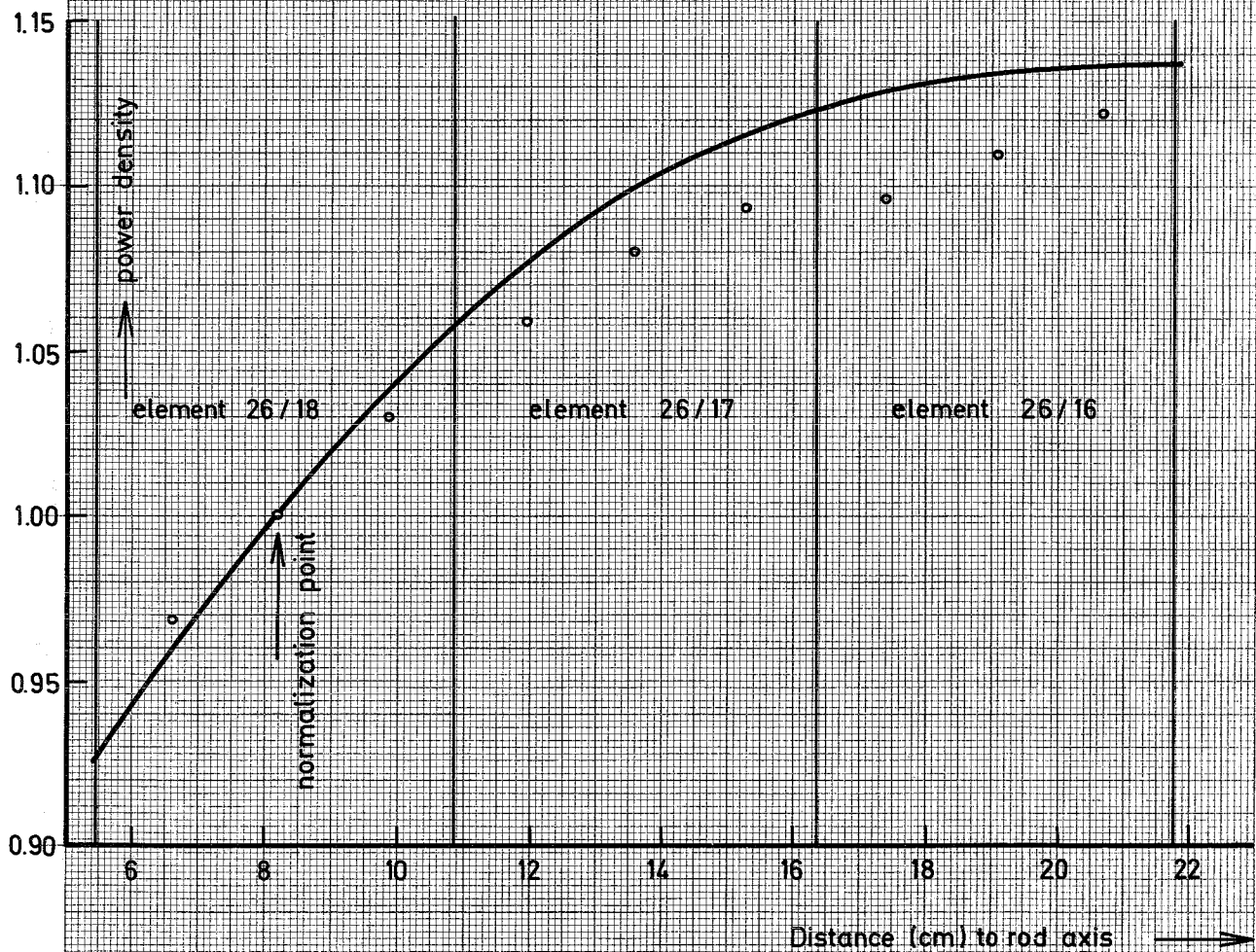
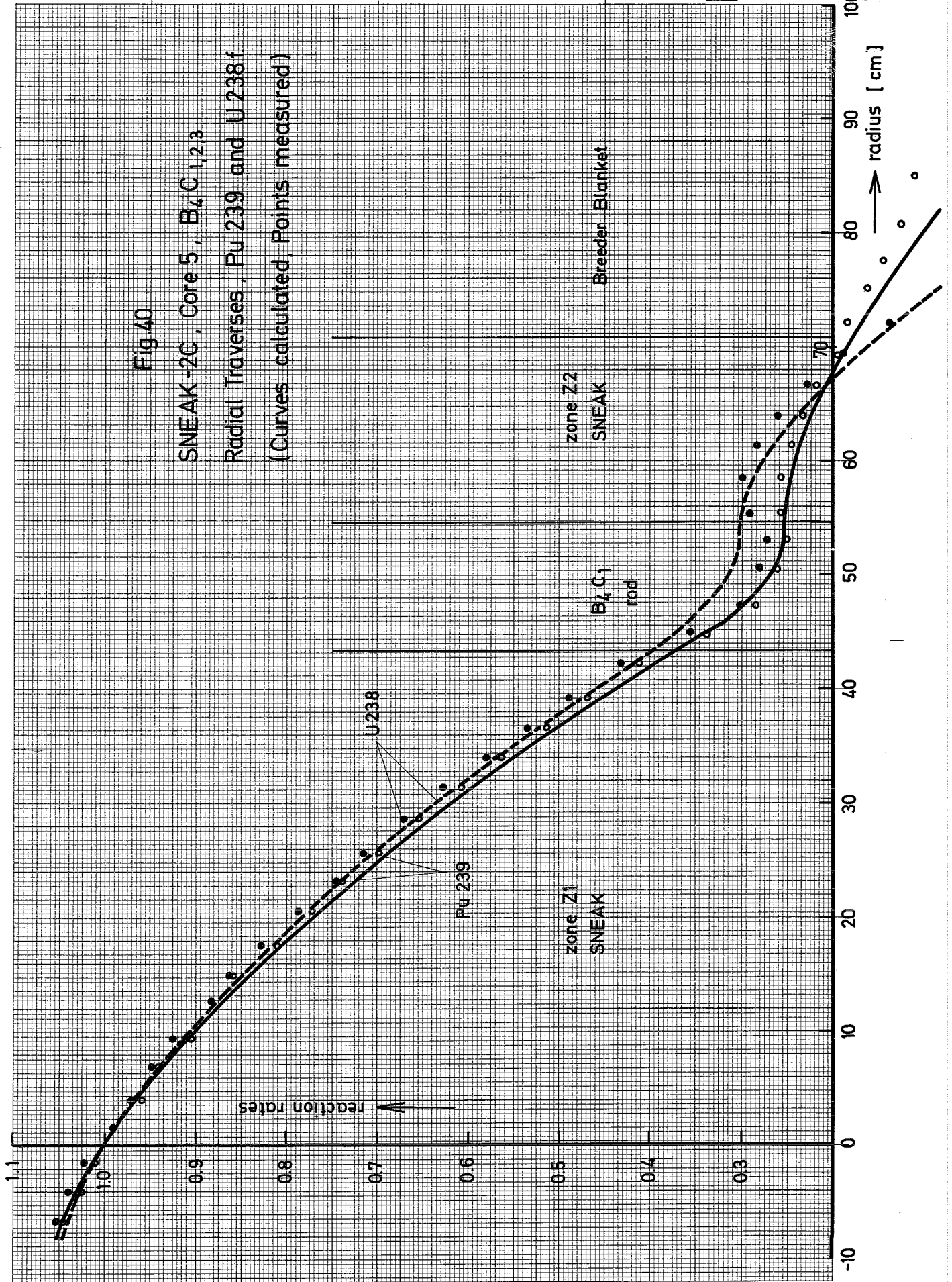




Fig.40
SNEAK-2C, Core 5, B₄C_{1,2,3}
Radial Traverses, Pu 239 and U238f
(Curves calculated, Points measured)



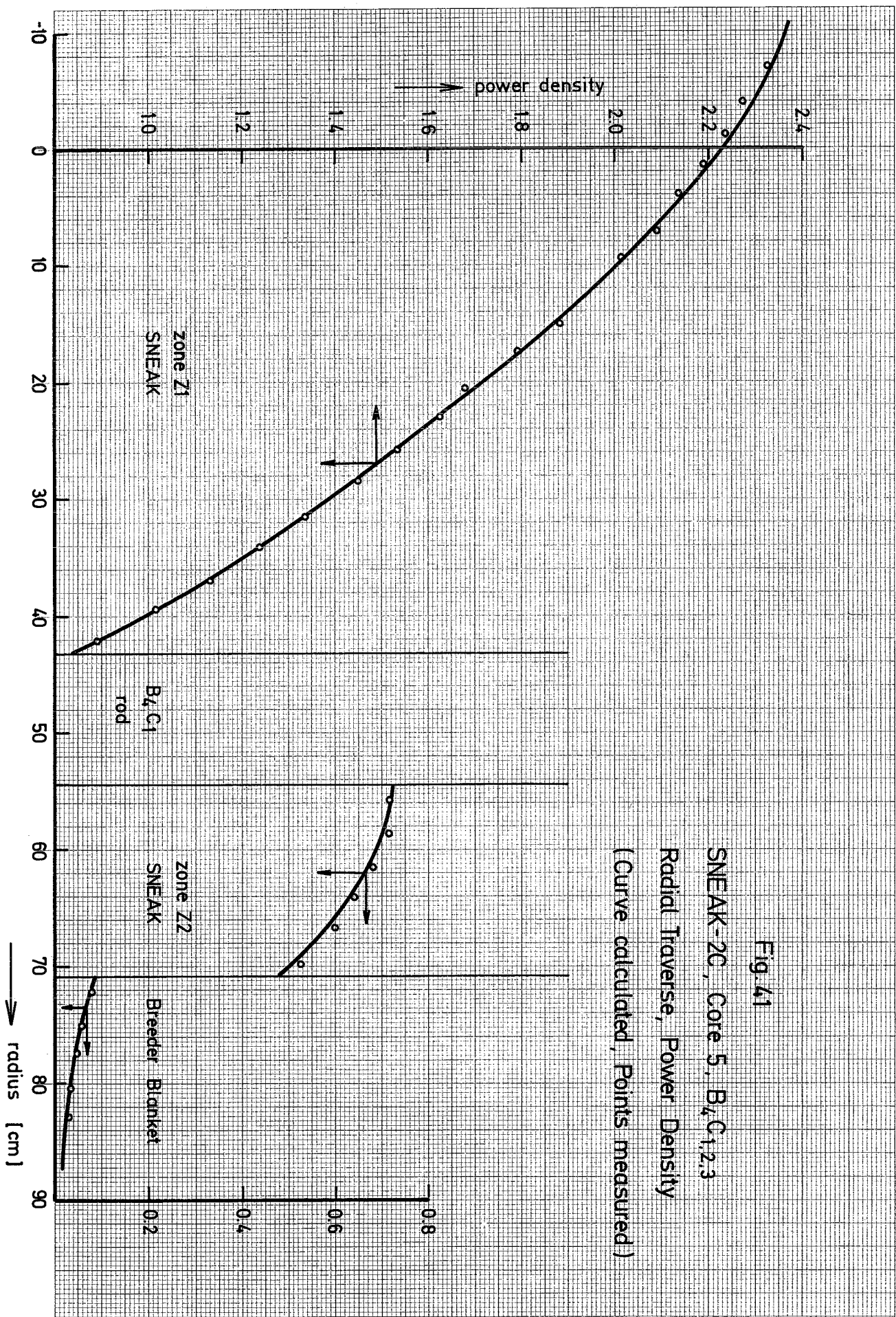


Fig. 41
 SNEAK-2C, Core 5, B₄C_{1,2,3}
 Radial Traverse, Power Density
 (Curve calculated, Points measured)

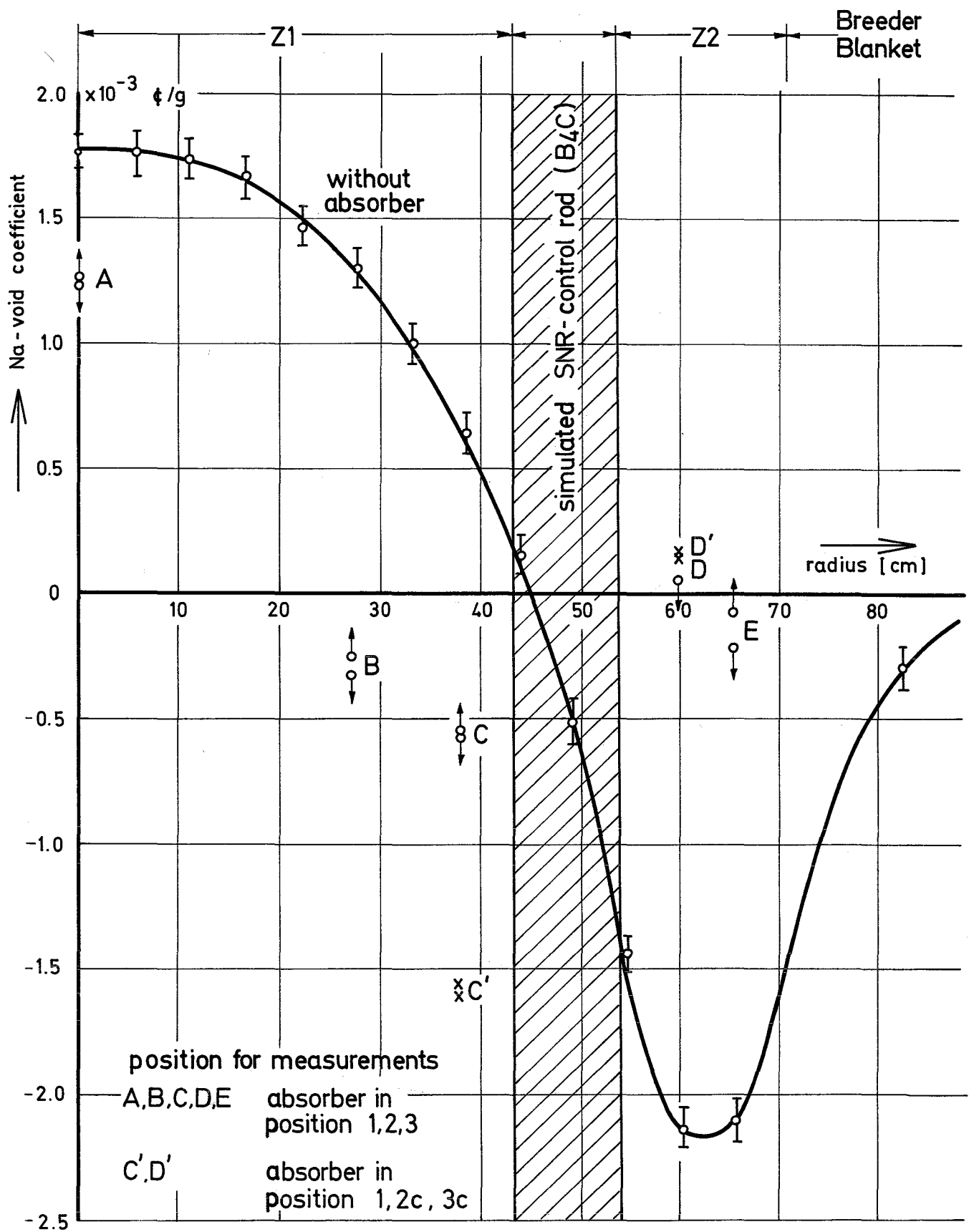


Fig.42 SNEAK-2C Na-Void Traverse with and without Absorbers

